A REVIEW OF AERONAUTICAL FATIGUE INVESTIGATIONS IN FINLAND APRIL 2017 – MARCH 2019

Presented at the 36th Conference of the
International Committee on Aeronautical Fatigue and
Structural Integrity (ICAF),
Krakow, Poland, 3-4 June 2019

Compiled by	Tomi Viitanen, Aslak Siljander
Confidentiality	Public

Preface

The Finnish Defence Forces Logistics Command, Joint System Centre (FDFLOGCOM JSC) initiated and supported this work. The editors are indebted to the following individuals who helped in the preparation of the review (organizations and individuals in alphabetical order):

Espoo 30 April 2019

Editors

Contents

1 Introduction

The coordinated aeronautical research in Finland - and its embodiment: the national research network - has over the decades been solely advocated and supported by the Finnish Air Force (FINAF). Their vision is that while the FINAF is concentrating to carry out its primary objectives, the national research network help FINAF to optimize the use of their prevailing fleet in a cost-effective way, and to make the most of their asset. The assigned research activities by the FINAF are of two kinds: on the one hand, the tasks are related to finding pragmatic solutions to be applied with little or no effort in every day's routine, but on the other hand, the tasks feature a more scientific flavor such that the possible solution goes beyond the obvious and requires more time to mature. The FINAF has also found it advantageous that Finland belongs to the international community of aeronautical fatigue research – i.e. is a member nation in ICAF. This will is manifested in the ICAF National Reviews since 2001. [24], [25], [26], [27], [28], [29], [30], [31], [32]

The Finnish Air Force is one of the oldest independent air forces in the world. It all began 101 years ago when the Swedish Count, Eric von Rosen, donated to the Finnish Air Force its first aircraft. A Thulin typ D reconnaissance plane (**Figure 1**) arrived at the city of Vaasa on the 6th March 1918, and that day has since been celebrated as the foundation date of the Finnish Air Force. [1]

Figure 1: *The first aircraft of the Finnish Air Force, Thulin typ D, shown in the city of Vaasa, March 1918. Figure courtesy of the Finnish Air Force. [1]*

In the early 1920s, the focus of the FINAF development was on maritime aviation, since it was then considered that the primary task of the Finnish air arm was, with procured floatplanes, to conduct surveillance and reconnaissance operations relying on Finland's territorial waters.

Present-day objective of the Air Force has basically remained the same: to monitor and secure Finland's territorial integrity. However, the tools to implement the objective are somewhat more capable than back in the old days. The current fixed wing aircraft inventory of the FINAF is summarized in **Figure 2**.
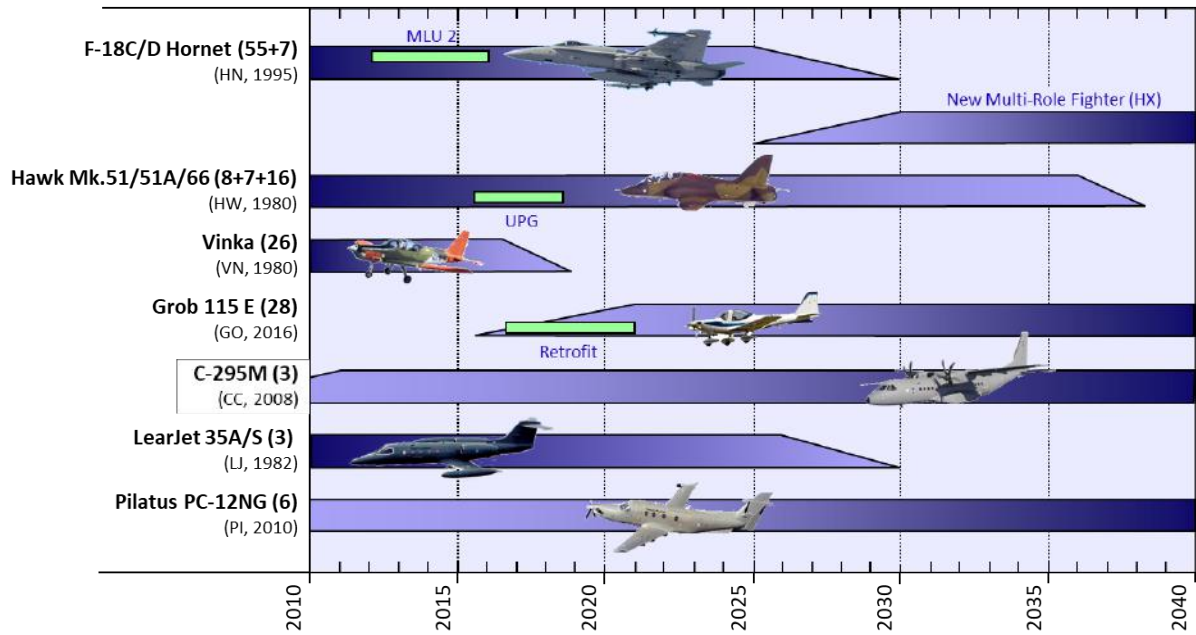
Figure 2: *An overview of the fixed wing aircraft inventory of the Finnish Air Force (FINAF). Figure courtesy of the Joint Systems Centre.*

The 20 TTH/SAR NH90 helicopters purchased earlier by the Finnish Defence Forces (FDF) were retrofitted (by Patria Aviation) and reached the Full Operational Condition (FOC) status. The retrofits (including the platform and various systems therein) started in 2014, and were completed in 2018. The helicopters of the FDF at the time of writing this review are summarized in **Figure 3**.
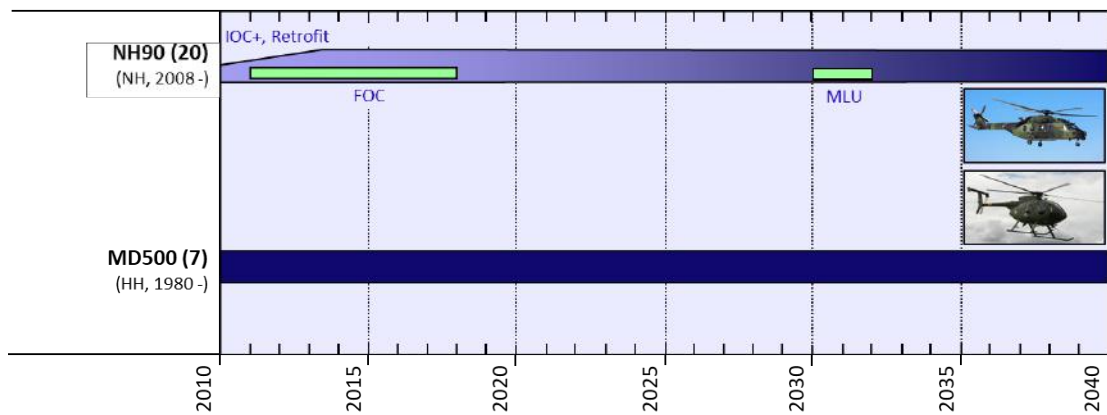
Figure 3: *An overview of the rotary wing aircraft inventory of the Finnish Defence Forces (FDF). Figure courtesy of the Joint Systems Centre.*

Before proceeding into the highlights of the structural integrity management activities, a brief update of the FINAF's fighter aircraft and associated pilot training aircraft is provided next.

1.1   Valmet L-70 Vinka

The Valmet L-70 Vinka is a three-seat piston-engine aircraft of Finnish design and manufacture (**Figure 4**). The Vinka is used by the FINAF in a primary training role since 1980 to teach basic flying skills to military pilots. Due to its long service life the Vinka has undergone several minor structural reinforcements and other modifications. 26 of the original 30 Vinkas remain in service with the FINAF. The German-built Grob G 115E will replace the Vinka aircraft in the primary and basic training role in the coming years (Chapter 1.2). [2]

Figure 4:   Valmet L-70 Vinka primary trainer aircraft (VN-5). Figure courtesy of the FINAF.

Previous activities related to the Valmet Vinka primary trainer of the FINAF were outlined in e.g. [32] Chapter 1.1. During the Life Extension Program (LEP) of the Vinka primary trainer fleet, each aircraft was equipped with a g counter. The structural life consumption and severity of the usage is monitored by Patria Aviation from the g counter data. Patria also issues recommendations on a yearly basis regarding the rotation of the Vinka fleet to obtain a more even rate of structural life expended.

Based on the g counter information, the severity of usage is more benign compared to the basis of the LEP analyses and tests, see **Figure 5**.

The first fleet leader was removed from operation in September 2015 after logging 7100 FH (it was given 100 FH extension to the official 7000 FH limit). After that the plane was disassembled for structural inspections. Most of the inspections were done visually but the most critical locations were inspected using NDT. No cracks or loose rivets were found. Based on the inspection results, and the fact that originally three fleet leaders were selected as a precaution, it was decided that the two other fleet leaders do not any more need to log hours differently compared to the rest of the fleet. In late 2018 loose rivets were found from the lower surface of the wing of the fleet aircraft. This finding could not be predicted based on the fleet leader inspection.
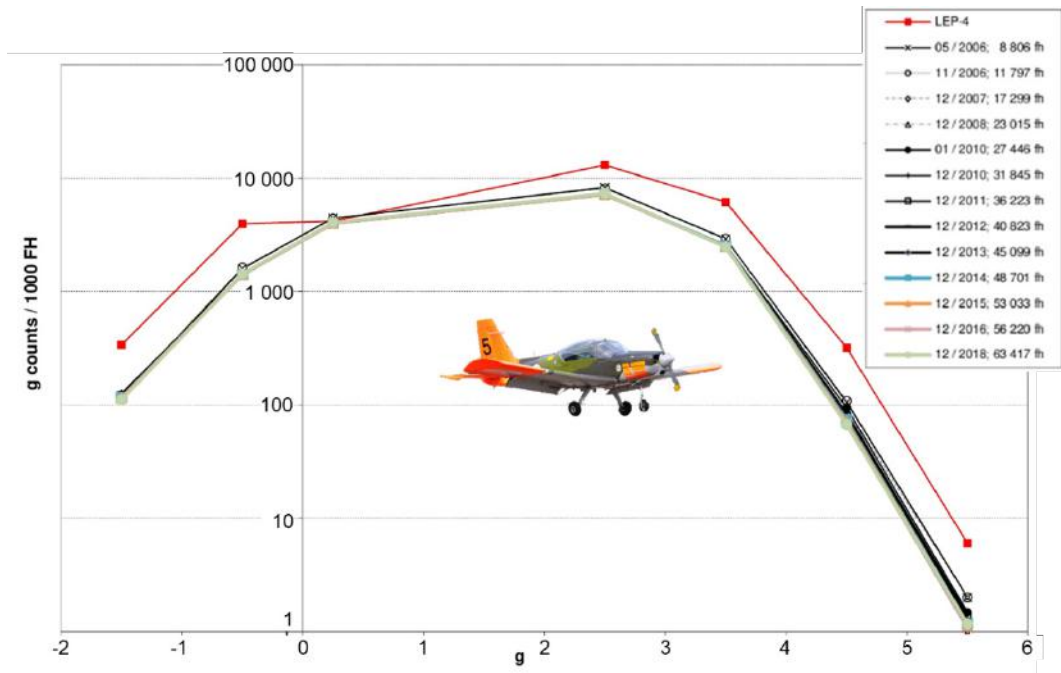
Figure 5: *The g counts per 1000 FH of the Valmet Vinka. From top to bottom: The spectrum representing the LEP design assumptions (LEP-4); the post LEP g counter spectrum as of May 2006; as of November 2006; as of December 2007; as of December 2008; as of January 2010; as of December 2010; as of December 2011; as of December 2012; as of December 2013; as of December 2014; as of December 2015; as of December 2016; and the update from the previous review: as of December 2018 including a total of 63 417 FH. All curves (excluding the red LEP-4) represent the fleet average from all Vinkas, as ranked according to the aircraft center of gravity normal acceleration. Figure courtesy of Patria Aviation.*

1.2   Grob G 115E

The Grob G 115E is a small, lightweight, two-seat piston-engine aircraft built in Germany by Grob Aircraft. In October 2016, the FINAF procured 28 pre-owned Grob G 115Es for the Defence Forces to supersede Valmet L-70 Vinkas (Chapter 1.1) in primary and basic training roles. The aircraft were purchased from Babcock Aerospace Limited, which had previously operated them as a training platform for the Royal Air Force. [2]

The Finnish Grobs are allocated GO-series military registrations and were delivered to Finland in 2016-2018. Before handover to the customer, the Grob fleet will receive an avionic and communication systems upgrade. State-of-the-art digital displays will be fitted in order to bring the cockpit layout compatible with the other aircraft operated by the Defence Forces.

On the contrary to its predecessors (Vinkas), the structure of Grob G 115E is manufactured of composite materials. It is constructed predominantly from carbon fiber reinforced composites, has a tapered low wing, a 180 hp engine with a 3-bladed variable-pitch propeller, a fixed tricycle undercarriage, fixed horizontal and vertical stabilizers and conventional flight control surfaces. The large glass canopy renders clear all-round visibility to the crew (**Figure 6**).

Figure 6:   *Grob G 115E primary trainer aircraft. Figure courtesy of the FINAF.*

1.3 Hawk Mk.51/51A and Mk.66

The BAE Systems Hawk is a British single-engine two-seat advanced jet trainer which is operated in Finland by the Air Force Academy, primarily in advanced and tactical training roles. The first Hawks, Mk.51s, entered Finnish service in 1980-1985. In 1993, the FINAF ordered an additional batch of seven Hawk Mk.51As that contain minor improvements in structure and avionics compared with the Hawk Mk.51. Finland augmented its Hawk fleet in 2007 by sourcing 18 low-hour Hawk Mk.66s from Switzerland. Externally, the former Swiss Hawks stand out from the grey legacy Hawks owing to their red-and-white paint scheme (see **Figure 7**). However, from 2017 to 2020 the Mk 66 aircraft will receive a grey livery similar to older model aircraft. [2]

Due to increasing signs of metal fatigue, a major structural reinforcement program (SRP) was performed to extend the operational life of Finland's Hawks. The Hawk SRP was completed during the late 1990s. Along with the Mk.66s, the Finnish Hawks underwent an extensive cockpit upgrade program carried out by Patria Aviation. The glass cockpit upgrade program included the replacement of analogue cockpit instruments with modern displays which narrows the gap between the instrument layout of the Hawk and F/A-18C/D Hornet (see Chapter 1.4). In the first phase, all 18 Mk.66s, seven Mk.51As, and one Mk.51 received the cockpit modification and were delivered to the FINAF by January 2018. Later, seven additional Mk.51s were modernised in 2016-2018 based on the refined Hawk life cycle plans and to compensate the loss of two already modernized Mk.66 aircraft. Thus, the 2019 fleet consists of 31 upgraded Hawks: 8 Mk.51s, 7 Mk.51As and 16 Mk.66s. They are expected to remain in service until the 2030s or beyond. [2]

Figure 7: *BAE Systems Hawk advanced jet trainer variants in the FINAF fleet (from left to right): Hawk Mk.51, Hawk Mk.51A, and Hawk Mk.66. Figure courtesy of the FINAF.*

The inherent fatigue tracking for each FINAF Hawk aircraft relies on counting g level exceedances and calculating a usage index i.e. Fatigue Index (FI) by the variant specific equations on a flight-by-flight basis. This method is adequate for monitoring the structural locations mainly influenced by aircraft normal acceleration (multiplied by weight). However, the current FI tracking does not take into account of buffet loading which is the main driver for the structural fatigue issues e.g. in the empennage of the Hawk aircraft. The Fatigue Index summary of the Finnish Hawk fleet is shown in **Figure 8**.
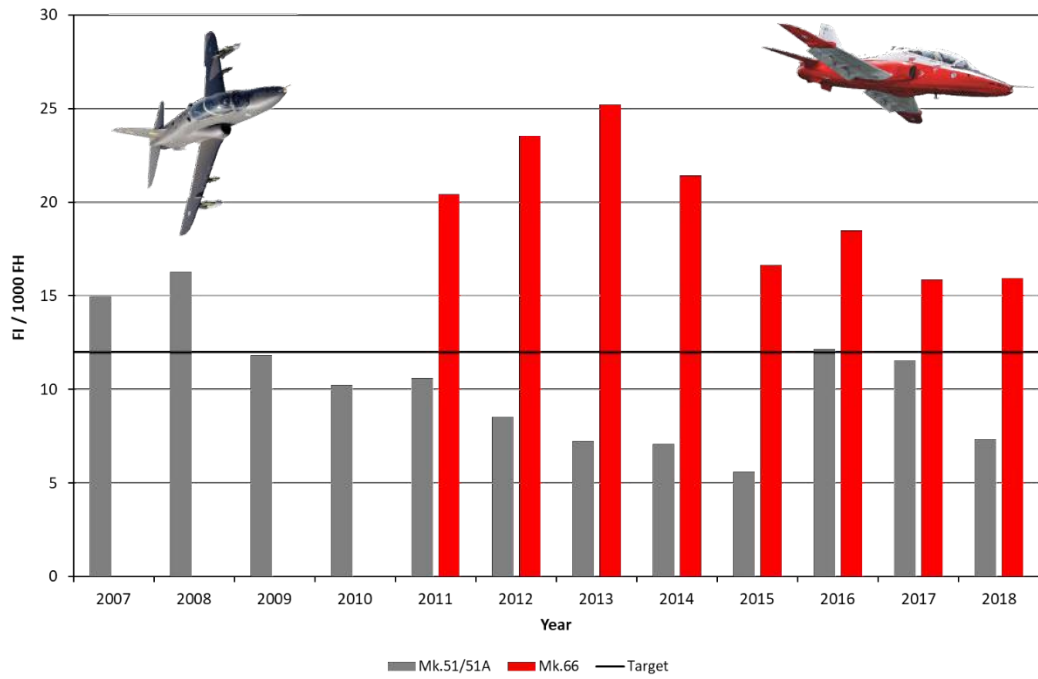
Figure 8: *Annual Fatigue Index (FI) development of the FINAF Hawk aircraft (Mk.51/51A in grey; Mk.66 in red) in the end of 2018. The annual target, average of all the types, is 12 FI/1000 FH. Figure courtesy of the FINAF.*

1.4   F/A-18C/D Hornet

The Boeing F/A-18C (single seat) and F/A-18D (two seat) Hornet are twin-engine, mid-wing, carrier-capable, multirole jet fighters (see **Figure 9**), that form the nucleus of the Finnish air defence. The late-production Lot 17 aircraft entered Finnish service in 1995-2000. The Finnish two-seaters were built in the United States by McDonnell Douglas which later merged with Boeing, while the single-seat aircraft were assembled at the Patria Aviation facility in Finland. The Hornet fleet of the FINAF consists of 62 aircraft: 55 C-models, and 7 D-models. [2]

It was recognized already in the initial stage of the Hornet program that technology of the 1990s would be obsolete way before the planned withdrawal date of the type, 2025-2030 time frame. Therefore, in order to keep the Hornet fleet at their highest level of performance, the fleet would be subjected to continuous and systematic development over its life cycle. The Hornet fleet's capabilities have been improved through midlife upgrades, and its relative performance will peak at the end of the 2010s. The partners in the upgrades were Boeing, Naval Air Systems Command as an upgrade design organization and equipment supplier, and Patria Aviation as a life cycle support service provider for the aircraft. The Finnish Hornets have undergone two mid-life upgrades, designated as Mid-Life Update 1 (MLU 1) and Mid-Life Update 2 (MLU 2) which were incorporated between 2006-2010, and 2012-2016 respectively.

Figure 9:   *Boeing F/A-18C Hornet multirole jet fighter. Figure courtesy of the FINAF.*

The focus in MLU 1 was to improve the Hornet's air-to-air capability. The aircraft were fitted with provisions for a helmet-mounted sighting system to improve close-range combat capability and the AIM-9X Sidewinder missile. [70]

The primary objective in MLU 2 was to enable the FINAF Hornets' air-to-surface capability by integrating various types of weapons, and self-protection, communication, navigation and information distributions systems which make the aircraft more interoperable in joint operations. Along with the MLU 2 upgrade, the FINAF Hornets have also gained the ability to perform air-to-ground operations. This will reflect on training programs and the use of the aircraft and thus, also the airframe stressing. The Finnish pilots are enabled to exercise the full potential of the Hornet in joint and combined operations with a wide range of air-to-air and air-to-ground capabilities.

Other significant MLU 2 upgrades were, for example, the cockpit upgrade with new displays and the BOL countermeasures dispensers. There are special arrangements to manage the C and D model differences between the USN and the FINAF in the MLU 2 induced configurations: The software testing will be done in Finland by the FINAFSAC ACC

(Satakunta Air Command, Air Combat Centre, Flight Test Section) and Patria Aviation's STIC laboratory (Software Test and Integration Centre). For the first time in the history of the Hornet, there is a foreign (Finnish) organization approved as a part of the approval process of the US software.

From structural point of view, the MLU 2 upgrade included structural strengthening and a purchase of Line Replaceable Units (LRU) and other spares to ensure the safe and reliable performance until the sundown of the aircraft type. All structural MLU 2 modifications were carried out by Patria Aviation, and the MLU 2 preparation work was done in cooperation with the Swiss Air Force. However, the combined effect of MLU 1 and MLU 2 will not extend the airframe's service life from late 2020s.

The FINAF Hornet fleet's fatigue tracking is currently based on: 1. Flight Hours (FH), 2. Wing Root Fatigue Life Expended (WR FLE) -value, and 3. T*-value (time spent in a buffet-dominating Point In The Sky, PITS) for the Vertical Tail [74]. Summary of the wing root fatigue life expended (WR FLE) of the FINAF F/A-18C/D fleet is presented in **Figure 10**.
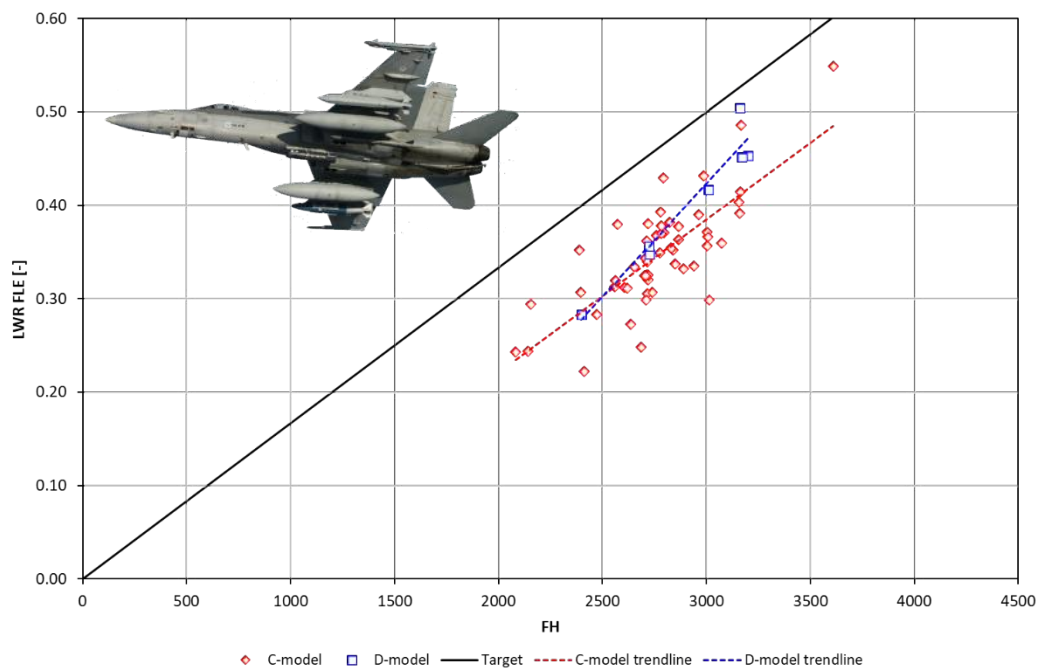
Figure 10: *Summary of the left wing root fatigue life expended (LWR FLE) of the FINAF F/A-18C/D fleet at the end of 2018. The data is from all 62 aircraft included [74]. The target is 4500 FH and 0.75 WR FLE simultaneously. Figure courtesy of the Joint Systems Centre.*

It is known, that the WR FLE is primarily dependent on the aircraft normal acceleration, so it does not provide useful fatigue information about the structural locations prone to the buffeting. As the Vertical Tail of the F/A-18 aircraft is typically buffeting-strained structure, a more useful usage index, developed by the international F/A-18A/B/C/D Hornet user's community, have been put into practice in the FINAF. A T* (T star) value indicates time spent in the PITS that contributes most of the fatigue damage for the Vertical Tail. Summary of the T*-values [h] of the FINAF F/A-18C/D fleet is presented in **Figure 11**. The interim limit for T* is 22 h.
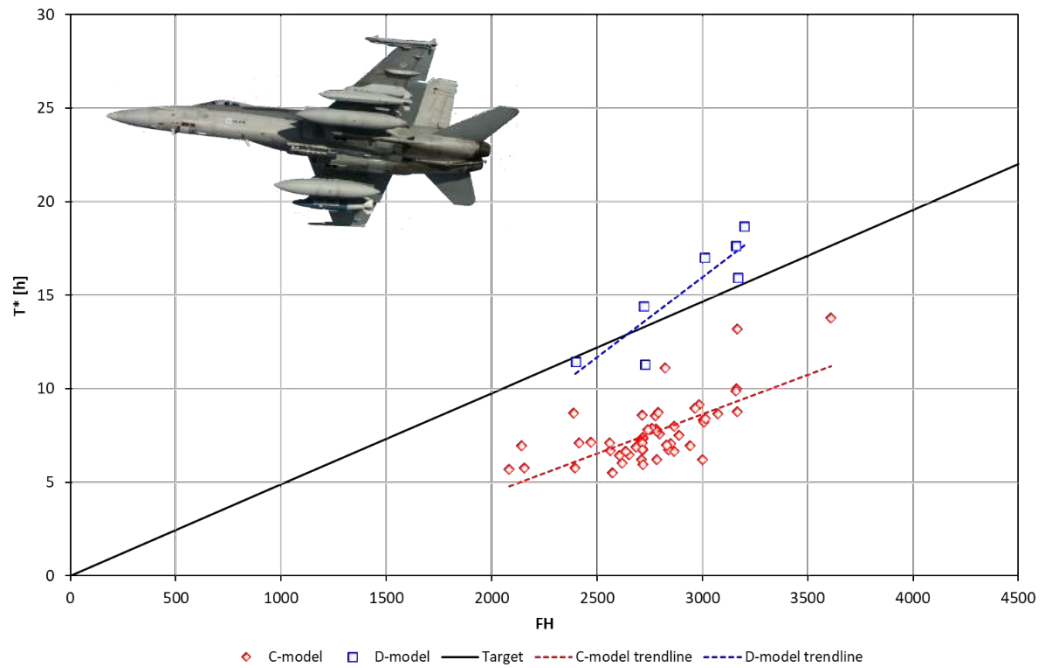
Figure 11: *Summary of the Vertical Tail fatigue tracking (T*-value) of the FINAF F/A-18C/D fleet at the end of 2018. The data is from all 62 aircraft included [74]. The interim target is 4500 FH and 22 T* FH simultaneously. Figure courtesy of the Joint Systems Centre.*

According to the structural analysis, and verified by the recorded measurement data from operational conditions, Finnish Hornets will reach their expected 4500 FH / 0.75 WR FLE service life without a need for further airframe work as planned.

There will be no post-MLU 2 upgrades; the Hornet will not be given any new capabilities. Only updates and modifications that are essential for the maintenance of flight safety and operational performance will be carried out. The Hornet is capable of accomplishing its operations safely and reliably until the mid-2020s. The decommissioning of the Hornet fleet will start in 2025. Phasing out the aircraft becomes a reality when they are about to reach their structural flight hour limits between 2025 and 2030. Then new multi-role fighters to be purchased through the HX Program will replace an obsolescent fleet (see Chapter 1.5). [2], [3]

1.5 HX Fighter Program

The planned service life of the Finnish F/A-18C/D Hornet fleet comes to an end by 2025–2030 as the aircraft reach the end of their 30 year service life. In parallel, the replaced capabilities must be phased in and be fully operational in service in 2030. There are three major factors that limit the service life of the fleet are [5], [6]:

1. Structural fatigue,

2. System support expires, and

3. Comparative operational capabilities are weakening.

The FINAF mission readiness requires flight training syllabi that include a great deal of air combat manoeuvring which stresses the structures of the aircraft – sometimes more than originally planned. Throughout the service history of the Hornet fleet the FINAF has been analysing its flight training syllabi with respect to structural life-limiting aspects and come to a conclusion that several structural modifications are required in order to achieve the targeted flight hours. The present service life model is based on an adjusted operations profile which together with structural modifications enables the Hornet fleet safe usage until 2030.

Extending the lifespan of the FINAF Hornet fleet into the 2030s, contrary to the present plans, would increase expenses in life-cycle management and increase the cost risks of system support. The relative capabilities of the Hornet fleet will degrade in the 2020s and the most significant degradation falls on its interdiction capability: the next generation multi-role fighters in Finland's neighborhood will technologically surpass the Hornet's capabilities. Extending its structural life and implementing a new, sizeable midlife upgrade would make it possible to delay the decision to replace the Hornet capabilities by five years, at most. It is estimated that the capability would be fully available no earlier than eight years after the financial decision is taken. As a result, substantial additional costs would be incurred in case of the service life of the Hornet fleet would be extended. This is neither a cost-effective solution nor would it be sufficient in terms of Finland's defence.

The aim of the HX Fighter Program is to replace the nationwide air defence capability of the Finnish Air Force F/A-18C/D fleet with the most cost-effective manner to Finland's state economy. This comprises a comprehensive solution that introduces a capable multi-role fighter. To rely solely on anti-aircraft weapons and/or unmanned aircraft is not a relevant option since both systems would only cover a part of the capabilities of the modern multi-role aircraft. [4], [5]

The capability, which will be created through the procurement, must be viable for at least 30 years, and it must be constantly sustained and developed. The HX Fighter Program will take about 10…15 years to complete as presented in **Figure 12**.
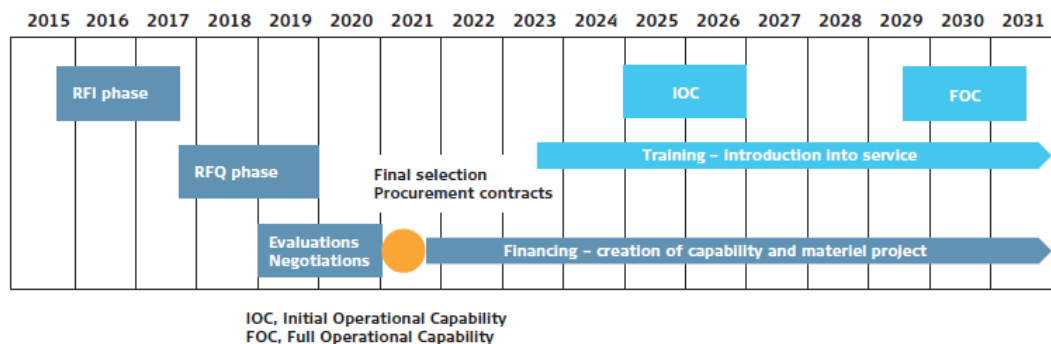
Figure 12: *HX programme schedule. RFI: Request for Information, RFQ: Request for Quotation, IOC: Initial Operational Capability, FOC: Full Operational Capability. [5]*

In April 2018, the Defence Forces sent a Request for Quotation (RFQ) to the governments of France, Great Britain, Sweden and the United States, to be forwarded to five manufacturers of multi-role fighters in these countries. The aircraft types in question are the Boeing F/A-18 Super Hornet (United States), Dassault Rafale (France), Eurofighter Typhoon (Great Britain), Lockheed Martin F-35 (United States) and Saab Gripen (Sweden). [7]

The deadline for submitting replies was set at the end of January 2019. The Defence Forces' Logistics Command received a preliminary RFQ for all five aircraft types. The replies contain binding information on the comprehensive solution and package, built around each multi-role fighter option; the aim is to create the best possible capability for Finland's defence system while replacing the Hornet fleet.

Apart from the 64 aircraft, the replies to invitations to tender contain technical systems needed for operating the aircraft, training systems, necessary maintenance tools, testing equipment and spare parts as well as weapons, sensors and other associated type-specific support functions. They may also include other supporting systems and capability elements.

The next phase after receiving the preliminary quotations is a content analysis that lasts several months. This is followed by the first phase of negotiations during which the quotations are further specified in cooperation with the manufacturers.

A more specific RFQ will be sent in the second half of 2019; this will be followed by the second phase of negotiations during which the content of procurement packages will be finalized. The second phase of negotiations will end in 2020; the manufacturers will then be requested to submit final tender documents i.e. their best and final offer (BAFO). The government will make the decision on the replacement of the Hornet fleet in 2021. The procurement will be the biggest arms trade in Finland's history. The projected cost of the program is EUR 7…10 billion. The timetable and phasing of the HX Program in 2018-2021 time frame is presented in **Figure 13**.
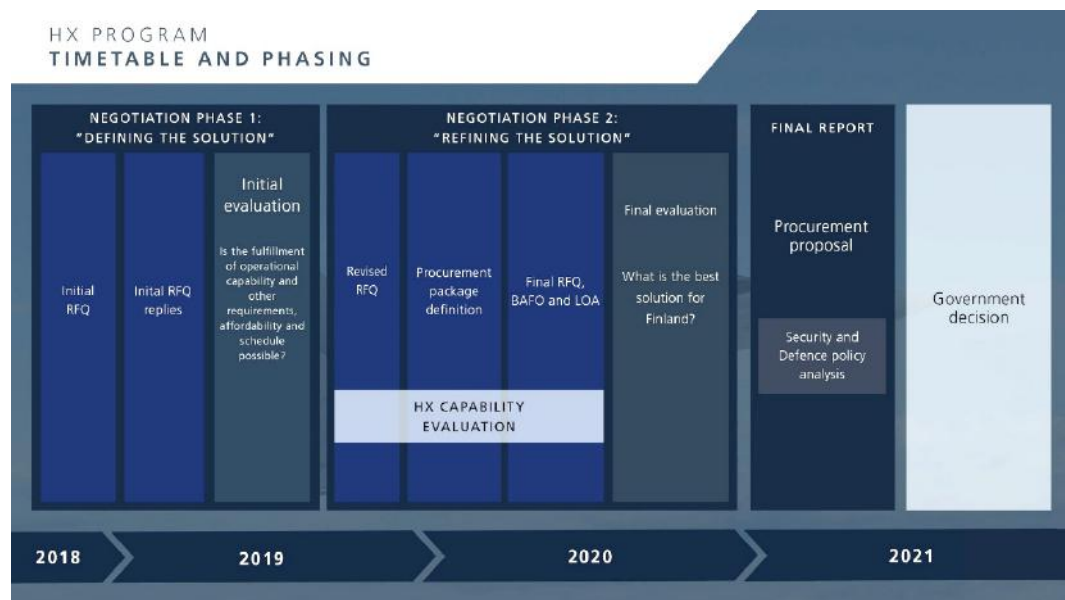
Figure 13: HX program, timetable and phasing in 2018-2021 time frame. The government decision on the replacement of the Hornet fleet will be made in 2021. Figure courtesy of Ministry of Defence.

1.6 Scope of the review

This national review on aeronautical fatigue concentrates on the fixed wing aircraft of the Finnish Air Force related to fighter aircraft and associated pilot training aircraft. The FINAF inventory includes: 62 F/A-18C/D Hornet fighters, 8 Hawk Mk.51, 7 Mk.51A and 16 Mk.66 jet trainers, 26 Valmet L-70 Vinka primary trainers, and 28 Grob G 115E primary trainers. By now, approx. 177 000 FH have been flown with the Hornets, 263 000 FH with the Hawks, and 186 000 FH with the Vinkas.

No FINAF aircraft of these type designations have been lost due to structural issues.

The severity of the Finnish usage in view of structural fatigue with the aircraft of noteworthy maneuvering capability (**Figure 8** (Hawk) and **Figure 10**, **Figure 11** (Hornet)) clearly demonstrates the need to maintain, further develop and apply concrete and systematic efforts to cope with the structural deterioration effects.

In 2005, the International Committee on Aeronautical Fatigue and Structural Integrity (ICAF) formally welcomed Finland as a full member of the ICAF, making Finland the 13th member nation. The 8th national review as a full member about aeronautical fatigue investigations in Finland April 2017 - March 2019 was compiled by Tomi Viitanen and Aslak Siljander (VTT).

The review comprises inputs from the organizations listed below (in alphabetical order):

Aalto	Aalto University, School of Engineering, Department of Mechanical Engineering, P. O. Box 11000, FI-00076 Aalto, Finland (https://www.aalto.fi/)
AFCOMFIN	Air Force Command Finland, Plans Division A5, Programmes Coordination Section, P. O. Box 30, FI-41161 Tikkakoski, Finland.
Elomatic/Finflo	Elomatic/Finflo, Vaisalantie 2, FI-02130 Espoo, Finland (https://www.elomatic.com/en/).
Emmecon	Emmecon Ltd, Tammitie 12, FI-53810 Lappeenranta, Finland (https://www.emmecon.fi/).
Eurofins ES	Eurofins Expert Services Oy, P. O. Box 47, FI-02151 Espoo, Finland (https://www.eurofins.fi/expertservices/)
FDFLOGCOM JSC	Finnish Defence Forces Logistics Command, Joint Systems Centre, P. O. Box 69, FI-33541 Tampere, Finland (*https://puolustusvoimat.fi/en/about-us/logistics-command*).
Patria	Patria Aviation Oy, Lentokonetehtaantie 3, FI-35600 Halli, Finland (http://www.patria.fi/).
TAU	Tampere University, Plastics and Elastomer Technology, FI-33014 Tampere, Finland (https://www.tuni.fi/en).
Trueflaw	Trueflaw Ltd, Tillinmäentie 3 Tila A113, FI-02330 Espoo, Finland (http://www.trueflaw.com/).
VTT	VTT Technical Research Centre of Finland Ltd. P. O. Box 1000, FI-02044 VTT, Finland (http://www.vtt.fi/?lang=en) + Trano Ltd. (VTT External)

2 Current activities: ASIMP 2017-2020

The Aircraft Structural Integrity Management Program (ASIMP) 2013-2016, as briefly outlined in [32], has been completed. The follow-on program, ASIMP 2017-2020 with its various sub-programs has been started and progressed according to the plans. An attempt is provided below to provide highlights of the ASIMP 2017-2020 achievements thus far.

2.1 Loads and stresses

2.1.1 Recent developments in helicopter flow simulations at Patria Aviation

In the ICAF 2017 report (Chapter 2.1.1 of Ref. [32]), recent helicopter CFD work related to modelling the flow field around NH90 fuselage was described. Three new versions of the helicopter model with open doors were then reported. Late in 2017, the model was further enhanced by a capability to add the heavy store carriers (HSC) and external fuel tanks attached to them [18]. The Chimera technique for the additions was applied, i.e. overset grids were utilized. The shape of the carriers is somewhat complicated, which required careful balancing of the grid resolution and omission of some details.

The new model version with just the HSCs and with the tanks attached was tested with the FINFLO flow solver in fast cruise with the doors closed. The solution for the full configuration is illustrated in **Figure 14**. The computations proceeded smoothly, but the flowfield remained mildly oscillatory because of the blunt carriers. The increase in the helicopter drag caused by the installation was noticeable, but the changes in the fuselage lift and pitching moment were small. At this stage, no reference results are available to assess the accuracy of the model.
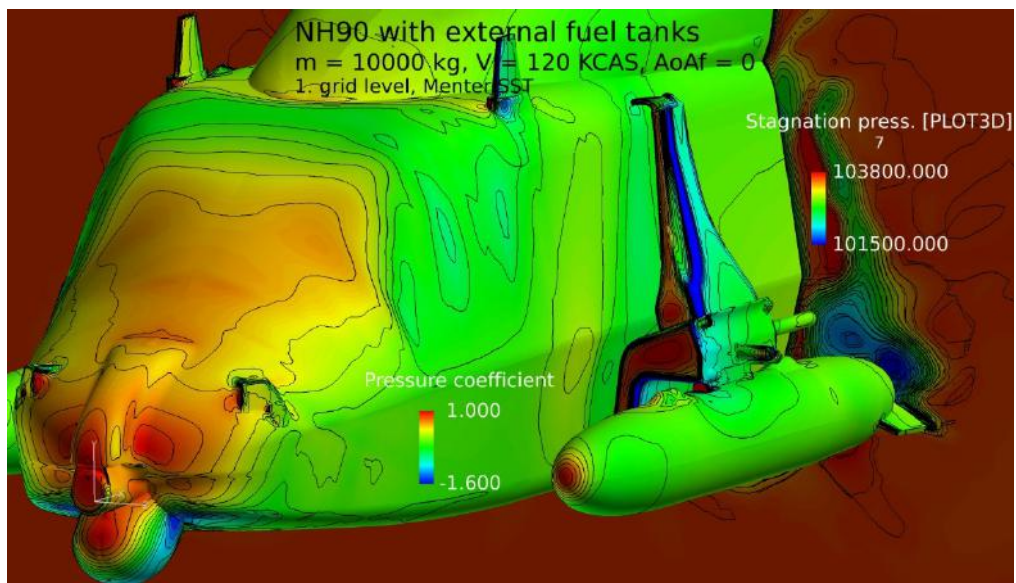
Figure 14: *Flow solution for NH90 with heavy store carriers and external fuel tanks as computed by FINFLO applying its current actuator disk rotor modelling. Figure courtesy of Patria Aviation.*

2.1.2 Enhancement of the Hawk Mk.66 flow simulation model

In the ICAF 2017 report (Chapter 2.1.2 of Ref. [32]), a completely new CFD model for BAe Hawk of the FINAF was described. The model was applied to predicting aerodynamic load distributions for the tailplane in different flight conditions to be utilized in a domestic fatigue test of the component. At that stage, the model only involved a movable tailplane but not movable ailerons, rudder or airbrake. Subsequently, the Hawk model was enhanced by adding the missing deflection capability of the control surfaces [19]. However, the flaps were still left as permanently retracted, because the critical structural loads for the aircraft tend to appear in the cruise configuration. The added features increased the overall grid cell count by about 6 per cent to 18.5 million, and the number of grid blocks grew by 9 per cent.

The surface grid on the left aircraft half with deflected control surfaces is illustrated in **Figure 15**. The ailerons and rudder modelled using overset grid blocks can be easily set to selected positions within their full movement range, but the airbrake must be either fully closed or the deflection must not be small. In the detail view on the right, the aileron actuator bulge on the wing lower surface can be seen, although its modelling is somewhat crude.
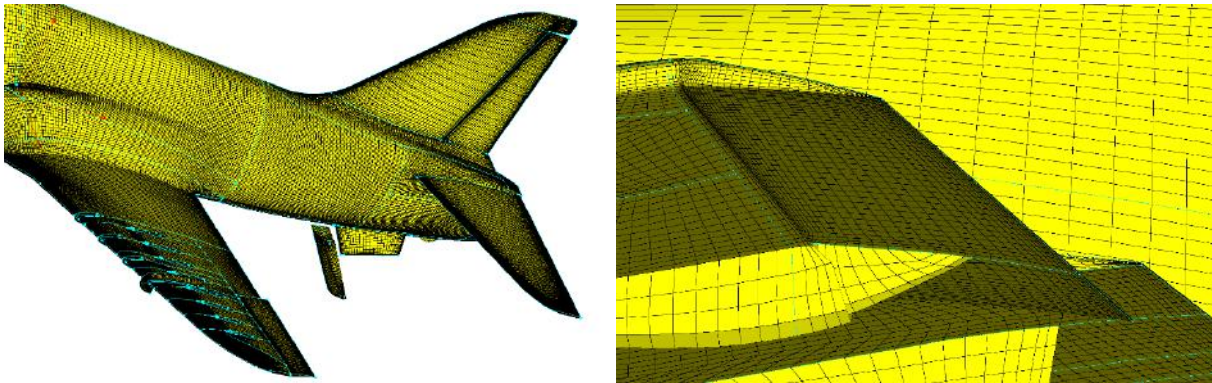
Figure 15: Surface grid of Hawk Mk.66 left side with deflected control surfaces and a detail of a fully deflected aileron. Figures courtesy of Patria Aviation.

An example of the results computed with the updated model using the FINFLO flow solver is shown in **Figure 16**, where the overall flow solution in a rapid steady roll is illustrated. The pressure coefficient on the aircraft surface, Mach number distributions at two chordwise planes and vertical flow velocity in the inertial reference frame below the aircraft are included. The ailerons are realistically deflected to their maxima, but the noticeable rudder deflection is actually unnecessary and applied only for the model testing purposes. Computations with the deflected airbrake were also performed without problems, and large-scale oscillations in the brake wake were obtained, as expected. Based on the test cases, the Hawk model enhancements work well, but the lack of reference data does not enable quantitative assessments.
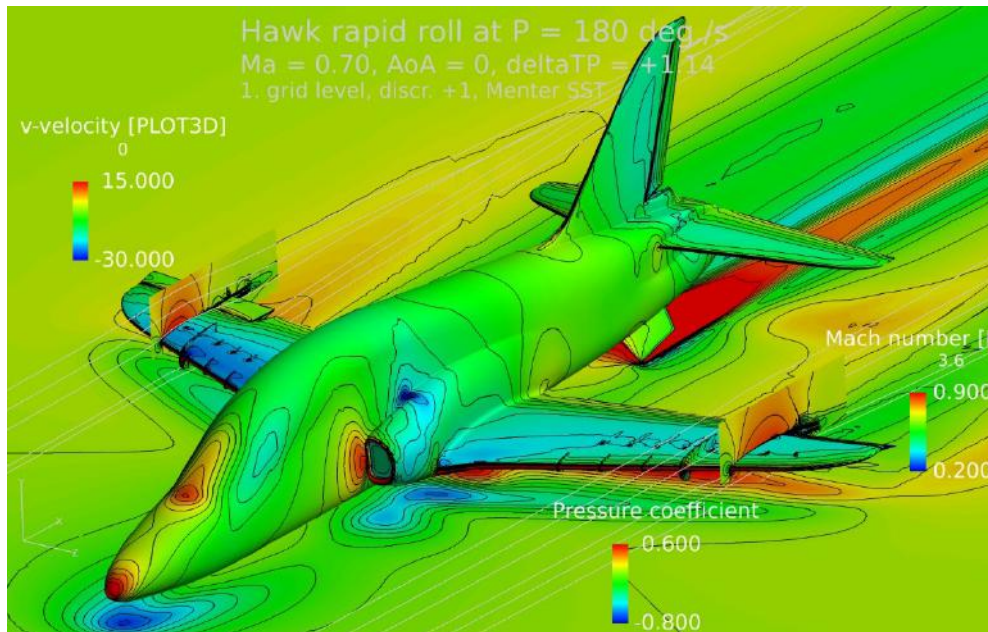
Figure 16: *Flow solution for the Hawk in a rapid roll to the right as computed by FINFLO. Figure courtesy of Patria Aviation.*

2.1.3 Aerodynamic limit load computations for the Hornet

Related to the aging of the Hornet fleet of the FINAF, structural limit load cases are to be studied to predict crack growth. To enable such studies, the aerodynamic limit load distributions for the whole aircraft in critical design load cases are required. The available Boeing (OEM) design documents contain partial distributions for several different load cases, but the information does not cover the whole aircraft. To complete the load distributions, a set of new CFD computations for the Hornet was recently performed [20]. The work was done in co-operation between Patria Aviation and Elomatic Ltd. that had bought Finflo Ltd.

For all the limit load computations with the FINFLO flow solver, the existing CFD grid generated by Finflo Oy was available. Just some minor adjustments were made to improve the robustness of the computations that involve some extreme flow features. The 13 load cases and flight conditions studied were selected on the basis of the available Boeing design documents. The cases included symmetric steady and unsteady situations as well as asymmetric maneuvers. However, the Boeing documentation did not include all the necessary definitions of the flight conditions needed in the CFD runs. To complete the input data for FINFLO, 6-DOF flight simulations had to be performed with an existing domestic software (e.g. Chapter 13.2.1.2 in Refs. [28], [30]) that models for example the operation of the actual Hornet flight control system and aeroelastic effects. When the appropriate design-case maneuvers were mimicked and the results were taken at proper short time periods, all the required parameters like the control surface deflections and prevailing aircraft angular rates were obtained.

At limit loads, the aeroelastic deformations of the Hornet wings and tail are noticeable and affect the aerodynamic load distributions markedly, which has to be taken into account. Therefore, many load cases for which the Boeing data did not contain all the relevant component load distributions were computed by FINFLO with periodic interactive calculations of the aeroelastic deformations by a global Nastran structural model. The CFD work was divided in such a manner that all the 8 steady-state symmetric cases were computed at Patria, and the unsteady and asymmetric cases were studied at Elomatic.

As an example of the computations performed at Patria, a transonic pull-up (at Ma≈0.85, α=5.53° and a nominal load factor of 7.5) is briefly described (see CFD collaboration

between Switzerland and Finland in Chapter 2.1.5 and **Figure 22** [82]). **Figure 17** shows the extent of the related aeroelastic deformations, where the final shape was reached via 8 iteration cycles with FINFLO and Nastran In **Figure 18**, the flow solution is illustrated. Even in this perspective, the wing bending can be seen. The surface pressure distribution contains typical steep gradients for a transonic case, and the flow separates partially downstream of the wing-fold hinge bulge.

In all the computed cases, the overall aerodynamic forces and moments of the aircraft could be compared with the nominal Boeing data. In general, the agreement was reasonably good, but not surprisingly, some discrepancies were also noticed. However, the evaluation of the load distributions remains limited because of incomplete reference data.
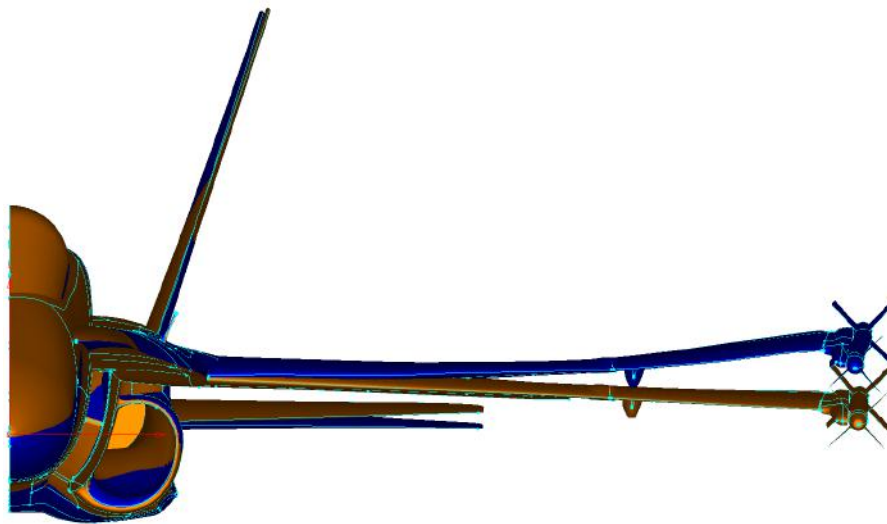
Figure 17: Surface grid shape of the Hornet in its nominal form (orange) and with converged static aeroelastic deformations (blue) in a symmetric steady pull-up case at the limit load factor. Figure courtesy of Patria Aviation.
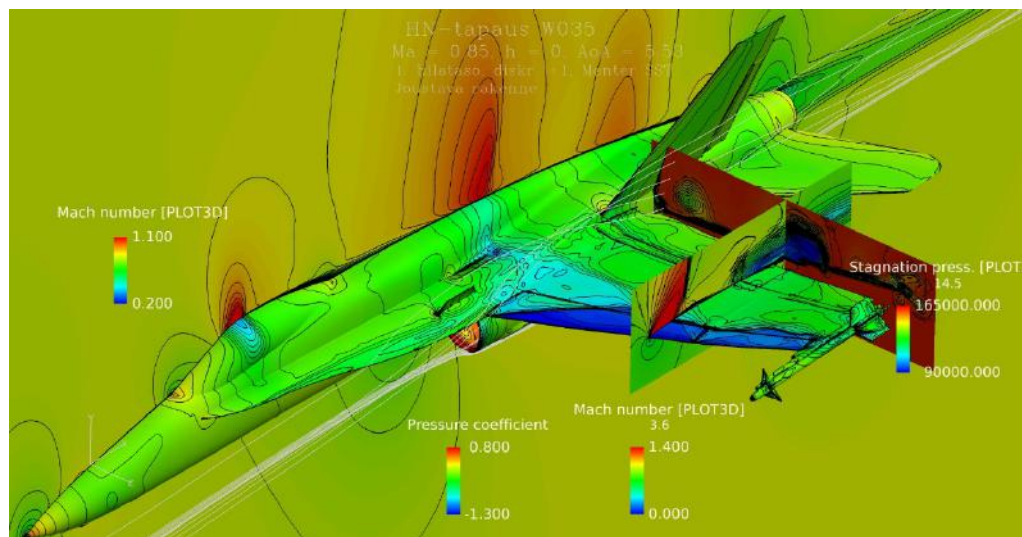
Figure 18: Flow solution for the Hornet in a symmetric steady pull-up case at the limit load factor as computed by FINFLO with aeroelastic deformations. Figure courtesy of Patria Aviation.

2.1.4 Aerodynamic modelling of Grob G115E and initial computations

Related to the domestic support of the Grob G115E fleet acquired by the FINAF from the UK, an aerodynamic model was created at Patria Aviation [21] based on 3-D scanned geometry of the aircraft. The idea is to be able to study the flight-mechanical characteristics of the type and to determine the aerodynamic structural loads and their distributions, as needs emerge.

The CFD model to be utilized by the FINFLO flow solver was to have movable control surfaces within their full deflection ranges and to cover the propeller slipstream effects. Actually, two versions of the model were generated. One version models just the left side of the aircraft without the propeller to efficiently perform symmetric studies without strong power effects. The second grid version for all kinds of studies covers the whole aircraft with the propeller modelled as an actuator disk. The full model contains 114 grid blocks, 38 of which are overset i.e. Chimera blocks to model the control surfaces, landing gear and the propeller disk. The overall cell count is about 17 million. The engine-bay inlet and outlet flows are modelled via through-flow boundary conditions.

The surface grid is illustrated in **Figure 19** with arbitrary control surface deflections. The flap and aileron actuating lever bulges and a blade antenna on the fin can be seen as modelled details, but small antennas and exhaust pipes are not included. The slightly asymmetric shape of the nose in front of the firewall and the skew propeller setting cannot be noticed in this kind of view.
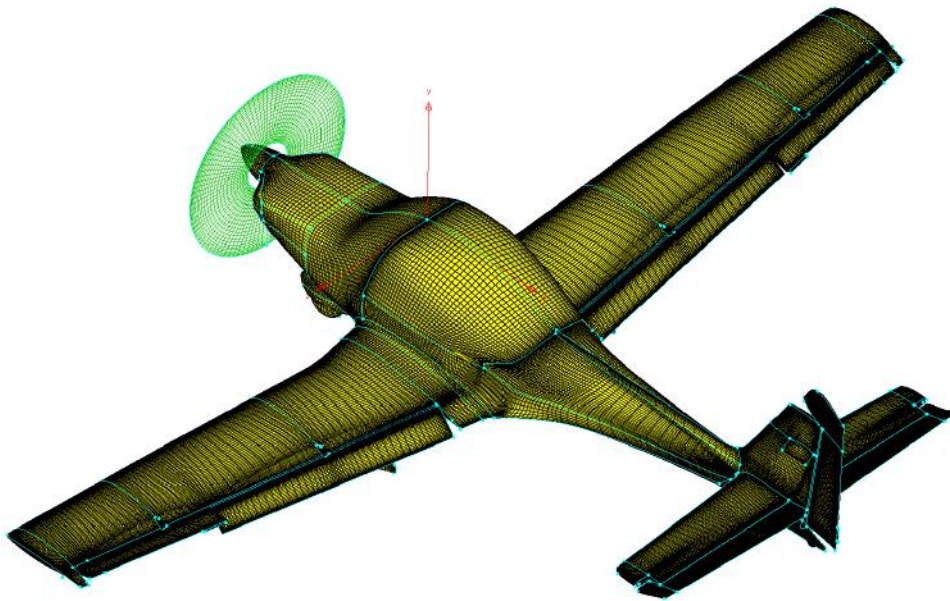
Figure 19: Surface grid of Grob G115E with deflected control surfaces and propeller actuator disk. Figure courtesy of Patria Aviation.

With the G115E CFD model, 20 steady-state flow cases were computed within the initial campaign. In all the cases, the flight Mach number was kept constant at 0.15, and the altitude corresponded to the sea level. Ten of the cases were computed with the symmetric half model, and ten were studied with the full model. In these cases, generally just one parameter was varied at the time, including the angles of attack and sideslip, control surface deflections, aircraft angular rates and engine power settings. The results provided an initial aerodynamic data package that was utilized to create a linear flight-mechanical model for the aircraft. Because of the low Mach number, a system for combining the basic computed aerodynamic load distributions via weighted superposition could also be crafted to quickly obtain realistic load distributions in desired flight conditions with moderate flow angles. For this special post-processing, different

combinations of inflow angles, control deflections, power settings, airspeeds, angular rates and centers of gravity can be defined via the flight-mechanical model.

As an example of the FINFLO computations, **Figure 20** illustrates the flow solution with moderate aileron deflections. All the other control surfaces are in their neutral positions, the nominal angle of attack is zero and there is no sideslip. The propeller operation corresponds to a low cruise power setting with mild slipstream effects. However, some asymmetry in the surface pressure distribution on the windscreen can be seen, and the vertical flow velocity distribution behind the wing around the fuselage is also asymmetric corresponding to the propeller rotation. Otherwise, the asymmetries are evident near the wing tip areas, where the aileron deflections modify the wing downwash.

In conclusion, the Grob G115E CFD model appears to work properly without apparent problems, but as in many other CFD applications, the lack of direct reference data hampers proper evaluations.
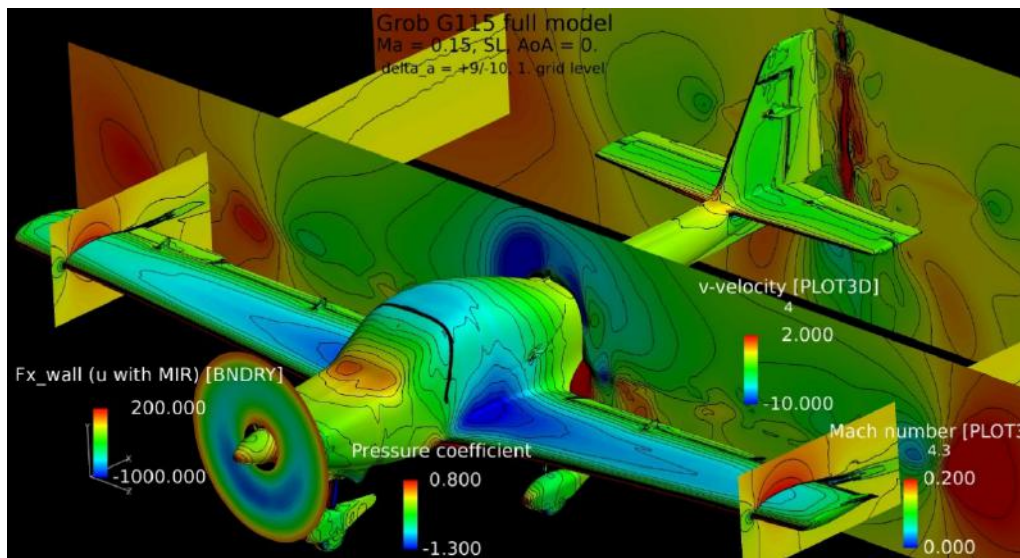
Figure 20: *Flow solution for the Grob G115E with aileron deflections as computed by FINFLO. Figure courtesy of Patria Aviation.*

2.1.5   Computational Fluid Dynamics at Finflo Ltd. and Elomatic Ltd.

Computational fluid dynamics (CFD) research at Finflo Ltd. is based on the in-house flow solver FINFLO. In September 2017, Elomatic Ltd. acquired Finflo Ltd. and inherited the CFD research made over the years at Finflo. Our research has been made in collaboration with Patria Aviation and VTT who also utilize the FINFLO solver.

In 2017 and 2018 time-accurate simulations of the F/A-18C aircraft were continued. The High Angle of Attack Research Vehicle (HARV) was used as a test case [8]. In the HARV case the aircraft is flying along a constant flight path with angle of attack α=30° and the Mach number is Ma=0.2755 (see **Figure 21**). Time-accurate simulations with different time-integration schemes (URANS, DES, and DDES) were performed and the results were compared to the flight test data and reference computations. The turbulence closure in the FINFLO simulations was the SST k-ω- model. It was found out that the grid resolution has a crucial impact on the results. Especially the DDES time-integration was vulnerable and the results changed dramatically when the grid density was changed. Pressure-difference data from two points on the vertical tail of the F/A-18C aircraft (ports 25 and 26) was transformed into a Power Spectral Density format (PSD). Results as a function of the Strouhal number are shown in **Figure 21** (bottom). The FINFLO results are compared to the reference simulation and the flight test data [67], [68]. The PSD transformation is not the same between the FINFLO and the reference results, thus the most important issue is to compare the shapes of the curves. As can be seen, FINFLO produces totally different results when the grid density is changed. On the densest grid in the FINFLO calculations the predicted PSD curves are close to the reference results. The coarser grid in our computations did not produce fluctuations in the pressure data. [33], [34]
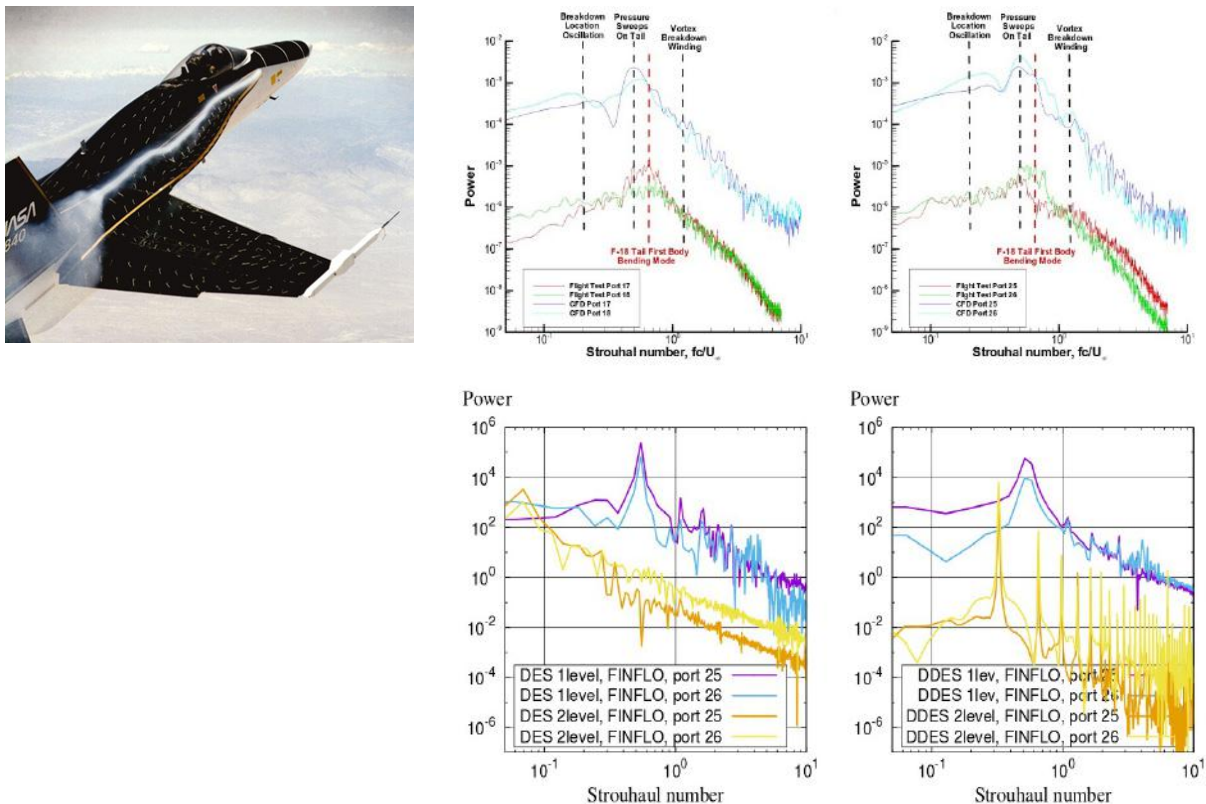
Figure 21: *NASA F-18 High Angle of Attack Research Vehicle (HARV) flight test (left) [8]. Power Spectral Density (PSD) comparisons between the reference results (top right), and the DES/DDES (bottom right). [67], [68]. Bottom figures courtesy of Elomatic/Finflo.*

CFD collaboration between Switzerland and Finland contains regular meetings of persons who work with the F/A-18C CFD models and develop the FINFLO and NSMB flow solvers.

The previous meeting was in Lucerne in 2017. In the year 2018, our collaboration resulted in a paper presented by Dr. Jan Vos at the 36th AIAA Applied Aerodynamics Conference in Atlanta [82]. For the Finnish part the research belonged to the Air Force project Management of the Aircraft Structures/Fluid-Structure Interaction (FSI). In this study, we compared the solutions obtained using the NSMB and FINFLO codes with and without FSI. To compute the flow solution two different grids were used, one generated in Switzerland and one in Finland. The grid topologies as well as the engine treatment are described by Vos et al. [82]. There are some differences between the grids. The Finnish grid includes the engine channel and the flow nozzle. Boundary conditions are applied on these surfaces to take into account the flow into and out of the engine. The Swiss CFD model does not have an engine, instead it considers flow through the engine duct. The volume grid resolution of the Swiss grid is higher than the resolution of the Finnish grid. The nominal first cell height of the Swiss grid is smaller but the cell height stretching is larger. The radius of the Swiss volume grid is about 250 m while the radius of the Finnish grid is about 500 m. For FSI the NSMB code has been coupled with a B2000+ solver and the FEM model used in this study was presented in detail by Vos et al. [83]. The Nastran BDF file of the F/A-18 FEM model was converted to the B2000++ format using an automatic conversion tool. The Finnish global FE model of the FINAF F/A-18C Hornet was developed at Patria Aviation by 2005. The model of the whole aircraft contains about 1.5 million DOFs and is applied within MSC Nastran 2012. The control surfaces can be set at desired deflections held in place with stiff rods modelling the actuators. A semi-automatic procedure is available for transferring the FINFLO-based load distributions onto the FE model.

The present case is a steady-state pull-up at Ma≈0.85, α=5.53° and a load factor of 7.5. The effect of different grids and turbulence models was studied by simulating the flow fields using the FINFLO code without FSI. Surface pressure coefficient distributions are shown in **Figure 22** (left) using both grids. It can be seen that the Swiss grid produces a bit more details inside the low-pressure area compared to the Finnish grid, but otherwise the overall results are very similar. Although not shown, the same concerns a comparison of results produced by different codes. However, when FSI is taken into account, there are differences as can be seen in **Figure 22** (right). The study revealed a clear need to develop FSI and that was considered to be a fruitful mutual research subject in the future.
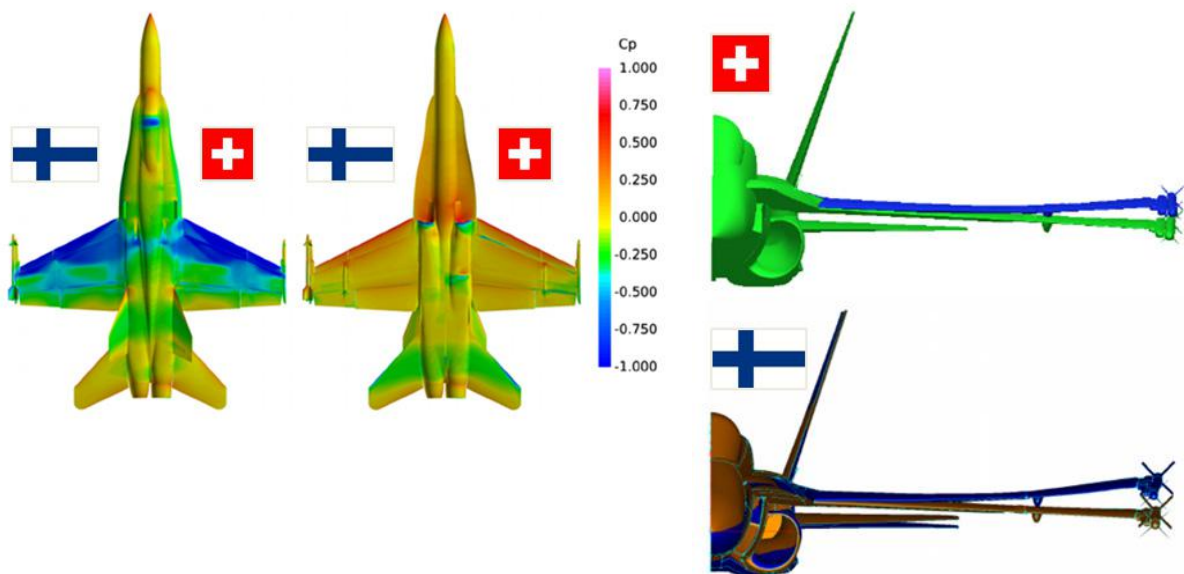
Figure 22: *Surface pressure coefficient distributions obtained using the FINFLO flow solver and the Swiss and Finnish grids (left). The Finnish grid solution on the left contains AIM-9M stores. Deformed and undeformed geometries as calculated by the NSMB-B2000++ coupling (top right), and the FINFLO-Nastran coupling (bottom right). Figures courtesy of Elomatic/Finflo.*

2.1.6 Hornet FE modeling - update

In the ICAF 2017 report (Chapter 2.1.4 of Ref. [32]), previous development phases of the global and detailed finite element (FE) modeling of the FINAF F/A-18C Hornet were outlined. Since then, new detailed FE models and crack initiation analyses based on the FINAF fleet usage representative FINAF BOS2 spectrum (Ref. [32], Chapter 2.2.5) have been prepared for the following structural locations: Bulkhead Y557.5 Vertical Tail Stub [57], Frame Y566 Vertical Tail Stub [58], Center Fuselage Dorsal Longeron area FS374-447 [69] and Aft Fuselage Upper Outboard Longeron area FS633-657 [77] (**Figure 23**). The Vertical Tail Stub locations were also added to parameter based fatigue tracking system (Chapter 2.2.2).
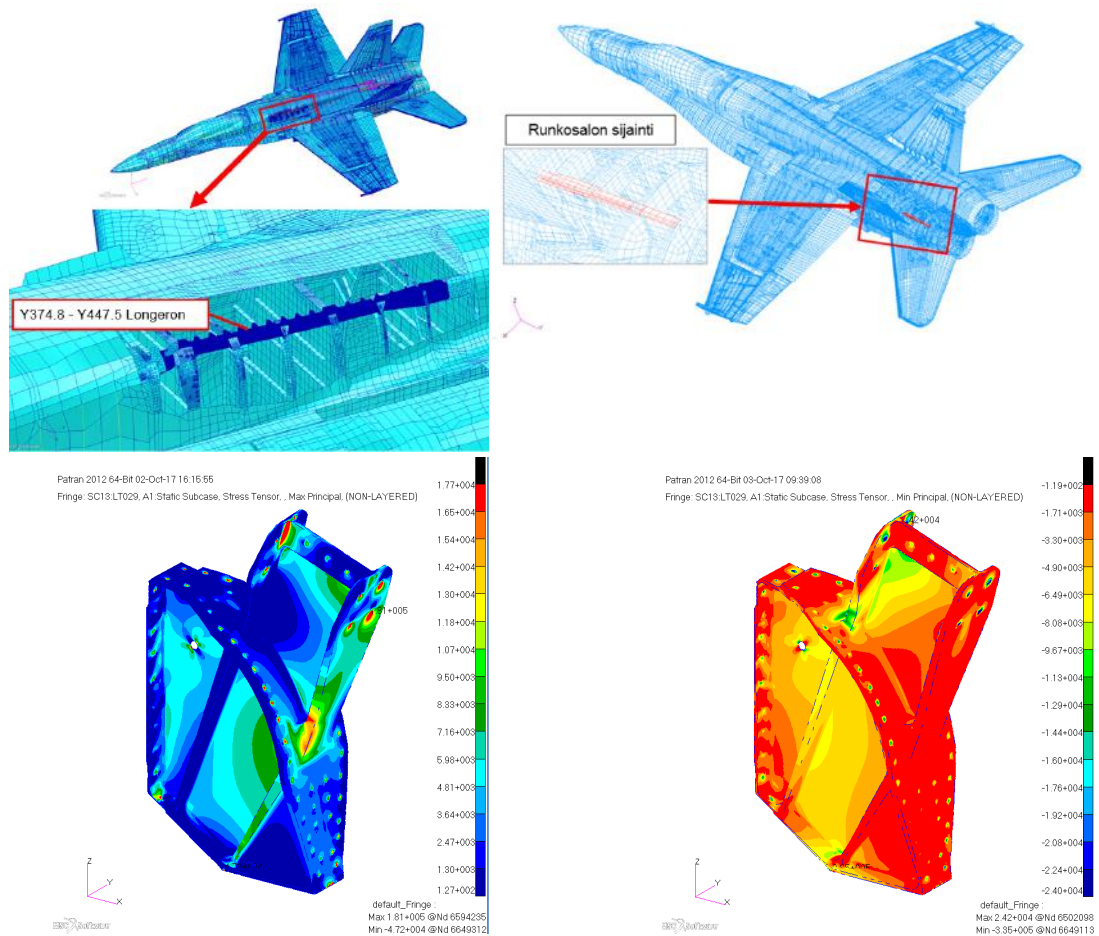
Figure 23: *Detailed FE models of Center Fuselage Dorsal Longeron FS374-447 (up, left), Aft Fuselage Upper Outboard Longeron FS633-657 (up, right), and results of the Vertical Tail Stub Y566 as maximum principal stresses (low, left) and minimum principal stresses (low, right) during 6 G Rolling Pull-Out maneuver. Figure courtesy of Patria Aviation.*

To enable prompt decisions about the required actions in case of possible crack findings in the structures of the aging FINAF Hornet fleet, critical crack sizes for the probable crack locations should be analyzed in advance. The highest loads occurring at these locations in service (i.e. appropriate Limit Load cases) should be applied in the analyses, and therefore aerodynamic loads for these load cases are needed in the FE analyses. A set of 13 OEM Limit Load cases was selected [22] taking into consideration coverage of the highest loads on different areas of the aircraft structure, availability of the initial conditions needed for the CFD analyses, and available OEM loads data and HOLM flight measurement data (Chapter 2.2.1) for comparison/validation. The CFD analyses for these load cases are presented in Chapter 2.1.3. The aerodynamic loads were transferred onto the global FE model and balanced load cases were built with appropriate aircraft inertia

properties and effects. Comparisons with corresponding OEM loads data and HOLM flight measurement data are currently going on.

2.2 Fatigue tracking systems

2.2.1 The FINAF HOLM aircraft in routine squadron service

The FINAF has routinely been running the Hornet Operational Loads Measurement (HOLM) program since 2006 [27]. The goal in this program is to quantify the effects of operational usage on the structure of the F/A-18 Hornet aircraft and thus support the national aircraft structural integrity efforts. The idea is that the recorded high fidelity structural response information from two extensively instrumented aircraft can be merged with data obtained from Neural Network (see Chapter 2.2.2) such that it will be possible to evaluate the structural life consumption of the whole Hornet fleet with adequate reliability. The HOLM program employs two Boeing F/A-18C Hornet aircraft (HN-416 and HN-432) with originally identical, but recently diverged onboard data acquisition systems and instrumentation (Ref. [32] Chapters 2.2.2, 2.2.4). In total, 44 strain sensors have been fitted on globally important locations as well as in the vicinity of structural locations addressed to be fatigue critical, and 4 accelerometers have been installed in top of the Vertical Tails. The optimized sampling rates of the strains vary from 1280 Hz in the highly vibrating structural locations (e.g. Vertical Tail) to 640 Hz elsewhere. The sampling rate of the accelerometers is 2560 Hz.

The Bootstrap area instrumentation (Chapter 2.2.4 of Ref. [32]) completed the HOLM on board system modifications, and currently there are no additional structural hot-spots to be monitored on the horizon. Bootstrap area instrumentation and mechanical ground calibrations have been summarized in Ref. [59].

The onboard HOLM instrumentation is periodically calibrated by VTT. The annual electrical calibrations of HN-416 and HN-432 reveals if any changes in the measuring chain have occurred or if the calibration coefficients need to be adjusted. Based on the calibration results, the quality of the system has remained outstanding: the quality of the strain signals is good and all the recordable strain data has been captured (minimal missing data). This all forms a solid base for all the analyses that are made based on the HOLM data. [62], [87]

To date, VTT has analyzed data from over 2800 recorded routine squadron flights of the two HOLM aircraft [95]. The extensively covered measurement data is utilized in in-country CFD [88] and FEA activities (see Chapter 2.1), but also as a part of the international F/A-18 cooperation (FISIF): the FINAF have assigned VTT to prepare HOLM data sets i.e. specific collections of measured data excluding the fatigue analysis results that have been supplied to the FISIF partners and to be used as they see fit. Time frame of this National Review covers four different data sets with various contents and their revisions that have been prepared and delivered to the FINAF. [89], [90], [91], [92], [94]

Since the previous National Review, there are neither new nor updated transfer functions within the HOLM damage analysis system at VTT. The HOLM ground analysis environment is now up to date, but is expecting some updated Bootstrap area transfer functions later to be implemented to the system (Ref. [32] Chapter 2.2.4). Current strain life analysis consists of 13 different structural areas including 39 separate transfer functions and fatigue critical locations.

Within the implementation process, almost all of these critical locations benefit from the specific Basic Operational Spectrum ver 2 (BOS2) flight set (Ref. [32] Chapter 2.2.5). This predefined data can be used e.g. to calculate preliminary and indicative fatigue lives prior to the actual flight-specific fatigue analyses including typically all the recorded flights.

In addition to the strain life method, the stress life analysis is also used, but directly at the strain gage instrumentation locations [48]. To achieve more usable results in the future, the commissioning of the damage tolerance analysis methods is ongoing [84].

The HOLM fatigue analysis database has been updated. The database works seamlessly with the data from the HOLM ground analysis environment. In addition to data from the fatigue tracking system the database includes all the needed information from the data analysis process. [93]

2.2.2 Parameter based fatigue life analysis - update

The parameter based fatigue life analysis is an individual aircraft fatigue life monitoring system developed for the FINAF F/A-18 Hornet fleet by Patria Aviation. The analysis utilizes inherently recorded flight parameter (Memory Unit) data, by standard aircraft systems, and created artificial neural networks (ANN) to model strain histories, and further, from which to produce flight-specific damage estimates for the fatigue critical structural locations. The technical background of the analysis is comprehensively explained in Ref. [79].

The ANN – on the basis of extensive HOLM data (Chapter 2.2.1) – enhances the nominal aircraft fatigue tracking in the fleet. For example, it enables the fleet to be sorted in FLE order (ascending/descending) for scheduled repairs, inspections, and structural part replacements. The method is schematically illustrated in **Figure 24.**
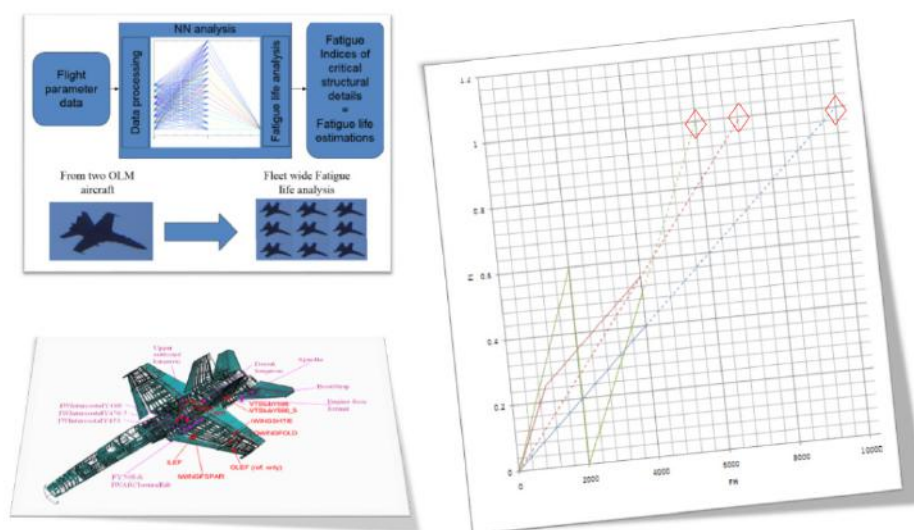
Figure 24: *Schematic of the applied monitoring method. Figure courtesy of Patria Aviation.*

Previous development phases of the parameter based fatigue life analysis system have been presented in Ref. [32], Chapter 2.2.6. A presentation of the usage and experiences of the monitoring method for the FINAF fleet management can be found in the ICAF 2015 Symposium presentation, Ref. [80]. The fatigue damage estimates are currently calculated for 19 structural locations, each consisting of 1-3 details (e.g. 1-3 fastener holes in the same structure).

Since ICAF 2017 [32], the coverage of the Parameter based analysis has been improved by running the analysis for the FINAF F/A-18 fleet flights between 2015-2016, so the analysis now covers flights for years 2000-2016. Also, two new vertical tail (VT) locations have been added to the system: VT Stub Y557.5 and VT Stub Y566. Monitoring of these locations is based on HOLM strain gage S35a data installed on VT Stub Y557.5. Training and analysis capability of the neural network for the strain sensor S35a is presented in [66]. The response of this strain gage was a difficult target to model and the fatigue analysis capability of its neural network is poor when compared to other locations.

2.2.3 Research efforts towards Hawk structural integrity management

The FINAF flight training syllabi have changed significantly in the last years. For example, glass cockpit modification (see Chapter 1.3) enables practising some training flights with the Hawk aircraft which earlier were flown solely by the Hornet. These changes may reduce the life of some critical structural components or locations well known from the older FINAF Hawk Mk.51/51A fleet.

The inherent fatigue tracking system for each FINAF Hawk aircraft is based on counting g level exceedances and calculating a usage index i.e. Fatigue Index (FI) by the variant specific equations. This method is adequate for monitoring the structural locations mainly influenced by aircraft normal acceleration (multiplied by weight). However, current FI tracking does not take buffet loading into account which is the main driver for the structural fatigue issues e.g. in the empennage of the Hawk aircraft.

2.2.3.1 Hawk Mk.66 mini OLM program completed

The FINAF Hawk Mk.66 mini OLM (Operational Loads Measurement) activities, as a collaboration of the FINAF, Patria Aviation, and VTT, were highlighted in the ICAF 2015 report (Chapter 13.2.2.3.2 of Ref. [31]) and in the ICAF 2017 report (Chapter 2.2.7.1 of Ref. [32]). In spring 2015 one Mk.66 jet trainer (HW-368) was equipped with a small-scale onboard system by VTT and Patria Aviation. The purpose of the temporary instrumentation consisting of ten strain gauges was to provide information about structural loads in different flight conditions, and to provide data for the creation of an average usage spectrum of the FINAF's later Hawk fleet. Also initial data for neural network development and training (Chapter 2.2.3.2) was obtained.

In the first phase a total of 14 test flights were successfully flown and analysed. Based on good experience, the FINAF decided to proceed collecting the structural response data on the instrumented Hawk Mk.66 aircraft. The mini OLM program continued until the end of year 2017. The mini OLM installation of HW-368 will soon be dismantled such that the onboard strain gauge instrumentation will stay intact but the DAU of the system will be adopted for other acute purposes. To date, number of recorded and analysed HW-368 mini OLM flights is approx. 350. Thus far the recorded data has been utilised e.g. to create the fatigue spectrum for the Hawk tailplane fatigue tests (Chapter 2.3.4), and in the Mk.66 tail neural network training (Chapter 2.2.3.2). [44], [61], [78], [85]

2.2.3.2 Hawk Structural Health Monitoring (SHM) update

Initial activities related to the Structural Health Monitoring (SHM) investigations for the FINAF Hawks were highlighted in the ICAF 2017 report (Chapter 2.2.7.2 of Ref. [32]). In the future the structural integrity of the FINAF Hawks' tail will be tracked by a neural network application which gets as input flight parameter data recorded by the mission data recorder from each individual aircraft. The measured strain data from the specifically instrumented aircraft is also needed in the neural network training and tracking phases. The onboard instrumentation consists of five strain sensors of which three are/were installed on the tailplane (**Figure 25**), one in the fin root, and one in the fuselage top longeron, left-hand side. The fuselage measurement point is highly influenced by the aircraft g-loads, and is therefore used for synchronising the strain gauge data with the flight parameter data.
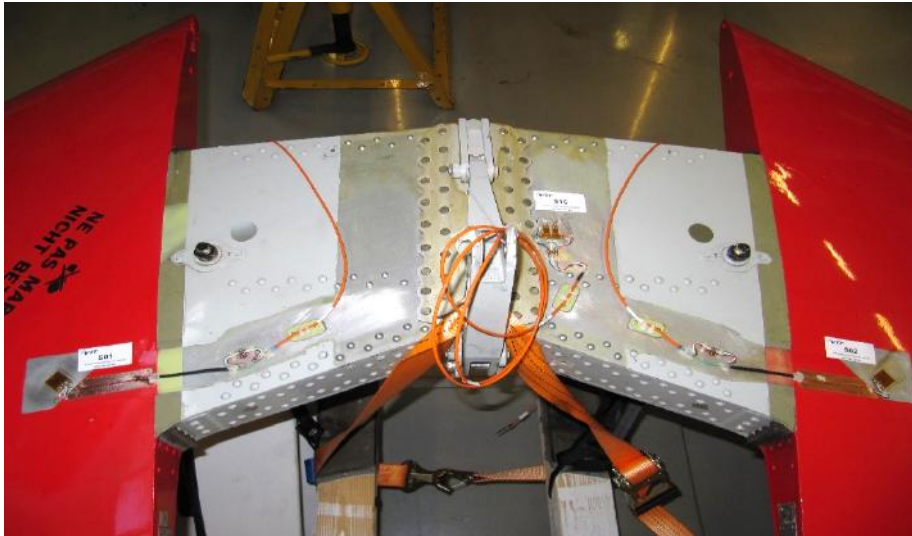
Figure 25: *Instrumented tailplane of the Hawk Mk.66 (HW-361), prior to applying wear protection.* *[64] Figure courtesy of VTT.*

Along with the instrumentation, the Hawk Mk.66's obsolete ESDA (Electronic Structural Data Acquisition) onboard monitoring system was replaced by Emmecon's Data Acquisition Unit (**Figure 26**) which has an ability not only to measure and store turning points of the strain signals but also to process the obtained stress data and store it in a Rainflow matrix form in a flight-by-flight basis. The stored Rainflow data can then be downloaded with a laptop computer during aircraft maintenance.
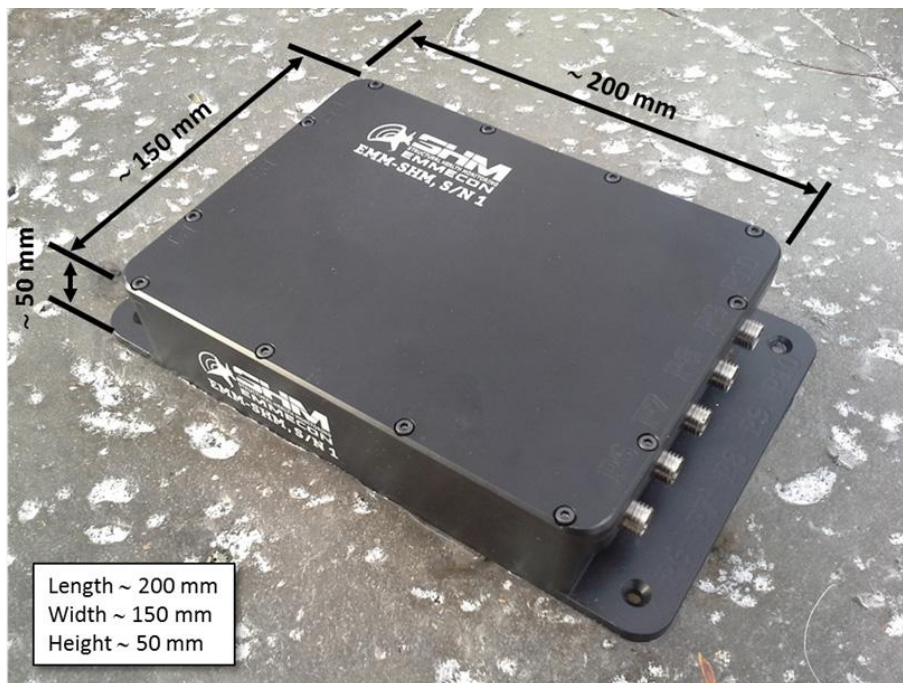
Figure 26: *An overview of Emmecon's onboard SHM system. Figure courtesy of Emmecon.*

The first EMM-SHM monitoring unit was installed to the FINAF Hawk Mk.66 aircraft HW-360 in autumn 2016. Until March 2019 altogether three Hawk Mk.66s and one Mk.51 were instrumented and equipped with Emmecon's EMM-SHM units. One more aircraft, Mk.51A, will be instrumented during spring 2019. Summary of recent instrumentations for the Hawk aircraft is presented in **Table 1**. [60], [61],[63], [64], [65]

Table 1: *Summary of instrumentations contributing Structural Health Monitoring for the FINAF Hawk aircraft. Strains: number of strain measurement channels, DAU: Data Acquisition Unit.*

Project	A/C Type	TailNo	Strains	DAU	Completed
HW mini OLM	Mk.66	HW-368	10	ACRA KAM-500	03/2015
HW SHM	Mk.66	HW-360	5	EMM-SHM	10/2016
HW SHM	Mk.51	HW-344	5	EMM-SHM	05/2018
HW SHM	Mk.66	HW-361	5	EMM-SHM	09/2018
HW SHM	Mk.66	HW-367	5	EMM-SHM	09/2018
HW SHM	Mk.51A	HW-355	5	EMM-SHM	ongoing

At the time of writing the review the neural network processing based on approximately 300 HW-368 mini OLM flights is under way and fatigue indices of the tail for each FINAF Hawk aircraft will be calculated by June 2019. The first neural network based on data acquired from the five aircraft with the EMM-SHM system is planned to be created until the end of the year 2019. Eventually, the FINAF Hawk's empennage will be monitored solely by the neural network based fatigue indices. As the mini OLM installation of the HW-368 will soon be dismantled, the SHM aircraft will remain as the only data source for the FINAF Hawk neural network.

2.3 Structural integrity of metallic materials

2.3.1 FINAF F/A-18C/D Hornet Structural Modifications

The FINAF F/A-18C/D Hornet fleet structural integrity is managed using an Aircraft Structural Integrity Program (ASIP) which is based on MIL-STD-1530 standard. To achieve the usage life target, several structural modifications must be done. The first Structural Refurbishment Program (SRP1) including 29 modifications was performed between years 2009-2014. Later the SRP1 was supplemented with 11 additional modifications and the new program was nominated as SRP1+ which started 2015 and is currently being performed to the last jets in the modification line. The SRP1 and SRP1+ modifications have been typical crack preventive modifications which have been performed before reaching analytical Crack Initiation (CI) life. The responsible for ASIP management, modification analysis and modification design has been Patria Aviation delegated by the FINAF.

Based on the ASIP group work, more modifications are needed for the F/A-18 fleet safe usage up to 2030. The Structure Sustainment Program (SSP) was established during years 2014-2016. The SSP includes 40 modifications, 17 On Condition repairs and almost 100 new inspections. At the moment, the modification line is in full production in Patria Aviation's facilities. The whole fleet will be in the SSP configuration at the end of 2021.

Typical for the SSP-modifications is that CI-life for the fatigue critical structural location has been reached before modification. That naturally causes some crack indications and leads to deeper material removals and larger oversize fastener installations than what has been done during the SRP1/1+. The Confidence Cut policy will be obeyed and because of that, Probability of Detection (POD) study (Ref. Chapter 2.3.3) for typical SSP flaws has been performed in collaboration with Patria Aviation, VTT, RUAG, FINAF and Trueflaw. The overview of the SRP1, SRP1+ and SSP modification locations is presented in **Figure 27** and **Figure 28**. [23], [42]
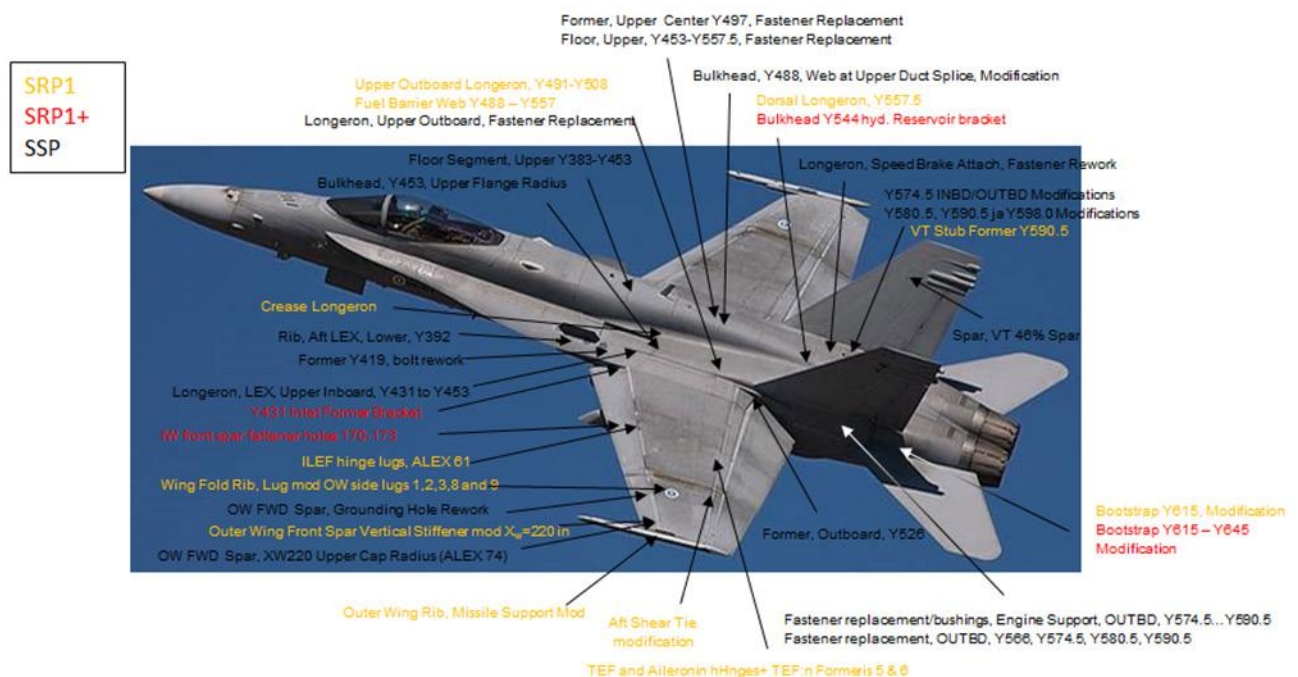
Figure 27: *The overview of the SRP1, SRP1+ and SSP modification locations. Figure courtesy of Patria Aviation.*
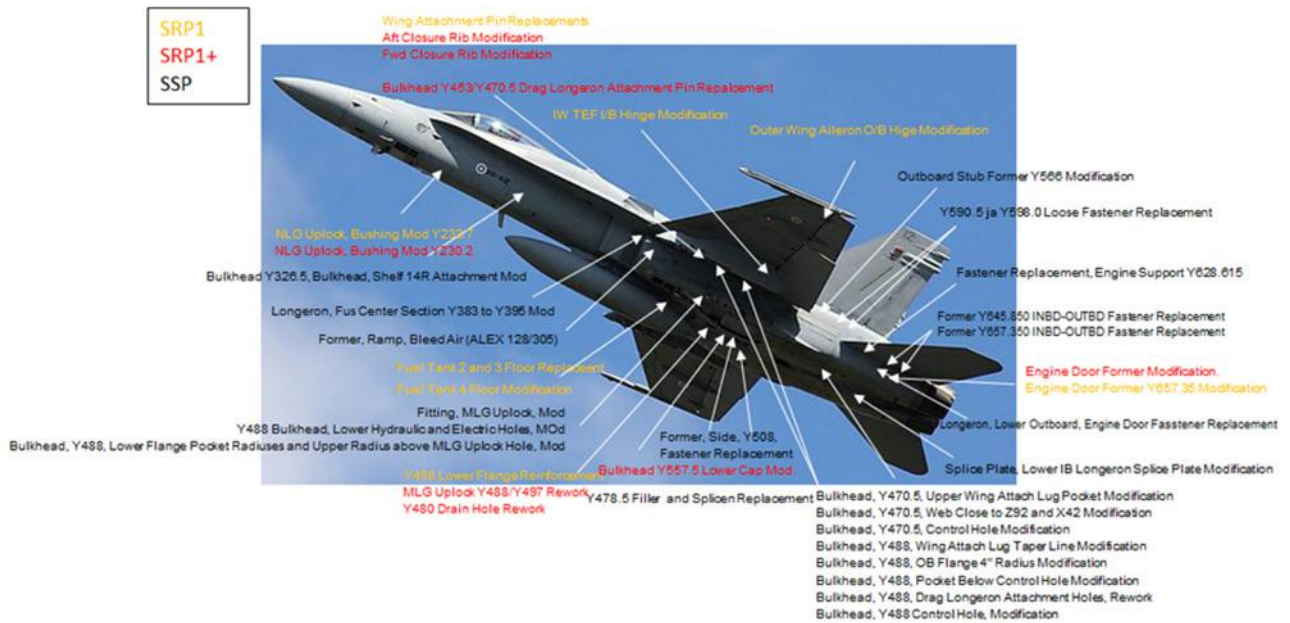
Figure 28: *The overview of the SRP1, SRP1+ and SSP modification locations. Figure courtesy of Patria Aviation.*

2.3.2 Study of small cracks growth

The growth of small cracks have been studied experimentally by fatigue tests. The objective was to find out the effect of different load spectrums, various surface working methods, and fastener hole tolerances and preparation methods on small crack growth. Test matrix included two kinds of test specimens: dogbone type specimens with shoulders in test section, and double lap shear joint specimens as presented in **Figure 29**. [86]

(a)

(b)
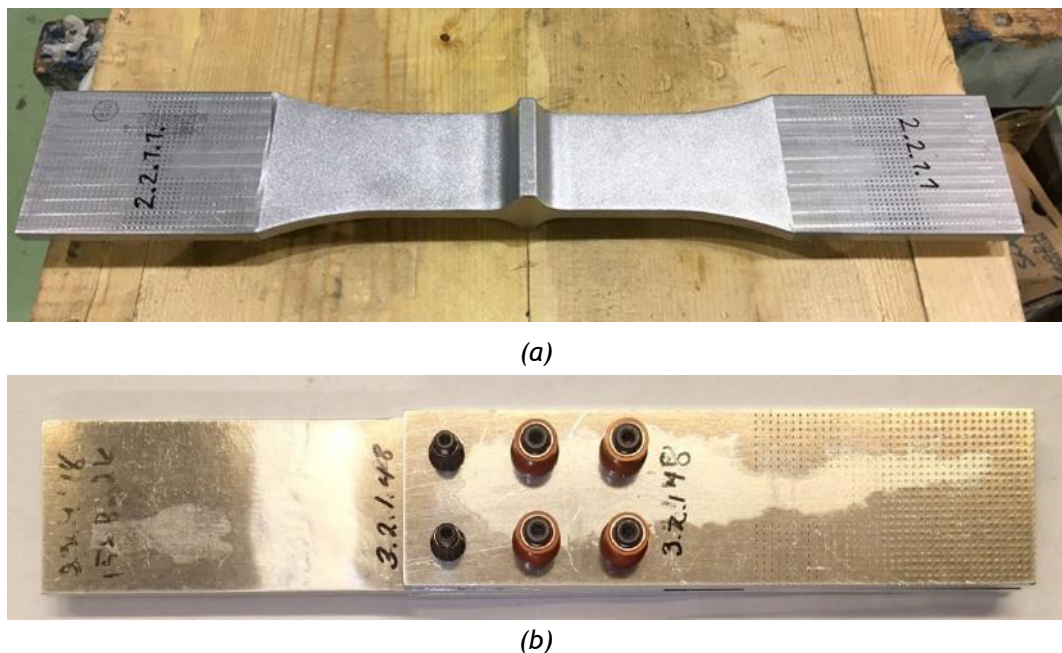
Figure 29: *Test specimens in the study of small crack growth: dogbone specimen with shoulders (a), modified double lap shear joint specimen (b). Figure courtesy of Patria Aviation.*

The dogbone specimens were made of 6 mm thick 7050-T7451 aluminium alloy and were chromic acid anodized, mimicking the OEM's production pre-IVD (Ion Vapor Deposition, corrosion preventive) process. It is known, that this chemical etching process weakens the fatigue properties of basic material because resulting etch pits serve as potential sources for the crack initiation.

The double lap shear joint specimens were made of á 4 mm thick 7075-T76 aluminium alloy. The number of fasteners per specimen was six, and applied fittings were: Class 2 fit, Interference fit, and cold working + Class 2 fit.

The specimens were loaded with three different F/A-18 wing root bending moment (WRBM) spectra until failure. The effect of different life improvement modifications on the fatigue life of the material were studied. The methods were: shot peening, polishing and reaming of the fastener holes. The effect of the three different fastener hole fittings together with the oversize hole modification were also tested on the double shear lap joint specimens. The implementation of the life improvement modifications took place after certain pre-cycling i.e. at various percentages of the average lifetime of the specimen and spectrum in question. After the modifications, all the specimens were cycled until fracture.

The quantitative fractography (QF) was carried out to some of the specimens in order to determine the small crack growth rates. The fracture surfaces were investigated in more detail with a scanning electron microscope (SEM). The applied load spectra included so called markers whose function was to improve the tracking of the crack growth. The crack growth was determined along one track per one fracture surface (**Figure 30**). The chosen track represented crack growth from a crack initiation point to deepest point of the presumed main crack.
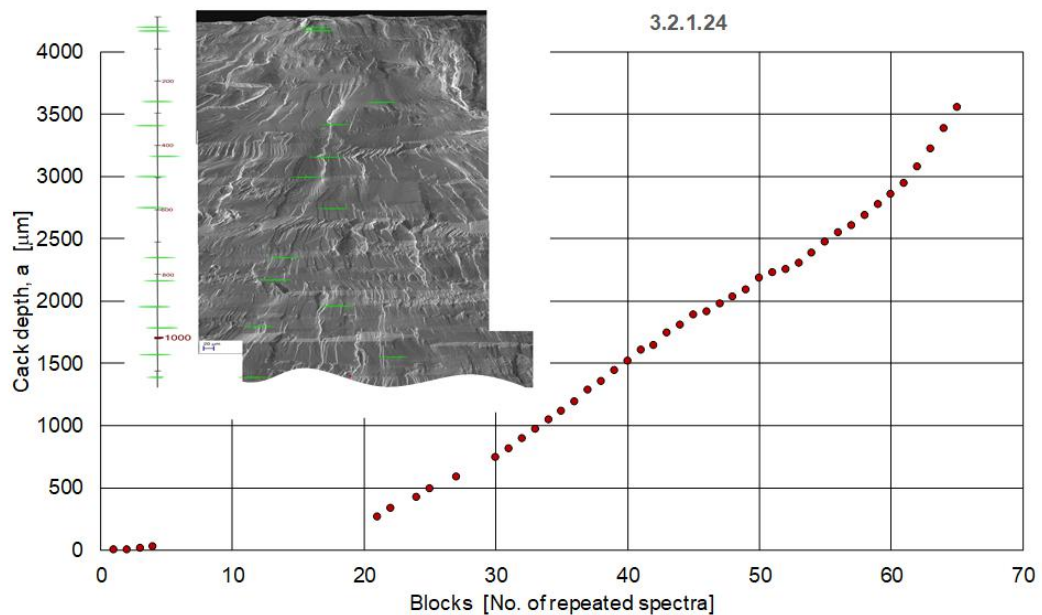
Figure 30: *A crack growth curve of a double shear lap joint specimen based on the fracture surface examination. Figure courtesy of VTT.*

As the fatigue tests are still ongoing, some of the results are not yet available, and the conclusions will be drawn later.

2.3.3 Probability of Detection in Non-Destructive Testing - Update

Non-Destructive Inspection (NDI) has evolved as a key element to monitor the integrity of structural components, especially in the age of Damage Tolerance. Along the inspection technology development it has emerged essential to quantify the reliability or performance of the used NDI method. Therefore a statistical concept called Probability of Detection (POD) has been developed.

In the ICAF 2017 Symposium (Ref. [76]), and national review (Chapter 2.3.2 of Ref. [32]), Patria's first experiences of POD using Eddy Current were presented. When inspecting holes with a rotating probe, the results showed that the performance was in the desired level. However, when inspecting surface cracks with a pencil probe, the performance was not as expected. Because of this, corrective actions have been introduced. To show their effectivity a new set of test specimens was needed as the earlier specimens were on loan and not available any more.

Using FINAF funding Patria manufactured a new specimen set – designed by RUAG Aviation - and cycled it together with VTT (**Figure 31**, **Figure 32**, **Figure 33**). As expected, producing well distributed cracks was challenging. However, the result was a good set of reusable specimens. At present the final preparations for the POD test are going on and the tests will be done in the near future. [13], [51]

Figure 31: POD test specimen under cycling in the universal test machine. Figure courtesy of VTT.

(a) *(b)*
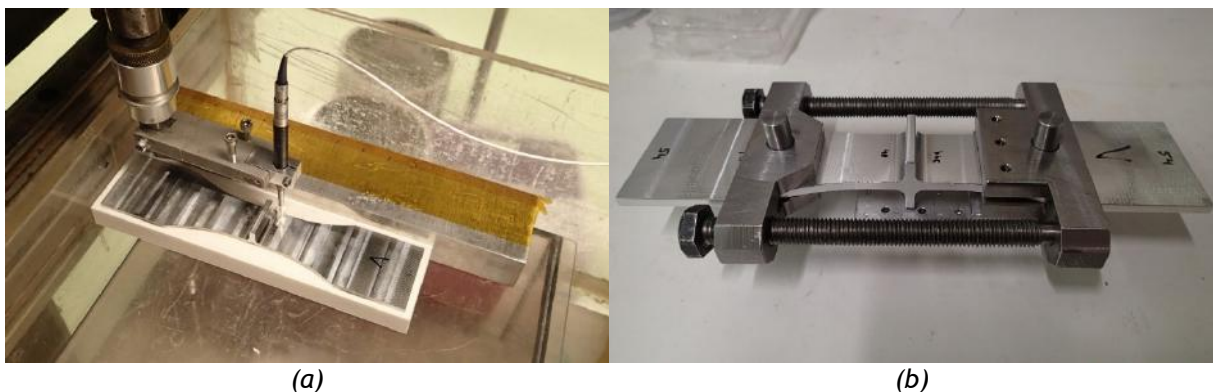
Figure 32: Automated Eddy Current inspections (subfigure a), static loading frame for SEM analysis (subfigure b). Figure courtesy of VTT.
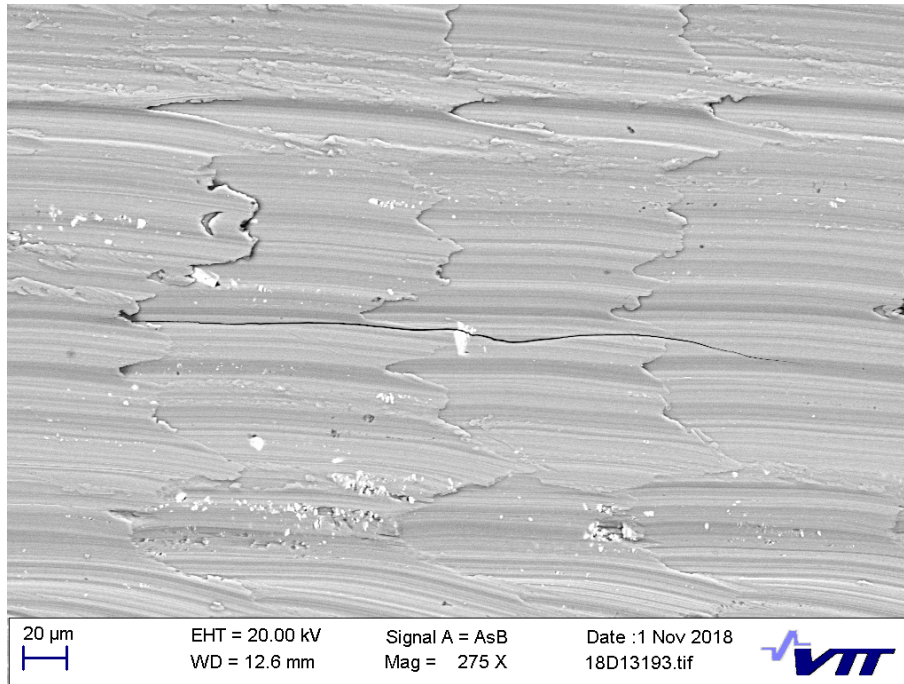
Figure 33: Produced surface crack for POD study. Crack length approx. 330 µm, after 55.000 cycles as shown in SEM figure under static tension load. The specimen was of Al 7075-T7351 as machined. Figure courtesy of VTT.

2.3.4 Hawk tailplane fatigue life assessment

The FINAF Hawk tailplane fatigue tests were introduced in Chapter 2.3.3 in Ref. [32], and the brief update is given below. Due to the uncertainty about the fatigue life of the Hawk Mk.51/51A/66 tailplane in the FINAF operational usage (see Chapter 2.2.3.1), the FINAF initiated in 2015 a full-scale fatigue tests (FSFT) to be performed on Hawk Mk.51/51A/66 tailplane's centre box buttstraps.

The FINAF's main objective is to get conclusive results to determine if the FINAF is required to procure additional tailplanes to keep its fleet operational until the planned withdrawal date of the aircraft type. The secondary objective was to obtain data about the crack growth rate, which could be used to increase the related structural inspection interval times. This was mainly achieved by means of the periodic non-destructive inspections (NDI) during the tests.

The fatigue tests (**Figure 34**) were performed by Patria Aviation Ltd. (prime contractor) with Elomatic Ltd. as a subcontractor for the load distribution plate design and manufacturing work, and VTT Ltd. with VTT Expert Services Ltd. (at present Eurofins Expert Services Ltd.) (main subcontractors) during year 2017.

The structural tests were conducted with two tailplane units, which both had flown approx. 4.000 flight hours (FH). The goal was to fatigue test the TP's up to 10.000 equivalent FH (EFH) to achieve additional 2.000 FH with a scatter factor (SF) of 5. The first unit had undergone structural repairs during its normal operational cycle at 3.330 FH; the latter had repairs repaired done just before the test at 4.000 FH. The tailplane's fatigue life is determined by its critical primary structural components: the upper and lower centre buttstrap plates, and centre spar (**Figure 35**). [49], [52], [53], [54], [55]

The FINAF Hawk Mk.51/51A/66 tailplane full-scale fatigue tests will be presented at the ICAF2019 Oral Session [50].

Figure 34: *The test set-up of the FINAF Hawk tailplane. Figure courtesy of Eurofins Expert Services.*
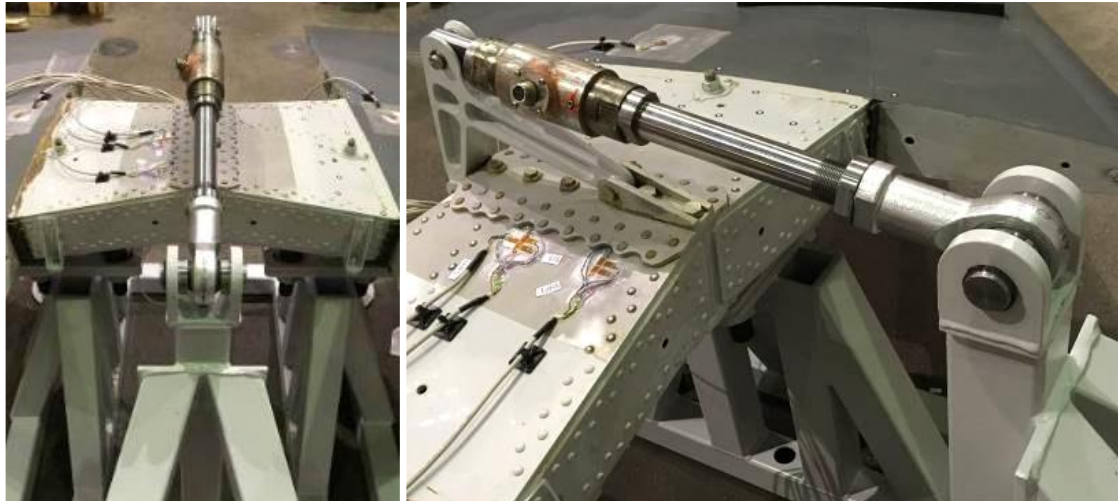
Figure 35: *The critical detail of the FINAF Hawk tailplane: the upper and lower centre buttstrap plates, and centre spar. Figure courtesy of VTT.*

2.3.5   Hawk Mk.66 centre fuselage fatigue issues

Some fatigue issues have occurred in FINAF Hawk Mk 66 centre fuselages. During 2000 FH maintenance many loosened rivets in pressurized fuel tank have been observed. Also, some aircraft have cracks in fuel tank floor support beam. In FINAF Mk 51/51A fleet those loosened rivets have never occurred and support beam cracks not earlier than 3500 FH.

Some vibration and stress measurements with inertia loggers and strain gauges have been done to better understand the loading of the centre fuselage. According to the latest observations the pressure in fuel tank rises significantly higher in some flight situations than purposed. The next examinations will be directed to Mk 66 fuel tank pressurization system. [43], [47]

2.3.6 Residual stress changes due to cyclic loading

Recent investigation carried out in Aalto University, Engineering Materials research group concentrated on residual stresses and fatigue life of the EN AW 7050-T7451 aluminium alloy. The objective of the investigation was to inspect the effect of shot peening on residual stresses and the influence of cyclic axial loading on residual stresses. The theory of the surface treatment method and residual stress measurements have been published in Ref. [97], and the focus here was on the description of the test set-up, results and analyses. [12]

2.3.6.1 Fatigue tests

Dog-bone test specimens were provided for the tests by Patria Aviation. Test specimens' (width 25 mm, thickness 5 mm) as machined surfaces were shot peened with coverage of 200 % and Almen intensity of 0.006-0.008.

Variable amplitude fatigue tests for the specimens were conducted on MTS 100 kN servo-hydraulic universal test machine (**Figure 36**). All tests were carried out as load controlled with 2 Hz loading frequency. Nominal peak-to-peak load levels were 55.3 kN/-25.6 kN resulting test section stress levels of 442 MPa/-205 MPa respectively. A buckling support was not applied/needed due to the relatively thick test specimen.
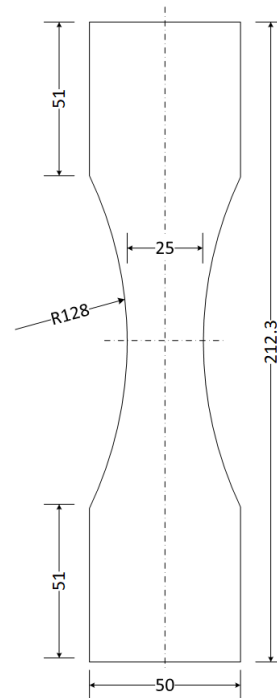
Figure 36: *A dog-bone specimen in the variable amplitude fatigue test. Figure courtesy of Aalto University.*

The number of test specimens was 12 (S1…S12). The first test specimen (S1) survived 10^6 load cycles, and was judged as a run-out. It turned out that the original test spectrum was not severe enough for the purpose, and had to be upscaled by a factor of 1.25, without exceeding the given ultimate load level. The next three specimens were tested with a new spectrum until failure, resulting an average life of $2 \cdot 10^5$ cycles. The test was continued such that five out of eight remaining specimens were delivered for re-peening in the halfway through their expected life time (approx. at 84.000 cycles).

2.3.6.2 X-Ray diffraction measurements

X-Ray diffraction is a non-destructive technique that provides detailed information about the crystallographic structure, chemical composition, and physical properties of materials. The method can also be used to determine residual stresses in the material. The X-Ray diffraction measurements were conducted with Stresstech X3000 equipment before and after the fatigue tests. The measurements for the flat dog-done specimens were tri-axial, including orientation angles 0° (transversal), 45°, and 90° (axial), thus allowing the calculation of principal stresses. Most measurements were conducted in the center of the test specimen (hot spot), but some dedicated measurements were also carried out in selected points in the longitudinal direction. The X-Ray diffraction test set-up is presented in **Figure 37**.
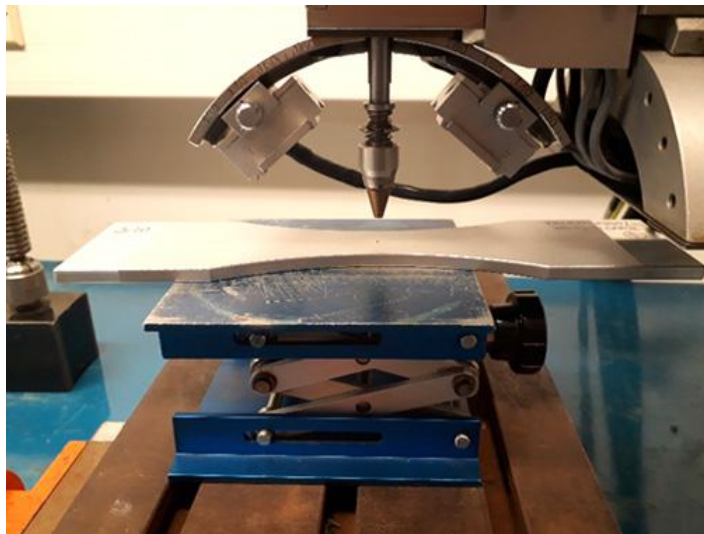
Figure 37: *Test set-up in the X-Ray diffraction measurements. Detector distance was 50 mm. Figure courtesy of Aalto University.*

2.3.6.3 Results

2.3.6.3.1 Residual stresses before fatigue testing

The residual stress measurements in different directions of the test specimens prior to the fatigue tests showed only minor variance for a single specimen and in between the test specimens. The residual stress direction was quite uniform in all cases, as illustrated in **Figure 38**.
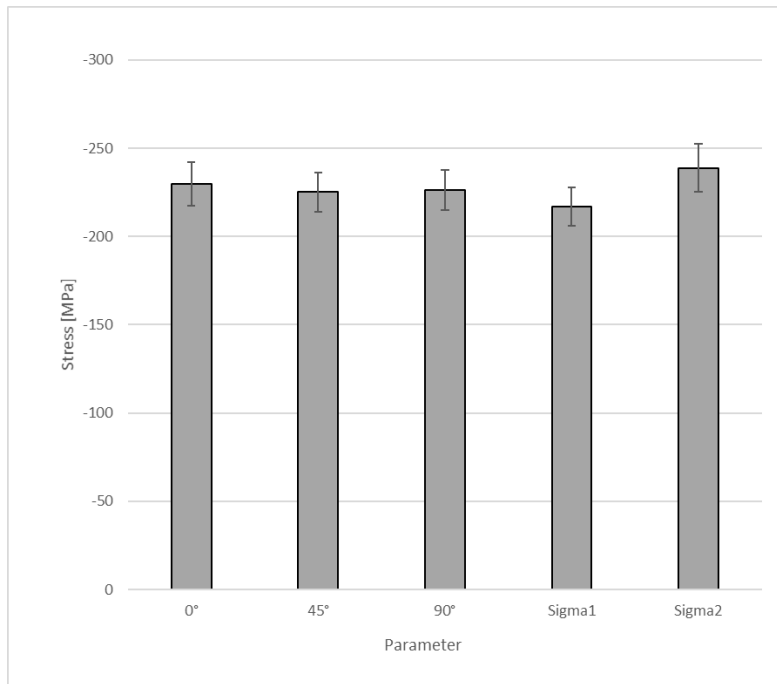
Figure 38: *The average residual stresses of 12 test specimens in 3 distinctive directions (0°, 45°, 90°), and max/min principal directions (Sigma1, Sigma2) from the X-Ray Diffraction measurements prior to the fatigue tests. Figure courtesy of Aalto University.*

2.3.6.3.2 Residual stresses after fatigue testing

High enough spectrum load levels had an effect on the residual stresses. The applied nominal stress for the test specimens varied approximately between 200…400 MPa. The residual stress relaxation was found in certain areas where peak stresses almost reached the yield stress of the material. With the given load spectrum the stress relaxation occurred during the first two load blocks after which the residual stresses remained unchanged although the cycling was continued. The phenomenon can be seen in **Figure 39**. Residual stress relaxation was most notable parallel to the loading direction, and least to the transversal direction.
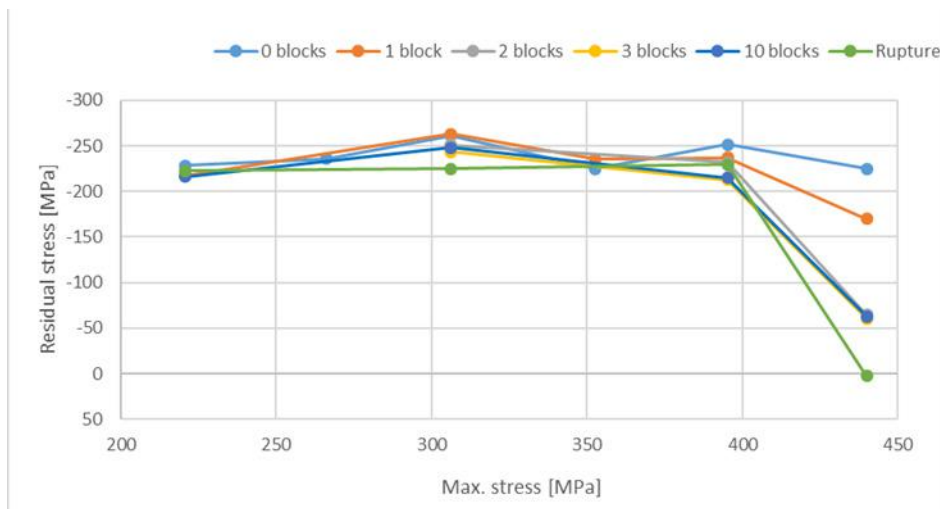
Figure 39: *The residual stresses of test specimen S8 measured in different points (indicated as varying max. stresses) along the axial (parallel) direction before fatigue loading and after selected number of load blocks. Figure courtesy of Aalto University.*

Shot peening is a cold working method whose purpose is to induce a favorable compressive residual stress distribution at some depth below the exposed surface, thus anticipating a beneficial effect on fatigue strength. Based on the test results of the shot peened specimens, the fatigue loading decreased the magnitude of the residual stresses, so it was assumed that re-peening (i.e. double shot peening) might increase the fatigue life. It turned out that re-peening reset the residual stresses back into their original level but had only minor effect on fatigue life. The effect of re-peening in different residual stress directions can be seen in **Figure 40**.
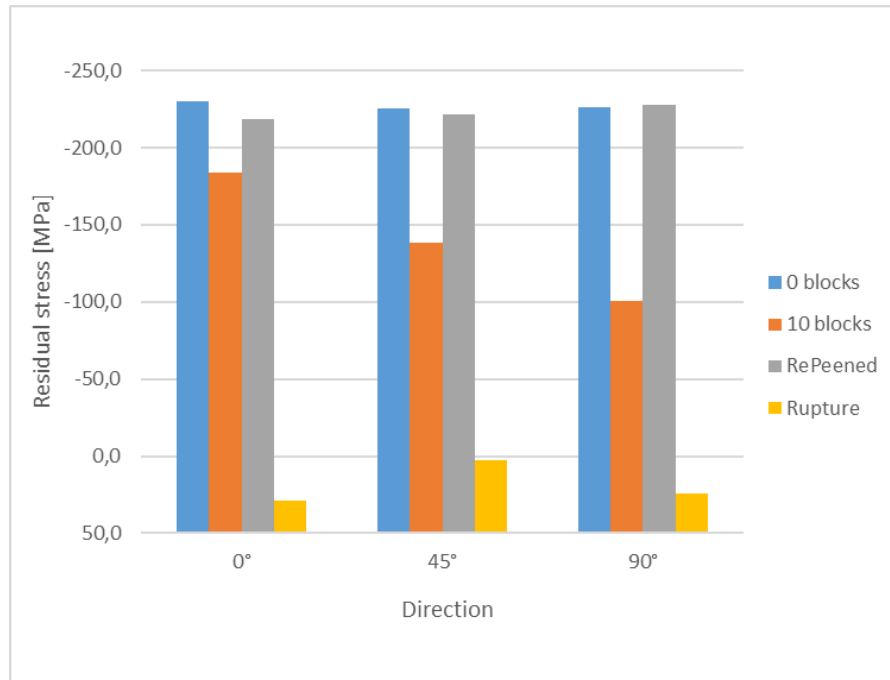
Figure 40: *The average residual stress of 8 test specimens in 3 distinctive directions (0°, 45°, 90°) before and after certain blocks of fatigue loading. Here, 90° is parallel to the loading i.e. axial direction. Figure courtesy of Aalto University.*

It can be concluded regarding the residual stresses after the fatigue tests, that the residual stress relaxation is significant during the first few loading blocks if the spectrum stress levels exceed 400 MPa. The relaxation was most evident parallel to the loading direction. Re-peening reset the compressive residual stresses back into their original level but the method had only minor effect on fatigue life.

Test specimen S8 had the shortest fatigue life (126.000 cycles). Post-mortem analysis done with Scanning Electron Microscopy (SEM) for the S8 specimen revealed that the fatigue crack had initiated from one side of the specimen, but fracture surface did not indicated any anomalies. The initiation point was located in the dent on the shot peened surface (**Figure 41**, **Figure 42**). Backscattered scanning electron micrographs of the fracture surfaces of the test specimen S8 after fatigue failure are presented in **Figure 43**, **Figure 44**.
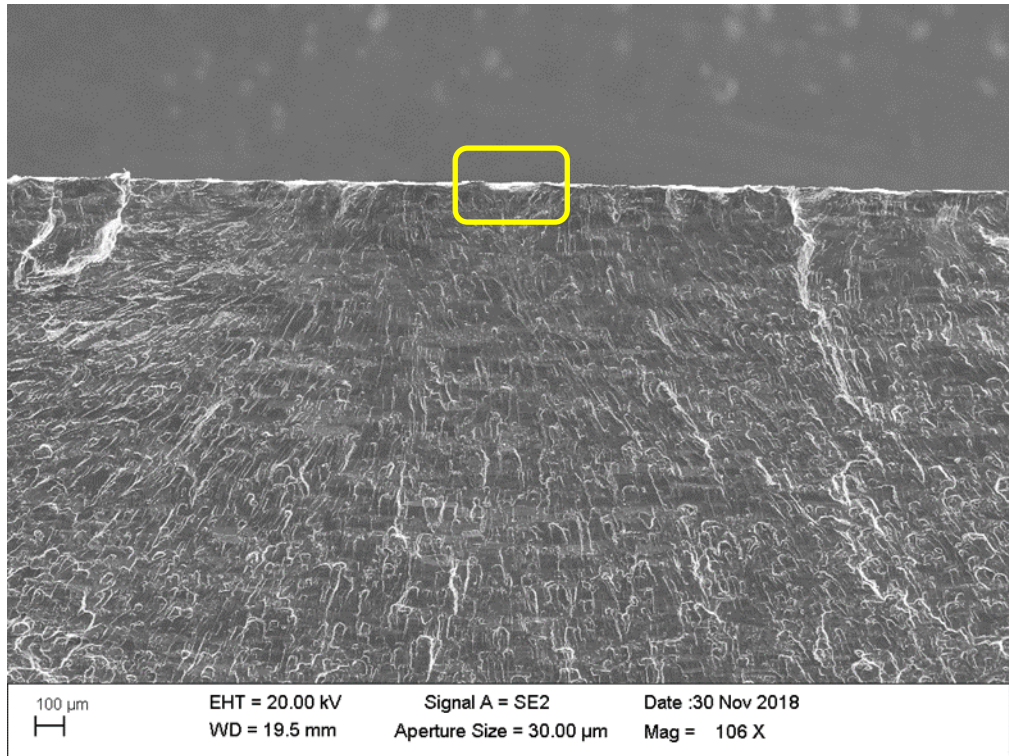
Figure 41: *The fracture surface of the test specimen S8. There appears to be multiple crack nucleation points (one of which is highlighted) along the shot peened surface. Figure courtesy of Aalto University.*
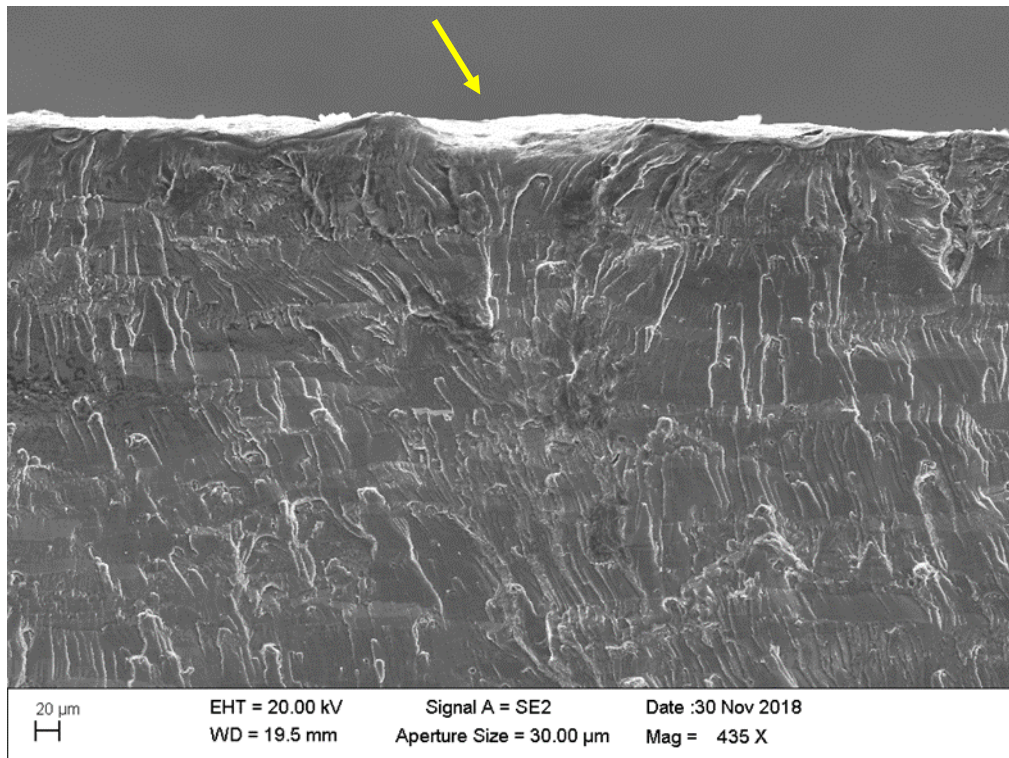
Figure 42: *Zoomed section of the crack nucleation point in the S8 test specimen. Figure courtesy of Aalto University.*
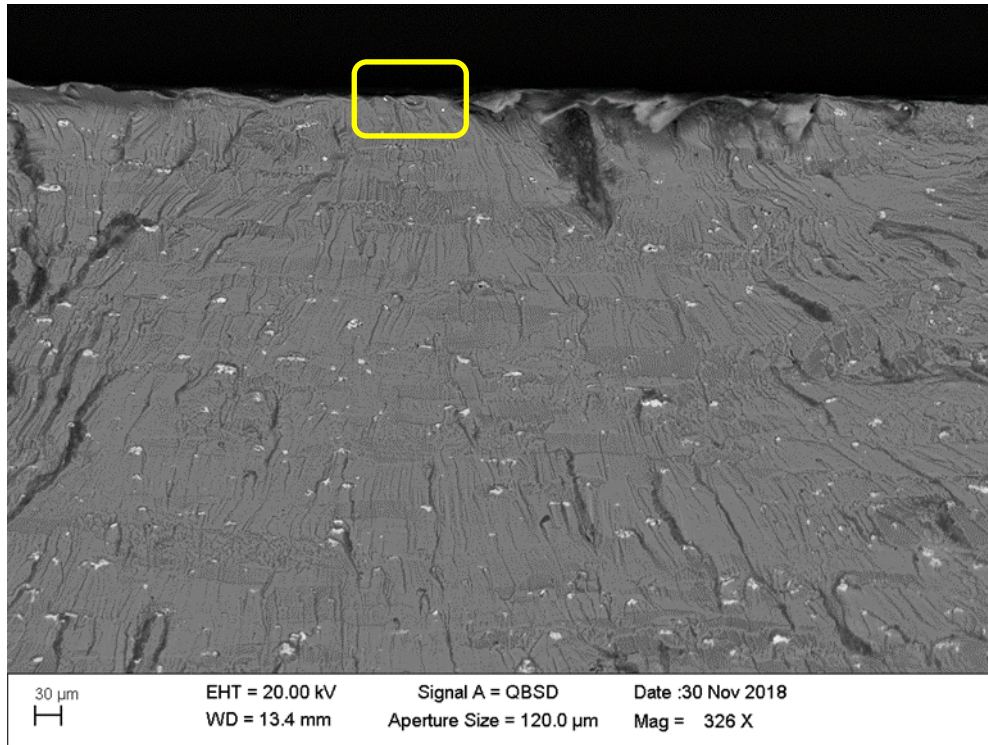
Figure 43: Backscattered image of the fracture surface of the test specimen S8. The crack nucleation point is highlighted. The presence of precipitates can be seen. Figure courtesy of Aalto University.
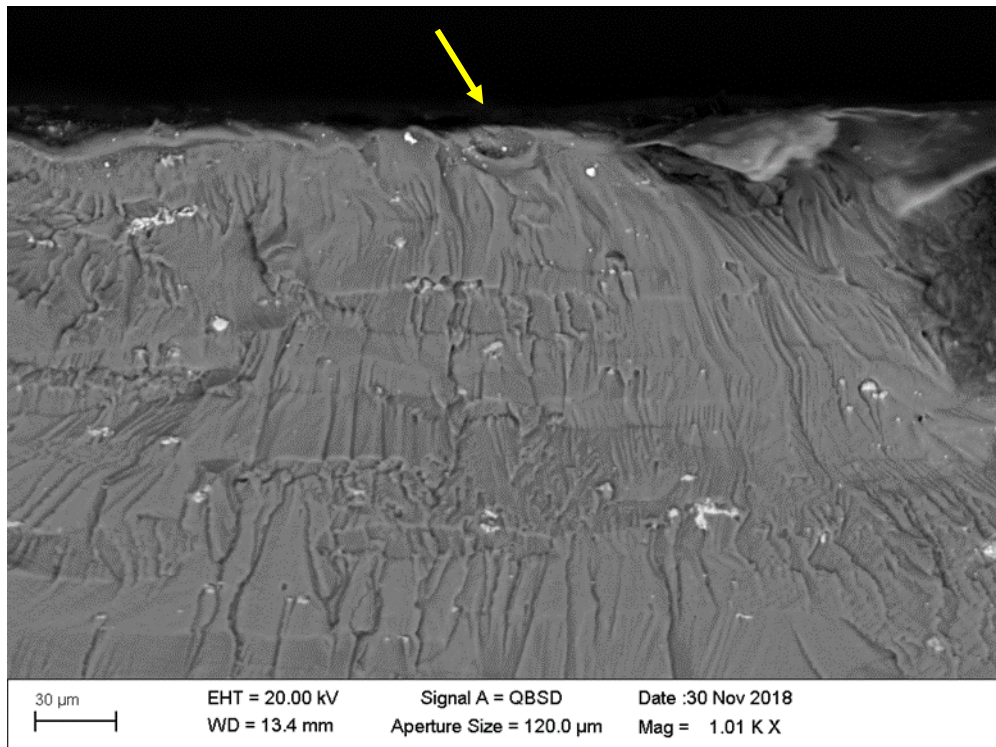
Figure 44: Zoomed section of the crack nucleation point in the S8 test specimen. Figure courtesy of Aalto University.

2.3.7 Development of data and method for fatigue sizing of bolted joints in AA7050-T7451 and AA2050-T84

This chapter highlights the international cooperation research activities in between Saab Aeronautics (Sweden) and VTT (Finland). The authors of the chapter are Zlatan Kapidžić and Hans Ansell, Saab AB.

2.3.7.1 Introduction

Current method for fatigue sizing of bolted joints in aluminium at Saab is based on data for joints in sheet materials AA2024 and AA7050. The methods and data for this purpose was developed in the early 1970s mainly for Saab 340 and Gripen A type of assembled thin sheet structure. Commencing with Gripen C/D and driven further in Gripen E/F is the vast use of machined integral structural solutions by use of thick aluminium plate product forms. Bolted joints in conventional AA7010/7050 alloys have been able to be handled with fairly accurate corrections of the original methods for Gripen C/D. Gripen E/F however will use AA2050 Aluminium-Lithium alloys to a huge extent which current corrections to existing methods and design data cannot handle in a proper way. New design data and modifications of the methodology are needed.

The aim of the work is to generate design data for bolted joints in thick plate alloy AA2050 and to adjust current stress severity factor method to fit to the stress analysis working process. Additional tests with specimens manufactured from thick plate alloy AA7050 are done on a limited basis. The work is split into two parts:

- Constant amplitude (CA) and spectrum fatigue testing of bolted joints
- Development of the fatigue sizing method

and will come together in a comprehensive methodology.

2.3.7.2 Test matrix principle

The principle for building up the test matrix and the expected outcome for evaluation is schematically outlined below. Complete SN-curves (three load levels) shall be generated only for R = 0 and R = -1 for AA2050 alloy and for R = 0 for the AA7050 alloy. Other variations, such as specimen type (single or double shear), number of fastener rows (2 or 3) , plate thickness (3 mm or 5 mm), fastener type (countersunk or protruding, Hi-Lite or Ti-screw), fastener diameter (6 mm or 8 mm), and variable amplitude loading are founded on fewer test specimen results. **Figure 45** shows the schematic representation of the test matrix principle for CA tests.
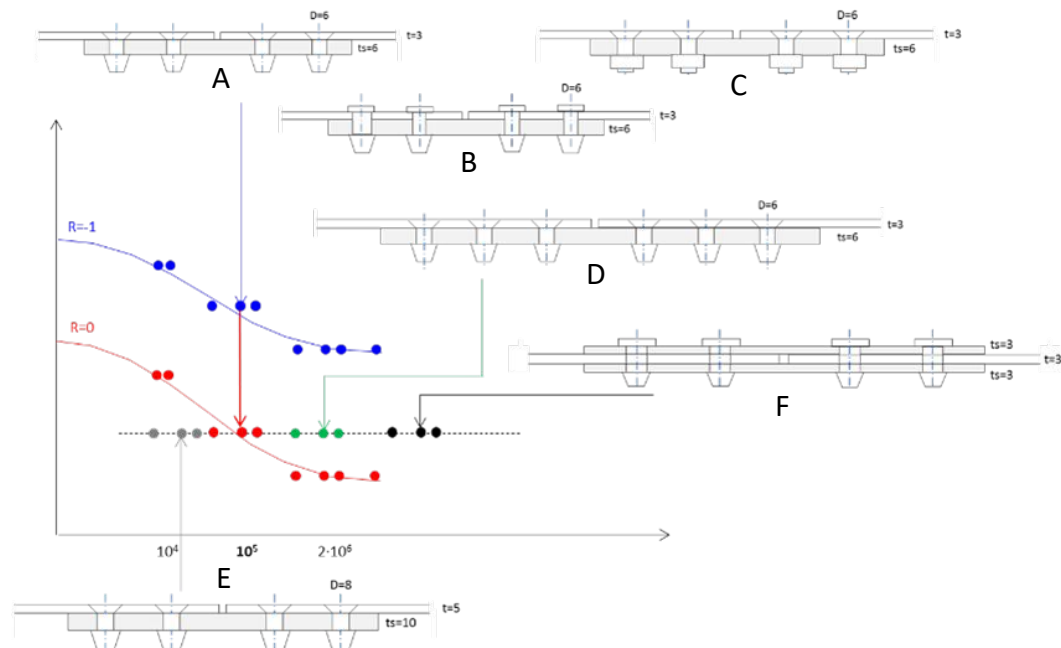
Figure 45:   Test matrix principle for CA testing. Figure courtesy of Saab Aeronautics.

The idea behind the variation of joint parameters included in the testing is to obtain a data set with varying amount of bolt transferred/by-pass load, secondary bending and stress concentration. All three of these parameters have an effect on the fatigue life and are included in the sizing method.

2.3.7.3 Test specimens

All specimens are two-column butt joints with a width of 8 D and with various fastener types (**Figure 45**): specimens A, D and E are bolted with countersunk Hi-Lites, specimens B and F are bolted with protruding head Hi-Lites and specimens C are bolted with countersunk Ti-screws. Four of the C specimens were assembled with low pretension torque (~2 Nm) and all other specimens were torqued to a level prescribed by the industrial standard (~6 Nm, referred to as "normal torque"). **Table 2** shows the number of tested specimen types at various stress amplitude (S_a) levels, the target life and load ratios (R) for both materials. The number of specimens tested in spectrum loading is also shown.

Table 2:   *Test matrix, number of tested specimens, totally 78 specimens tested (kFH = 1000 FH).*

Mat.	Spec Type	R = 0			R = -1			S_{min} = 60 MPa	Spectrum tensile		Spectrum tensile/ compressive	
		S_a = High 10^4	S_a = Mid 10^5	S_a = Low $2 \cdot 10^6$	S_a = High 10^4	S_a = Mid 10^5	S_a = Low $2 \cdot 10^6$	S_a = Mid 10^5	S_{max} = High 30 kFH	S_{max} = Low 60 kFH	S_{max} = High 10 kFH	S_{max} = Low 20 kFH
AA2050	A	4	4	4	2	3	4	3	2	2	1	1
	B		3	2								
	C		4	1								
	D		3	2								
	E		3	2								
	F	2	3									
AA7050	A	3	4	4		3			3	1		
	C		4	1								

Two spectra were used with about 60 cycles/Flight Hour (FH), a tensile dominated wing bending spectrum and a tensile/compressive fin spectrum. The results from spectrum tests are used subsequently for validation of cumulative damage calculations.

2.3.7.4 Test setup

Two uniaxial tensile/compressive machines were used in order to speed up the testing time. The specimens were installed in the grips with shimming plates at each end. Initially, seven tests were performed without any lateral support and a very significant secondary bending was observed. Three of these specimens failed in the joint plate whereupon it was decided that a lateral support shall be used, see Ref. [45]. **Figure 46** shows an early sketch of the lateral support and its realisation later on. The support had a significant influence on the secondary bending and its effects were evaluated using non-linear FE-model of the setup.
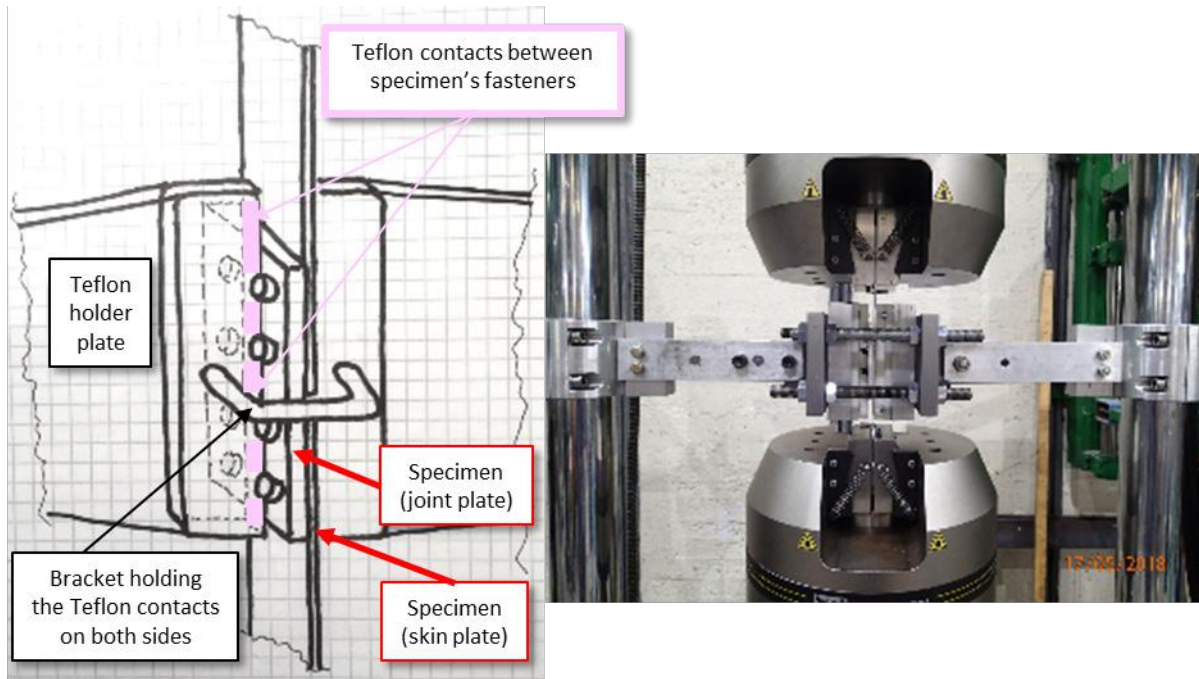
Figure 46: *Test setup with in-house designed lateral anti-buckling support. Figure courtesy of VTT.*

2.3.7.5   Test results

Figure 47 shows all test results in terms of applied gross stress amplitude σ_a and number of cycles to failure N_f.
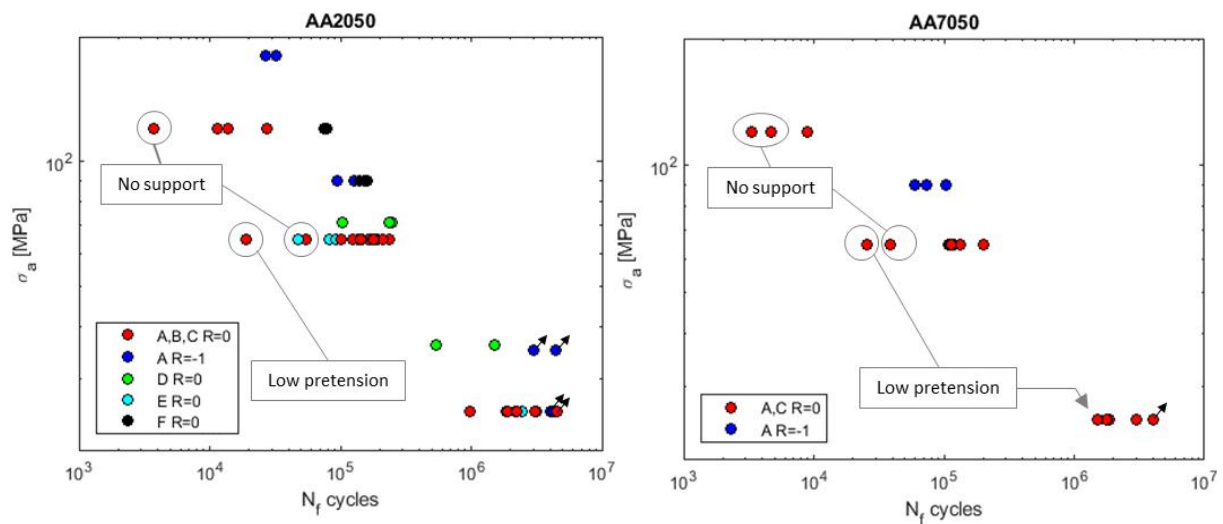
Figure 47: *Test results, gross test amplitude (σ_a) and number of cycles to failure (N_f). Figure courtesy of Saab Aeronautics.*

Some general comments about the test results presented in **Figure 47**:

- Specimens A, B and C had roughly the equally long fatigue lives, which is why they are presented in the same category.
- Specimens with no lateral support had significantly shorter fatigue lives than the ones with the support.

- Specimens with low pretension (2 Nm) had significantly shorter fatigue lives than the ones with normal pretension (6 Nm).
- Specimens E tend to have a slightly shorter lives than specimens A, B and C and specimens D and F tend to have longer lives.
- Tests at R = -1 gave longer lives than the tests at R = 0, as expected, cf. **Figure 45**.
- AA2050 specimens had on average 1.5 times longer life than AA7050 specimens.

The observed failure/cracking modes of all specimens are categorized in the following four groups as shown in **Figure 48**:

I   Cracking though the net-section of the outer bolt hole row of the skin plate
I* Cracking though the gross section of the skin plate near the outer bolt hole row
II Cracking though the gross section of the skin plate at the joint plate edge
III Cracking through the joint plate at the inner bolt hole row.
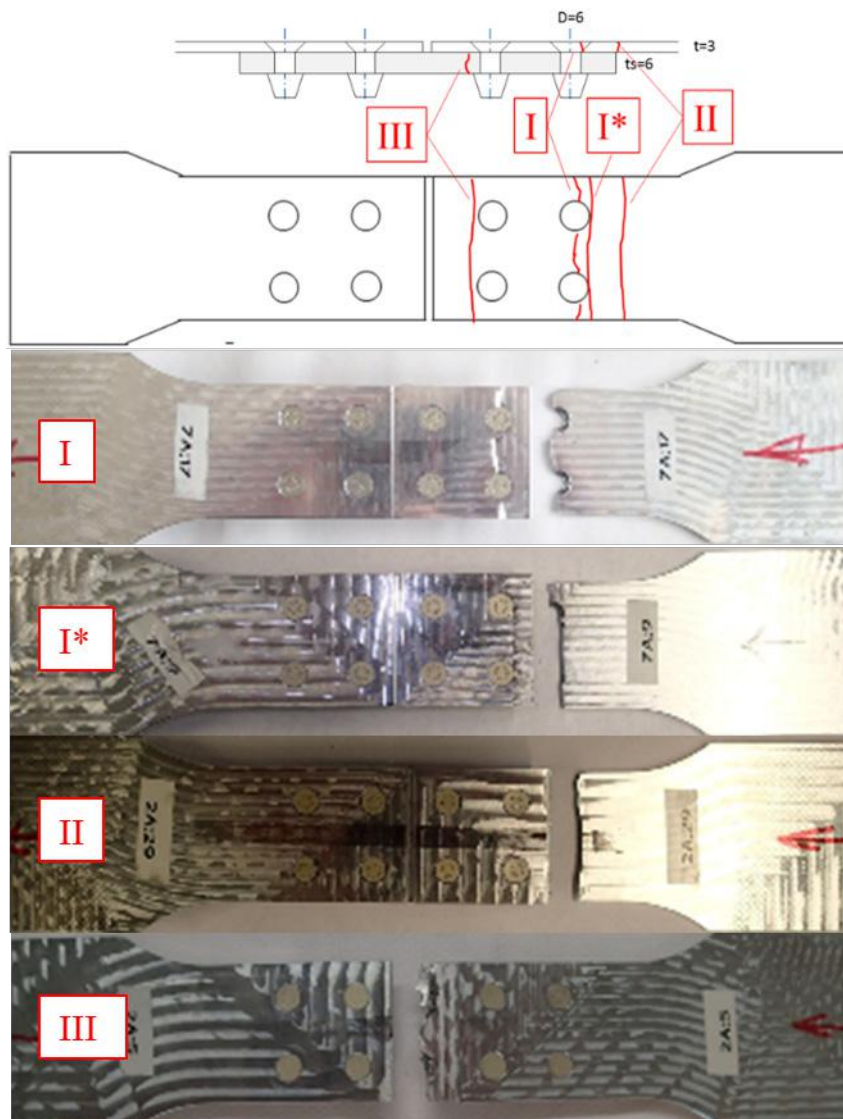
Figure 48: Observed failure modes. Figure courtesy of Saab Aeronautics.

Failure modes I and I* were observed in ~70 % of the test specimens and are the modes of interest for formulation of the sizing method. A fractography study of the fracture surface of six specimens that failed in modes I and I* was performed by VTT [101], see **Figure 49**. In normally pretorqued specimens, the cracks typically initiated at the faying

surface of the skin plate at some distance from the hole in both mode I and I*. In specimen with low pretension, the cracks initiated from the hole edge at the faying surface. These findings suggest that the stress concentration created by the bolt hole is probably of less importance than the amount of load transfer and secondary bending in normally pretorqued joints.
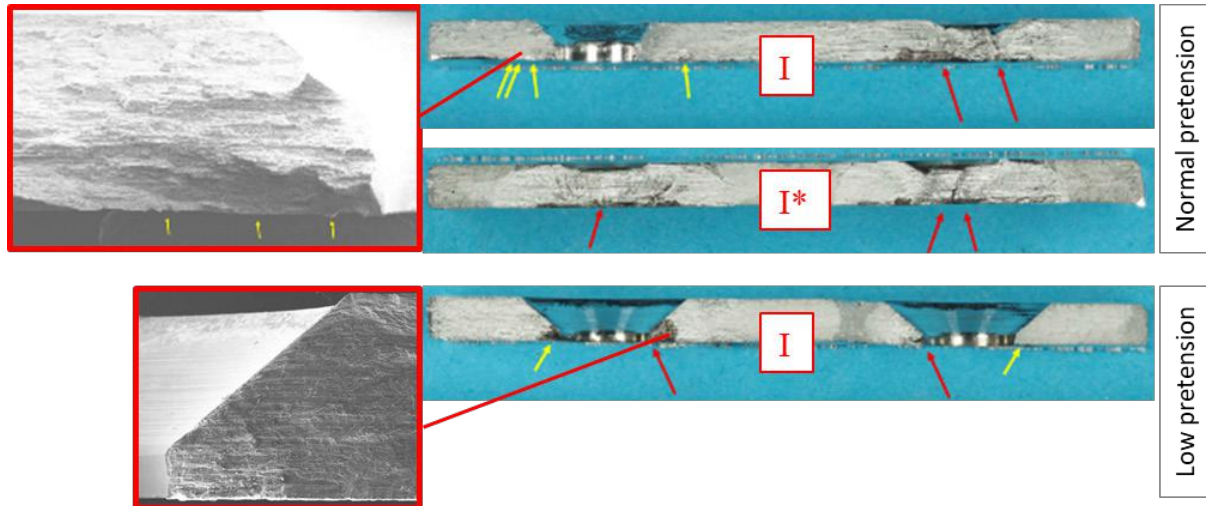
Figure 49: Fractography images of the typical crack initiation sites. Figure courtesy of Saab Aeronautics.

2.3.7.6 Fatigue sizing method

The present method is based on the concept of reference geometry method presented in Ref. [56] and outlined below. Consider the critical (mode I) bolt row in the skin plate and the stresses applied on it, see **Figure 50**.

σ = gross stress
σ_{bp} = by-pass stress
σ_b = bending stress
F_t = transferred load
$\sigma_t = F_t/Wt$ transferred stress
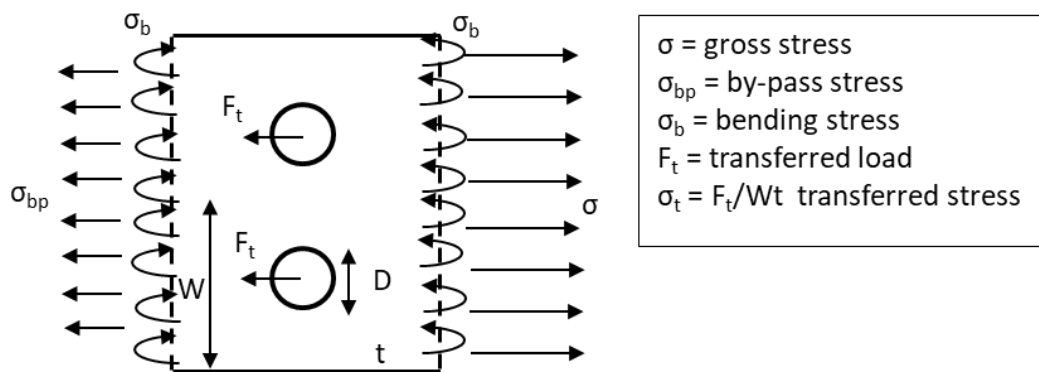
Figure 50: Stresses in the skin plate at the critical bolt row. Figure courtesy of Saab Aeronautics.

The net section stress σ_n is written as

$$\sigma_n = \frac{\sigma(1 + k_b)}{1 - \frac{D}{W}}$$

(1)

where k_b is the bending to gross stress ratio σ_b/σ. A log-linear type relation is assumed between the net-section stress amplitude σ_n, fatigue life N, stress concentration K_t and load ratio R. Expressed in terms of gross stress amplitude σ_a, via (1), this relation yields:

$$\sigma_a = C(K_t)^p(1-R)^q N^{-1/m}\frac{\left(1-\dfrac{D}{W}\right)}{(1+k_b)}$$ (2)

where C, p, q, and m are material parameters and K_t is defined as:

$$K_t = \left((1-f)K_{tg} + f\frac{W}{D}K_{tt} + k_b K_{tb}\right)\frac{1-\dfrac{D}{W}}{1+k_b}$$ (3)

where $f = \sigma_t/\sigma$ is the transferred load ratio and K_{tg}, K_{tt} and K_{tb} are stress concentration factors for by-pass, pin and bending load, defined as ratios between max stress at hole edge and gross stress, bearing stress and bending net-stress respectively. The parameters in Equation (3), including the bending ratio k_b, are determined using FEM for all specimens.

Equation (2) is logarithmised and fitted to the data by the least squares method. Modes II and III are considered to be outside of the scope of the method at hand and will not be regarded as such within it. The test results related to failure mode II and III are, however, included in the data for method formulation if the fatigue life is equal to or longer than the life of mode I for same specimen type. The results for tests with no lateral support are included in the data, considering increased secondary bending which is calculated using FEM. The tests with low pretension are not included. All fatigue lives for AA7050 specimens were scaled by 1.5 in order to reduce the data to a single set. There was not enough AA7050 data points to fit the materials separately. A log-linear regression is performed on the gross stress amplitude normalized by the K_t, R, D/W and k_b factors in Equation (2) (referred as to S_a) and the result is shown in **Figure 51**.

Equation (2) can be solved directly for N for any set of joint parameters and the cumulative damage can be obtained for any gross stress spectrum. However, the relation (2) is valid only in the range of the test data (10^4 … $4 \cdot 10^6$) and all stress amplitudes evaluated outside that range will yield unrealistic fatigue life. Therefore, it is more feasible to adopt the concept of reference joint [56] in order to suit the already established methodology at Saab.
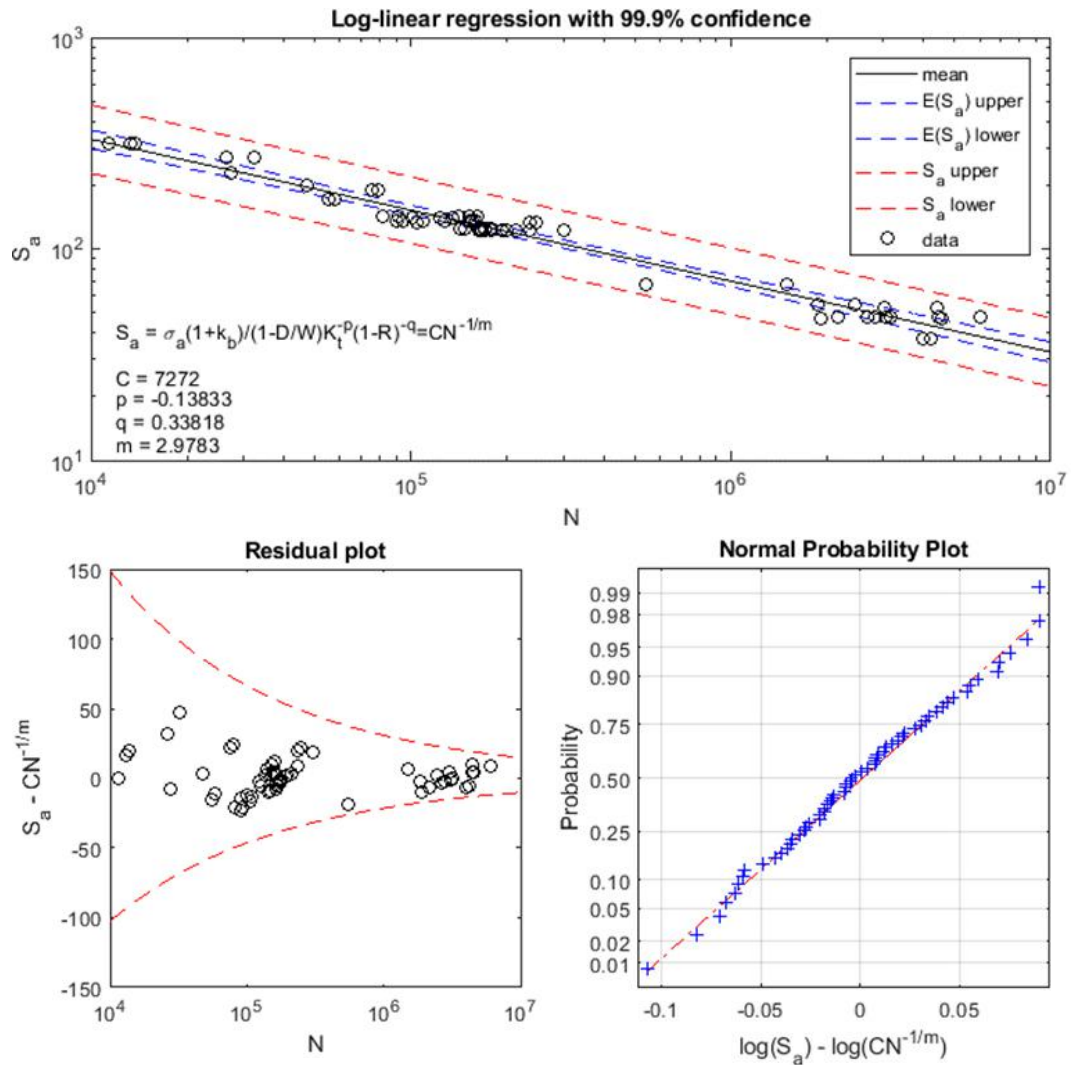
Figure 51: *Log-linear regression of the fatigue data, with the confidence interval for the mean $E(S_a)$ and the prediction interval based on log-normal distribution of the error. Figure courtesy of Saab Aeronautics.*

First, a Haigh diagram is constructed for a reference geometry (in this case type A specimen) based on Equation (2) with joint type A parameters. The tails of the SN-curves are provided with asymptotes at R = 0, tending towards 250 MPa at 10^3 and to 25 MPa at 10^7. This is an ad hoc correction based on evaluation of earlier data and is used for now until some more elaborate method can be established. Haigh diagram for AA7050 reference joint is scaled down by using C = $7272 \cdot (1.5)^{-1/m}$ in Equation (2), because we have previously scaled the data up by a factor of 1.5, and is shown in **Figure 52**.
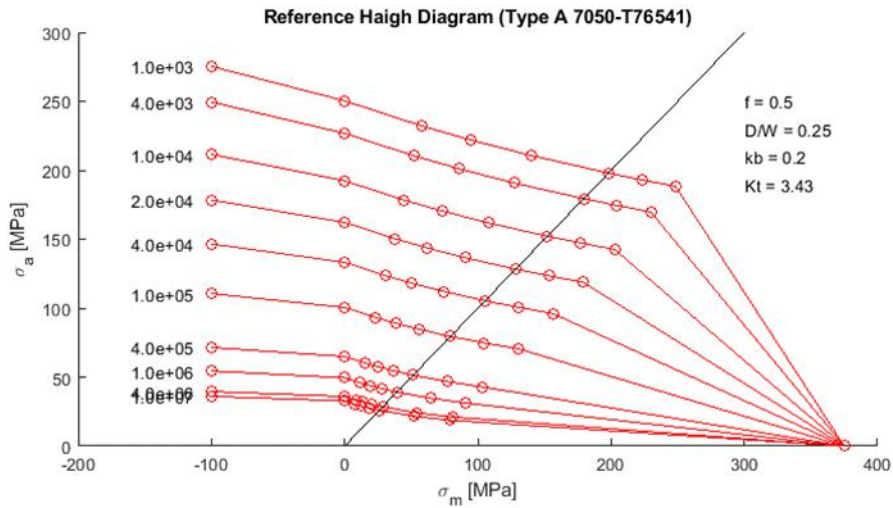
Figure 52: *Reference Haigh diagram, Type A joint, AA7050. Figure courtesy of Saab Aeronautics.*

In line with the method in [56], a Haigh diagram for an actual joint geometry is calculated from the reference Haigh diagram as

$$\sigma_a = (\sigma_0)_a \cdot \phi \tag{4}$$

where $(\sigma_0)_a$ are the gross stress amplitudes for the reference geometry and the correction factor is

$$\phi = \left(\frac{K_t}{K_{t0}}\right)^p \frac{\left(1 - \frac{D}{W}\right)}{\left(1 - \left(\frac{D}{W}\right)_0\right)} \frac{(1 + k_{b0})}{(1 + k_b)} \tag{5}$$

where the subscript 0 refers to the reference geometry. The mean stresses σ_m are scaled by the same correction factor. Cumulative damage is based on the Palmgren-Miner rule.

2.3.7.7   Evaluation of the fatigue sizing method

The method outlined above is applied for calculation of cumulative damage for spectrum loaded specimens of Type A. **Figure 53** shows the comparison of test results with the method predictions assuming failure at damage equal to one.
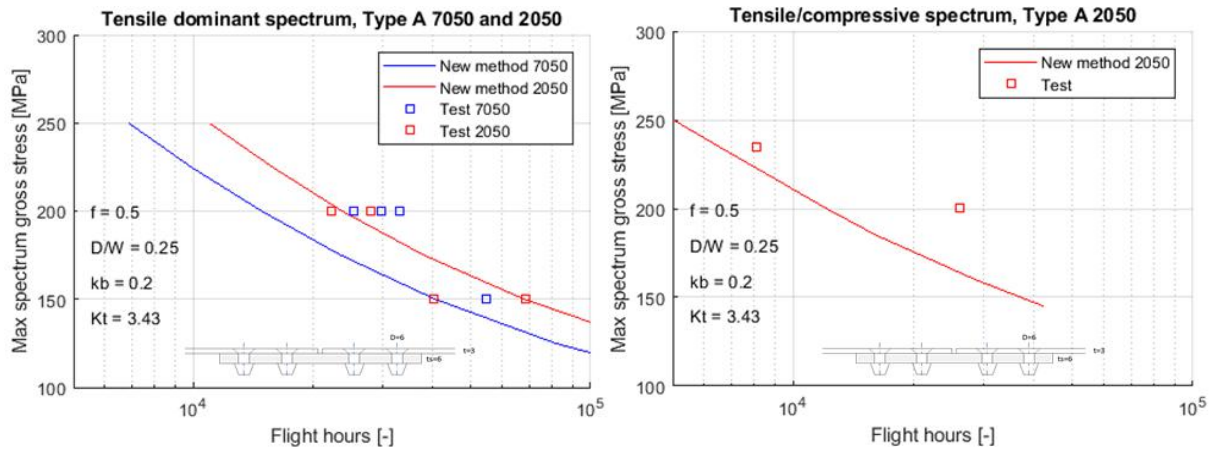
Figure 53: *Test results and prediction for Type A specimens. Figure courtesy of Saab Aeronautics.*

Further comparisons are performed to data presented in [17] and [75] where several types of 7050-T7651 specimens with Hi-lok fasteners were tested using FALSTAFF spectrum. The same secondary bending and transferred load as measured with strain gauges [17] are used in the predictions. The comparisons are shown in **Figure 54 … Figure 57**.
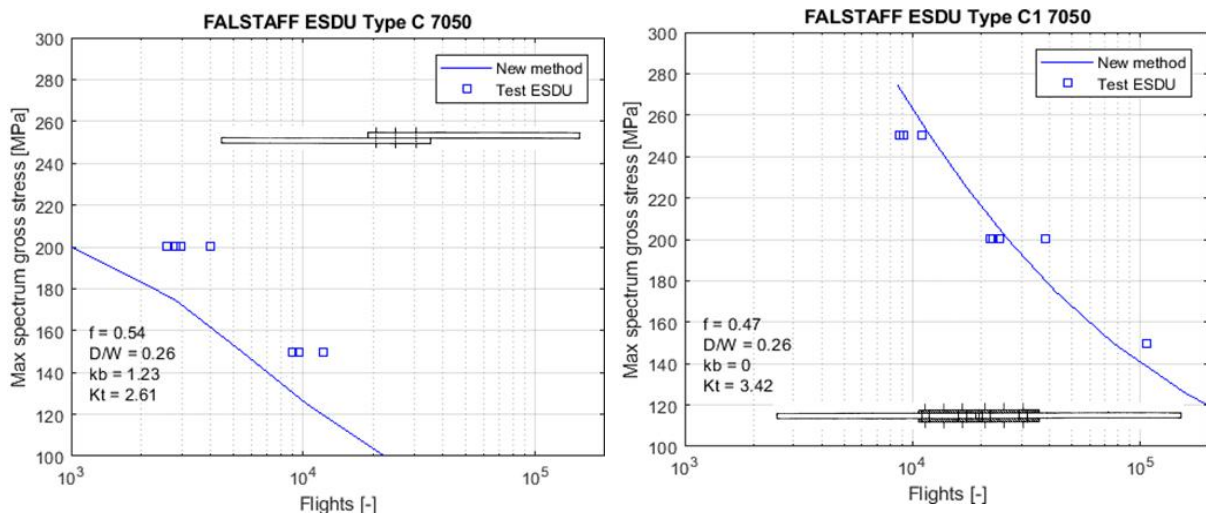
Figure 54: *Test results and prediction for Type C (single shear) and C1 (double shear) specimens [17]. Figure courtesy of Saab Aeronautics.*
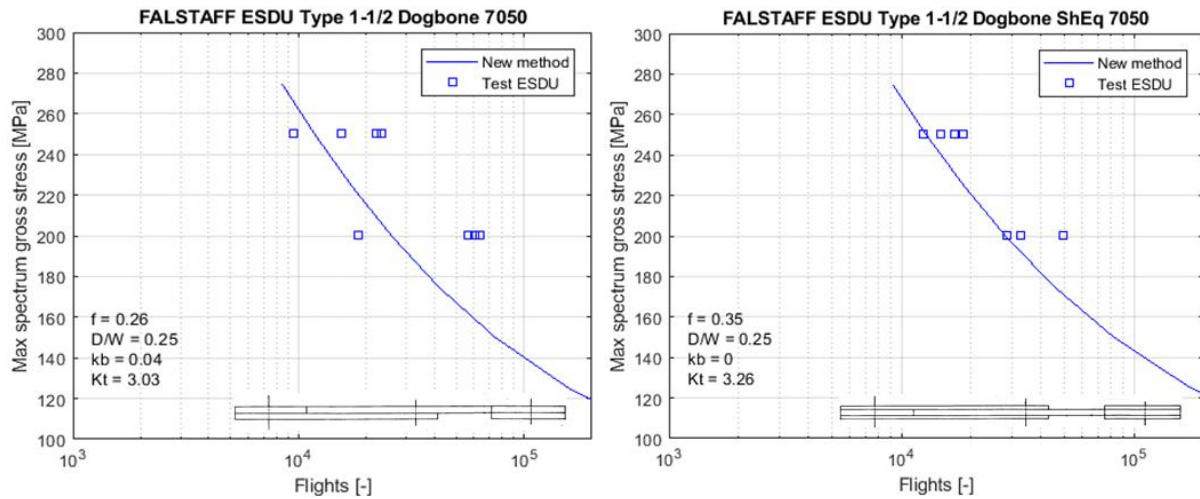
Figure 55: *Test results and prediction for Type 1-1/2 Dogbone and 1-1/2 Dogbone shear equivalent specimens [17]. Figure courtesy of Saab Aeronautics.*
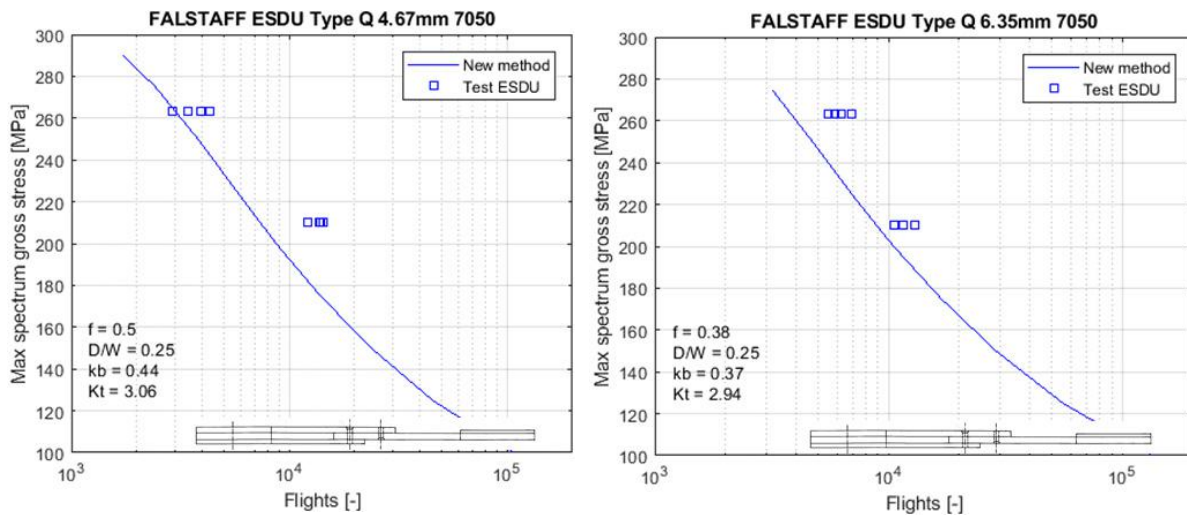
Figure 56: *Test results and prediction for Type Q 4.67 mm and Q 6.35 mm specimens [17]. Figure courtesy of Saab Aeronautics.*
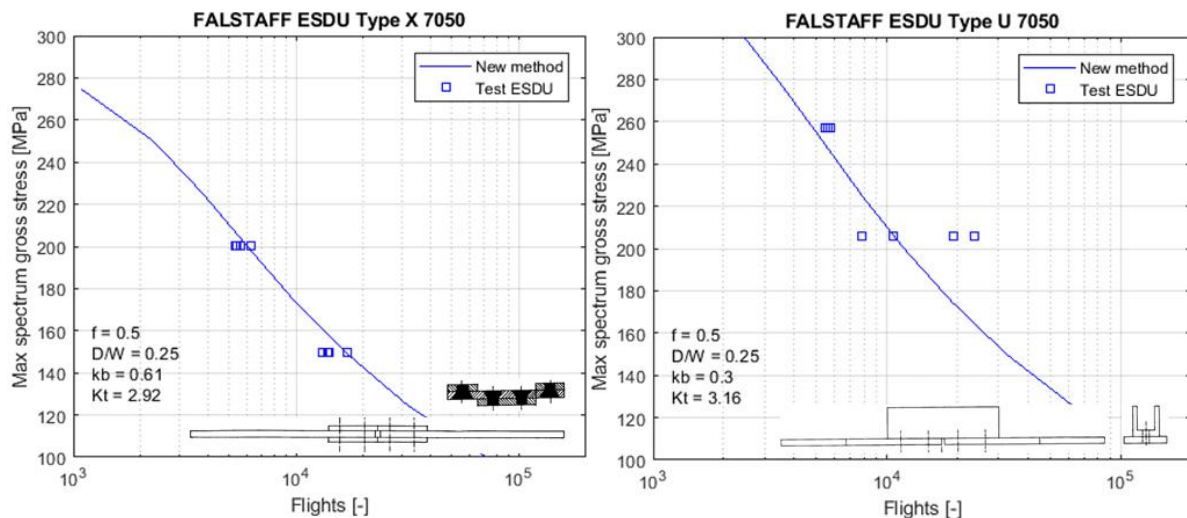
Figure 57: *Test results and prediction for Type X and U specimens [17], [75]. Figure courtesy of Saab Aeronautics.*

2.3.7.8 Conclusions

- A fatigue test series including varying joint configurations in alloys AA7050 and AA2050 were conducted.
- A fatigue sizing method, based on the concept of reference geometry is developed and fitted to the test data. The method takes into account the amount of transferred load, secondary bending, stress concentration and spectrum loading and is valid for normally torqued joints.
- Predictions of spectrum fatigue life of several tested specimens and tests of eight different types of joints from the literature were in satisfactorily correlation with the test results.

2.4 Structural integrity of composite materials

2.4.1 Structural integrity of composite materials and adhesively bonded multi-material joints

During the current research period, Tampere University has been continuing the work related to the structural integrity of composite materials and adhesively bonded joints. The roots of this work are in the research originally initiated at Aalto University. The work by Tampere University is focused on the development of analysis methods of computational continuum thermodynamics and on the practical usage of finite element applications of Virtual Crack Closure Technique (VCCT) and Cohesive Zone Modelling (CZM). The target is to provide analysis procedures for delamination and debond-predictions for specific aircraft structures. In detail, the current work deals with the simulation of multi-site damage and related interactions. Moreover, the case studies are typically applicable to not only quasi-static loads but also to dynamic loading schemes.

In the studies, VCCT has been considered the main analysis method whenever a pre-existing delamination or debond exists in the structure considered. The main advantage of VCCT is that only single fracture criterion based on Energy Release Rate, ERR, is needed for analysis and fracture toughness for considering the criticality per actual material. For computations with a mode division, an interaction law is additionally to be applied. This use of VCCT simplifies analysis and the experimental procedure due to essentially standard procedures are available for fracture toughness. The work by Tampere University also covered detailed studies about the applicability of VCCT in the event of extensive residual stresses and bi-material interfaces – typical of hybrid laminates [35], [36].

The fact that VCCT implementations by definition require pre-modelled flaw, a pre-crack, can be seen as a limitation for general fracture simulation. For various real-world cases, the main crack or alternatively additional cracks can for due to loading – being either static of dynamic. For this reason, an extension of VCCT was studied and a Combined CZM-VCCT method was developed [37], [38]. The term combined refers to a simulation where both the crack nucleation process as well as (stable) crack propagation process are predicted by as practical as possible means. As a first step, the developed method is intended to expand VCCT's limitation about the pre-existing crack. The Combined CZM-VCCT method separates the crack nucleation and propagation (i.e. onset and evolution) along the fracture path (**Figure 58**). The method utilizes CZM for the physically complex crack-onset phase and the propagation phase utilizes VCCT. The Combined CZM-VCCT method was successfully used in predicting the crack growth in a Double Cantilever Beam (DCB) test and also in a Cracked Lap Shear (CLS) test – these tests represent the mode I and mode I+II cases in terms of mode division [35], [38]. The next step in the development of the Combined CZM-VCCT method would be to understand limits of implicit and explicit solution processes and effects of multiple simultaneously growing cracks.
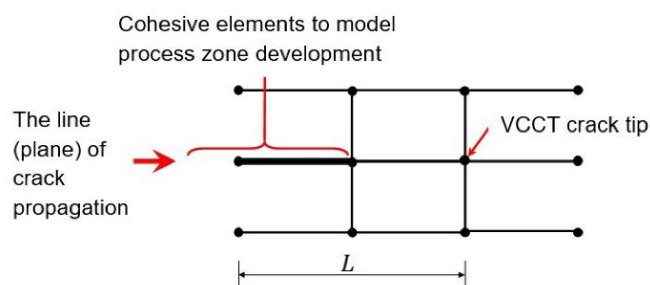

Figure 58: *The transition zone of the Combined VCCT-CZM method [38]. Figure courtesy of Tampere University.*

The experimental research program 2017-2019 had two targets. First, the mixed mode fracture of adhesive was studied in order to further validate the mode-division based analysis with the interaction law. Second, multi-material stepped lap joints were studied to understand the failure mechanisms and capabilities of analysis methods compared to real behaviour of stepped lap joints with metal-composite interfaces.

The first work task focused on the epoxy adhesive FM-300-2 material-wise. To gain results efficiently, a new test method was developed with a new test specimen design. Finally, the fracture criterion was determined based on a single mixed-mode specimen, which provided two mixed-mode ratios according to the use of the specimen during testing. The results of the tests were analysed using both VCCT and CZM numerical simulations. The result was a fast-preparable test specimen with a straightforward test setup and output two different mixed-mode fracture toughness allowables.

The second work task of the experimental program was focused on the stepped lap joint (SLJ) specimen made of carbon fibre reinforced plastic (CFRP) and a titanium alloy. SLJ specimens are in general representing structures where damage and cracking can start at several 'critical' locations and even simultaneously. In the work by Tampere University, the SLJ specimen involved three steps where one of the steps included a pre-inserted de-bond. Therefore, three different test configurations were created. The different SLJ specimens were tested under quasi-static tensile loading. Due to the materials and the debonds, the failure can initiate in three main failure modes (cohesive, adhesive, and delamination). Also, a debond at a step can merely work a stress booster for failure other than the step in question. It was seen necessary to apply specialized methods for following the failure progression. At Tampere University, the instrumentation included a sophisticated setup combining traditional strain gauge monitoring along with Digital Image Correlation (DIC) related data analysis. The DIC is a technique based on image processing and it offers numerous different ways to focus and magnify the spatial resolution of the 3D field data for strain and displacement. The DIC has been shown to be a valuable tool in the measurements for determining elastic constants for composite materials [73]. For the SLJ specimen experiments, the DIC was used for defining the fracture onset-related mechanisms. The analysis was interpreted in terms of displacement and strain fields to specify the critical points and failure mechanisms (**Figure 59**).
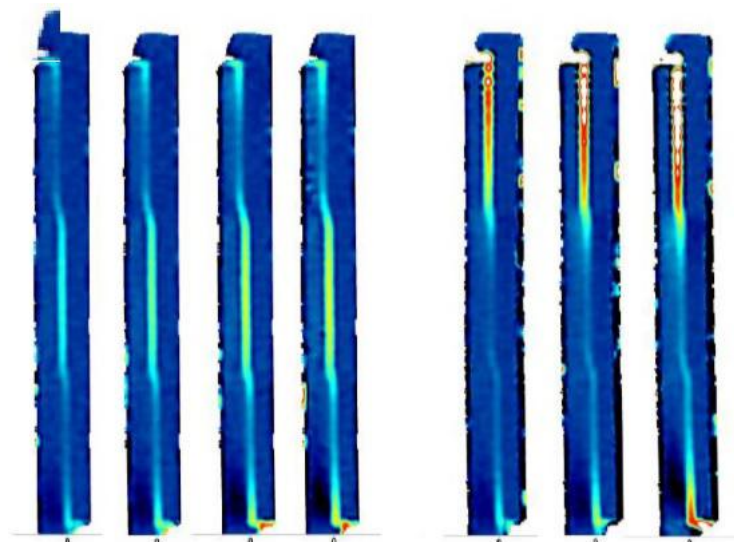
Figure 59: Stepped lap joint specimen tested in tensile mode and the DIC analysis used for monitoring the shear strain accumulation as a function of experiment time laps. Figure courtesy of Tampere University.

The damage tolerance/criticality analysis of an F-18 trailing edge flap (TEF) with fixture point delamination was continued at a part of the analysis work. The results presenting the TEF analysis with the existing delamination have been presented in our previous work [39]. The current work focused on understanding the interaction between several simultaneous delamination sites – i.e. a multiple delamination interaction in the TEF spar (**Figure 60**) [40]. The numerical analysis included several computation cycles and sensitivity mapping of numerical parameters applied in VCCT when using Abaqus/Standard. The influence of pure software-related computational parameters was shown to be small, which remarks the independency of the analysis in operator-determined (or default), non-physical parameters. Along with the parametric study, the effect of the delamination location in the laminate stacking direction was studied. The location of delamination was shown to have a significant influence on the delamination onset.
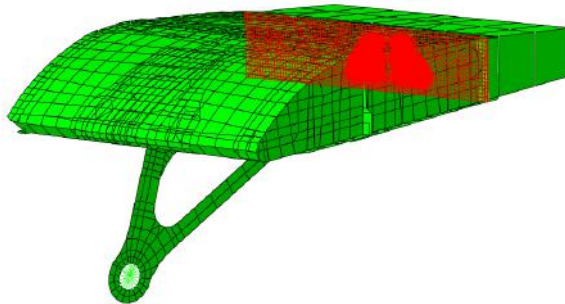
Figure 60: *The sub-model used in the analysis of the F-18 trailing edge flap damage [39]. Figure courtesy of Tampere University.*

For all of the above described structures, dynamic, cyclic loads are important in practice. Fracture and delamination growth due to cyclic loads is a challenging research topic and the experimental procedures are awkward. Currently, Tampere University is developing computational procedures to predict failure propagation in composites during impact loading (low velocity to high velocity impacts) and also crack growth in adhesive joints due to cyclic loading. The work has been initiated by launching extensive experimental test programs (**Figure 61**). The impact experiments take advantage of standard drop-weight apparatus, DIC, high-speed DIC, high-speed thermal cameras, and Hopkinson Split Bar (HSB) apparatus for high velocity impacts at the Tampere University premises.
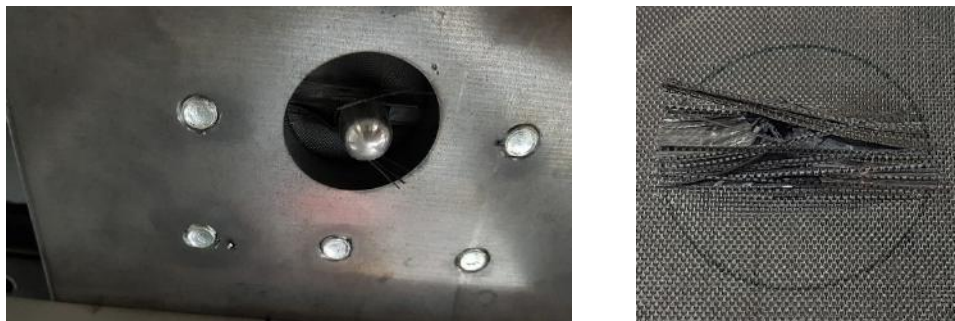
Figure 61: *Perforation damage in a CFRP laminate due to low velocity impact. Figure courtesy of Tampere University.*

In general, the experiments with fatigue of adhesive require fundamental development. The mode II related testing for fracture toughness of composites (end notched fracture, ENF) has previously been standardized by ASTM. For fatigue, especially for negative load

ratios (R < 0), there is no feasible setup standardized. Therefore, a proper test setup has been conceptualized (**Figure 62**) at Tampere University. Various concepts are being considered taking into account the easiness of testing and the accuracy (in terms of operator dependency, deviations, and load definition).
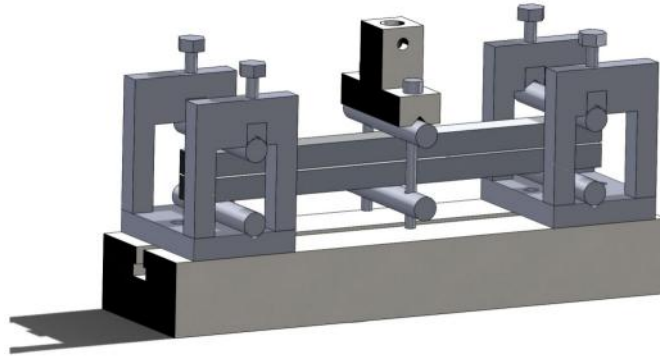
Figure 62: *Conceptual studies of test fixtures for mode II adhesive fatigue fracture. Figure courtesy of Tampere University.*

2.4.2 Thermographic studies – update

The number of penetrated water-induced failures within the FINAF F/A-18 rudders is on the rise. Thus, penetrated water in the composite structures operating in arctic conditions has been a research activity in Finland for several years. VTT and Patria Aviation have been working in close co-operation to develop a method to detect moisture and efficiently remove it from the structures.

Detailed inspection and drying procedure is explained in the ICAF2015 National review (Chapter 13.2.3.1 in Ref. [31]). The thermographic inspection method has shown to be the only method that detects small amounts of penetrated water from large areas without removing aircraft composite parts from the aircraft – and the only method within the FINAF, which can detect small amounts of water. The costs of thermography inspection + drying are far less than the costs of repair planning + repair, not to mention the costs of new rudders. The chronology of the rudder inspections has been as follows:

1. The selected rudders are delivered to Patria Aviation's repair shop.

2. Patria inspects the rudders using their X-ray method. In case moisture ingress is detected, the rudder undergoes a drying procedure. The dried rudder is inspected again using the X-ray method.

3. After the above X-ray inspections, VTT inspects the rudders using thermography. If moisture is detected, the rudder undergoes the drying procedure. The dried rudder is then re-inspected with thermography, but now only from those areas in which moisture was detected.

VTT has now inspected all the rudders in the FINAF F/A-18 fleet to reveal the water penetration or moisture ingress in the composite sandwich structures. During the Period 2017-2019, 31 rudders were inspected of which 6 displayed positive indications of moisture ingress. All of the above 31 rudders had undergone the X-ray inspections prior to the thermographic inspections. If the X-ray had given a suspicion of water ingress, the rudder was dried prior thermographic inspection. All together 164 thermographic inspections were made from the beginning of this study (2014). 25 % of thermographic inspections revealed moisture in the structure.

An overview of the rudder thermography inspections is provided in **Figure 63**.
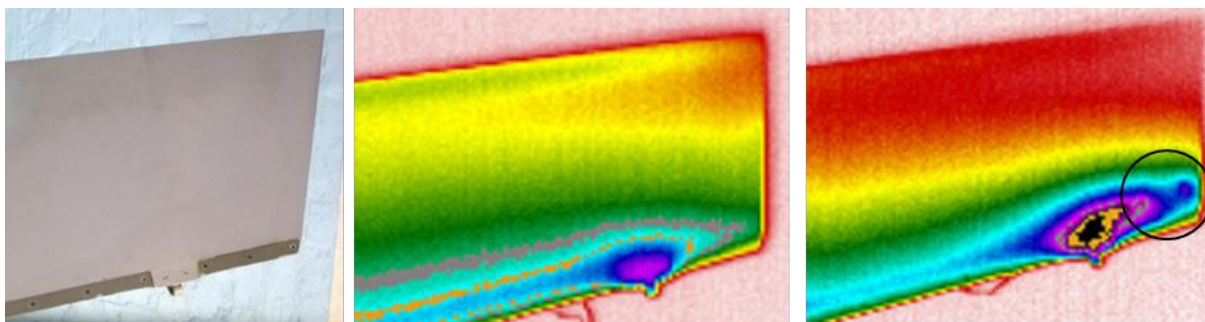
Figure 63: An overview of the rudder thermography inspections. **Left:** Actual rudder. **Middle:** Normal thermal pattern image i.e. no moisture ingress (LYK0059 (U22-2803)). **Right:** Abnormal thermal pattern image, which was verified by analysis as a positive finding of moisture ingress (LYK0132 (U22-2940)). Figure courtesy of VTT.

2.5 Repair technologies

2.5.1 Design and analysis of composite step-lap joint repair

The inner wing root of F/A-18 fighter aircraft is a double-sided titanium-composite stepped lap bonded joint. A repair concept for a case where two innermost steps are damaged is designed and analyzed. The repair concept is illustrated in **Figure 64**. The research program started by development of analysis tools followed by validation of these tools and will be continued by test program to fully validate and certify the selected repair concept at coupon level. The inner wing root step lap joint (IWSLJ) research program is based on a building block approach as illustrated in **Figure 64**.
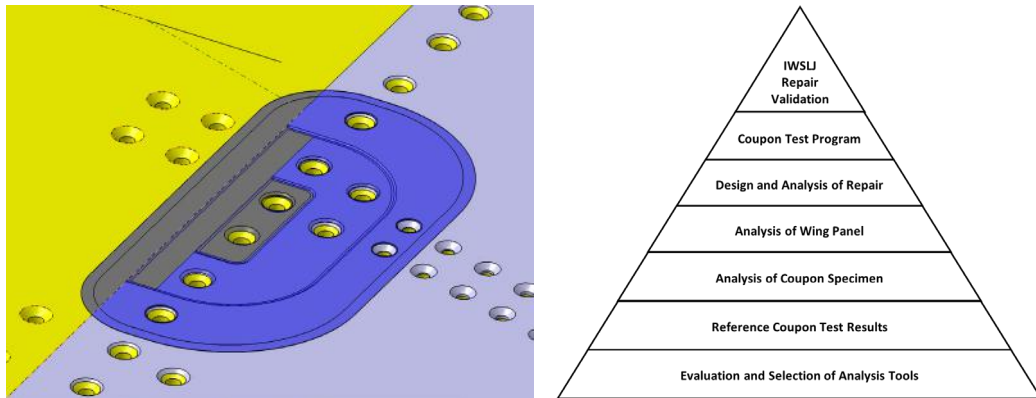
Figure 64: The IWSLJ repair concept and building block approach for the repair validation. Figure courtesy of Patria Aviation.

The analysis tool selected for the work is based on nonlinear finite element method (FEM). The results obtained from the model are fully comparable to the results from analytical tool used in original design (A4EI). However, with FEM more details are possible to include in the model to obtain deeper knowledge about the behavior of the joint. Most of the models are 2D strip models with plane strain elements and symmetrical along the centerline of the joint. The software used for modelling is MSC PATRAN/MARC. One of the models used in the analysis and typical results are shown in **Figure 65**.
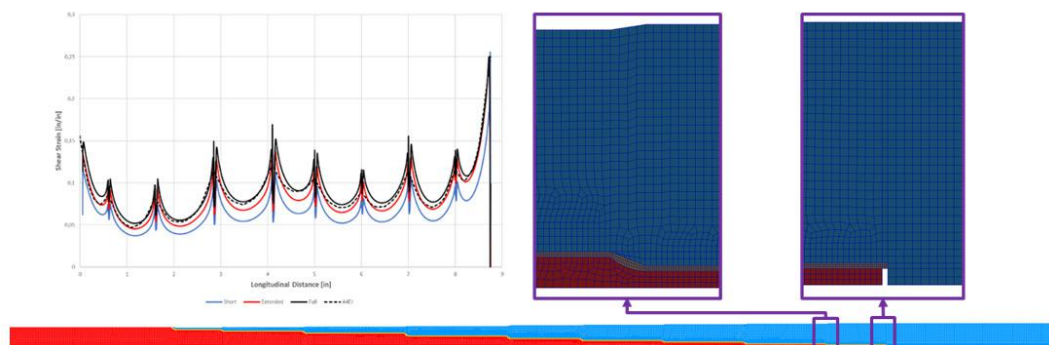
Figure 65: Typical FE model used in the analysis. Figure courtesy of Patria Aviation.

The repair concept selected for validation tests consist of removal of two full innermost steps and bonding a custom CFRP patch on the removed area. A similar concept with titanium patch was also considered but revealed difficulties in NDT of the repaired area.

A test program is developed for certification of the repair and full validation of the analysis tools. The test program consists of static and spectrum fatigue tests of both repaired and unrepaired specimens. The specimen geometry used in the tests is the same as used in original joint certification program. The specimens are obtained from a scrapped wing and the repair manufacturing methods and tools will be the same as would be used in actual wing repair. The test program is scheduled for year 2019. [46], [98], [99], [100]

2.5.2 Continued DIARC plasma coating activities at Aalto University

Previous metal bonding activities related to DIARC plasma coatings have been reported earlier in Ref. [9], Chapter 13.2.5.1.1 of Ref. [31], and in Chapter 2.5.1 of Ref. [32]. The recent achievements are outlined below.

The fatigue performance of DIARC® vacuum plasma surface treatment for titanium, stainless-steel and aluminium structural bonding was tested with double lap shear test specimens. In the metal surface treatment, a nanoscale DIARC Bindo coating is deposited on the substrates in a vacuum chamber. The DIARC-treated surface is ready for bonding and does not require any additional treatments, chemicals or primers containing hazardous CrVI chromium. Finite element method was used in analysing the test specimens. The tests were performed at room temperature dry and at room temperature after hot and wet exposure. The specimens were cycled with constant amplitude loading until failure or until 10 million cycles. The fatigue performance of the DIARC coating was found acceptable. There were no interfacial failures between the DIARC coating and metal or between the DIARC coating and adhesive. The residual strengths of all specimens after 10 million cycles were comparable to the static strength. Due to the copyright restrictions, further in-depth information of the study and the results can be found in [10].

3   Related activities

3.1   Hornet Main Landing Gear research – revisited

The study of the FINAF F/A-18C/D Hornet Main Landing Gear was briefly introduced in the ICAF 2009 report (Chapter 13.3.3 of Ref. [28]). At that time, the FINAF funded the development of a fully functional model of the F/A-18C/D Hornet landing gear by Patria Aviation – called HoLGer - in order to investigate reasons for landing gear failures (so-called Planing Link failures) that had caused several aircraft landing mishaps in Finland and elsewhere. The simulation helps examining the landing gear function under different landing conditions and the effect of different landing gear components.

The Hornet's landing gears have been modeled using MSC Software's Adams mechanical simulation software. The model consists of the nose landing gear (NLG) and both main landing gears (MLG) allowing asymmetric touchdown simulation capability. To achieve realistic approach flight path (including ground effect) and desired aircraft orientation, Matlab/Simulink based HUTFLY2 flight simulation software with the F/A-18C Hornet aircraft model had been used in conjunction with the HoLGer. In two-folded process, VTT first performed the approach phase according to the landing spectrum close to a ground contact altitude and delivered the necessary input data to Patria for the Landing Gear co-simulation to be performed, secondly, in touchdown. [96], [102], [103], [104]

After several upgrades/modifications of the FINAF F/A-18C/D Hornet fleet (Chapter 1.4) it became necessary to re-evaluate the Landing Gear simulation results. In 2018-2019, Patria Aviation is conducting a Hornet Main Landing Gear study under the FINAF's commission. The goals of the study are [41]:

1. to find out the effect of mass distribution change on landing behaviour,

2. to improve Landing Gear model (HoLGer) realism by coupling it to a complex Shock Absorber (SA) model, and

3. to find out stress concentration locations of three main parts: Trunnion, Lever and Lower Sidebrace.

Several modifications were made to the original Landing Gear simulation model to achieve the goals. Also, new approach flight paths and aircraft orientations were defined and simulated because of the changed inertial properties. The three main parts for both MLG's were modelled as flexible parts according to their geometry and material properties. In addition, a more detailed shock absorber model, which was done in Tampere University of Technology, was included in the simulation (**Figure 66**).
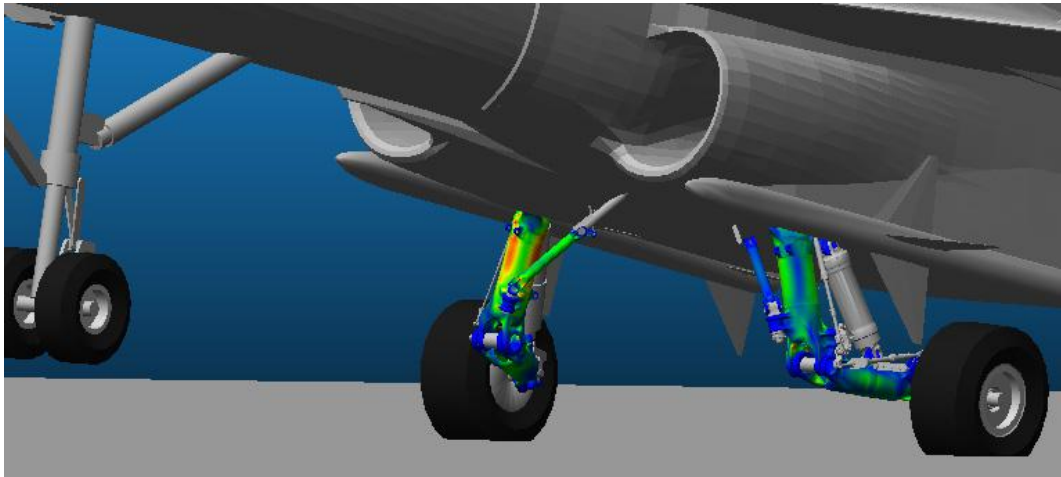

Figure 66: *Updated Main Landing Gear model of the FINAF's F/A-18C/D Hornet. Figure courtesy of Patria Aviation.*

Flexibility of the components was obtained with the finite element (FE) models' modal analysis (normal models + Craig-Bampton method). The FE-models were created by meshing the solid bodies obtained from the 3D scanning of the parts. This was needed to have realistic flexible part behaviour in multibody dynamics simulation.

The shock absorber modelled in Simcenter Amesim software was included to the co-simulation using the Functional Mock-up Interface standard. The co-simulation consists of Siemens Amesim shock absorber model, MSC Adams mechanical model and Matlab/ Simulink F/A-18C flight control model. Results of the new shock absorber model were compared to the measurements of real landing cases which proved that the output from the upgraded model is closer to the measured results than the output from the old model.

By using flexible parts, the stress concentration locations were found (**Figure 67**). Also the stresses of single nodes can now be tracked during transient simulation. In addition, the flexibility revealed interesting dynamic phenomenon of the MLG at touchdowns. Depending on the aircraft orientation, immediately after touchdown the lateral movement of tire was oscillating at an amplitude of more than one inch. The oscillation was larger when the side slip angle of an aircraft was increased and vice versa. The reason behind the lateral movement was a combination of tire dynamics and deformable parts which allow tire to move more in lateral direction before slipping. Similar oscillation was seen in video recording of the MLG Shock Absorber during landing event.

Figure 67: The stress concentrations in updated Main Landing Gear model of the FINAF's F/A-18C/D Hornet. Figure courtesy of Patria Aviation.

3.2   EDA Patchbond project

The EDA Patchbond project was broadly introduced in the ICAF 2017 report (Chapter 3.1 of Ref.[32]). The four-year "*Bolt free battle and operational damage repairs of metal and composite primary aircraft structures (PATCHBOND)*" project is being executed in the framework of the European Defence Agency (EDA) R&T Category B projects. The project focuses on the permanent bolt free composite patch repair of damaged composite primary structures on a military rotary wing platform. The primary goal is to specify a certification approach that fulfils the airworthiness requirements for permanent bonded composite patch repair in a highly loaded primary structure of the platform. The secondary goal is to investigate and define materials and repair processes that are capable of repairing the composite structure to comply with the required operational capability.

The project embraces the methods of repairing in-service damages whose size or location falls beyond the ASR/SRM (Aircraft Structural Repair/Structural Repair Manual) limits; i.e. damages in a highly loaded monolithic or sandwich structure and areas therein where

drilling of additional fastener holes is prohibited, thus enabling adhesively bonded repair the only feasible repair solution. The project covers the whole spectrum of methods starting from damage assessment, analytical and numerical analysis, repair design procedures, materials and processes, inspection, structural health monitoring and quality control, up to the certification aspects.

The work is performed by an international consortium consisting of 14 industrial and scientific partners from five European countries enabled to participate in EDA's projects, alphabetically: Finland: Aalto University (until 2017), Patria Aviation, VTT Technical Research Centre of Finland Ltd.; Germany: Airbus Defence and Space, Bundeswehr Research Institute for Materials, Fuels and Lubricants (WIWeB); the Netherlands: NLR, Fokker Services B.V., KVE Composites Repair; Norway: Norwegian Defence Research Establishment (FFI), Norwegian Defence Logistics Organization (NDLO), DolphiTech, FiReCo, Light Structures; and Spain: Spanish Institute for Aerospace Research (INTA). Project Lead Contractor is NLR (the Netherlands), and Patria Aviation is the Finnish coordinator of the project. The Finnish Defence Force Logistics Command is the national bill paying authority of the project.

The EDA Patchbond project has been divided into nine different Work Packages (WP) which in turn are divided into one or more Work Elements (WE). At the time of writing the national review the EDA Patchbond project was still ongoing, so the final conclusions are not included in this report.

3.3 Recent advances in optical distortion, scratch and dent quantifications on aircraft transparencies

There is an apparent need to automatically characterize and quantify optical distortions transparencies. The topic has been studied since 1960 [11] and methods has been developed for film photography e.g. the double exposure method, ASTM F733-09 [14], Grid Line Slope method, ASTM F2156-11 [15] and also fully automated systems based on digital imaging and machine learning has been developed [16], [81].

The FINAF expressed an interest to have a fully automated capability for measuring and quantifying optical distortions on aircraft transparencies with the following FINAF-specific requirements:

- Systematic, reproducible results
- Remove subjectivity related to human observers with an automated system
- Measure distortions and classify transparencies to pre-defined categories regarding their usability (pass/fail/subject to repair)
- Provide information for maintenance
- Track changes in transparencies (service history in view of sustainment aspects),
- Measure without removing transparencies from aircraft.

With the above requirements in mind, the FINAF tasked VTT to develop a fully automated optical distortion detection system for measuring and quantifying optical distortions on the FINAF F/A-18 transparencies. VTT executed the project in two phases in close collaboration with the FINAF and Patria Aviation (**Figure 68**):

- Phase 1 consisted of a laboratory-level demo system, in which an F/A-18 "off-aircraft" windshield (removed from the aircraft), could be inspected in a controlled laboratory environment, including the testing of ideas on how to develop the system further.
- Phase 2 consisted of an "on-aircraft" proof-of-concept system, in which the F/A-18C windshield and canopy could be inspected on-site (indoors e.g. hangar environments) while these transparencies were routinely installed in the aircraft.

XPARENCY Phase 1 Lab system
ASTM F733 & F2156

XPARENCY Phase 1 Lab system
Projector-based Approach (new)

2013   2014   2015

2016

XPARENCY Phase 2 Lab system
Yearly evolutionary steps
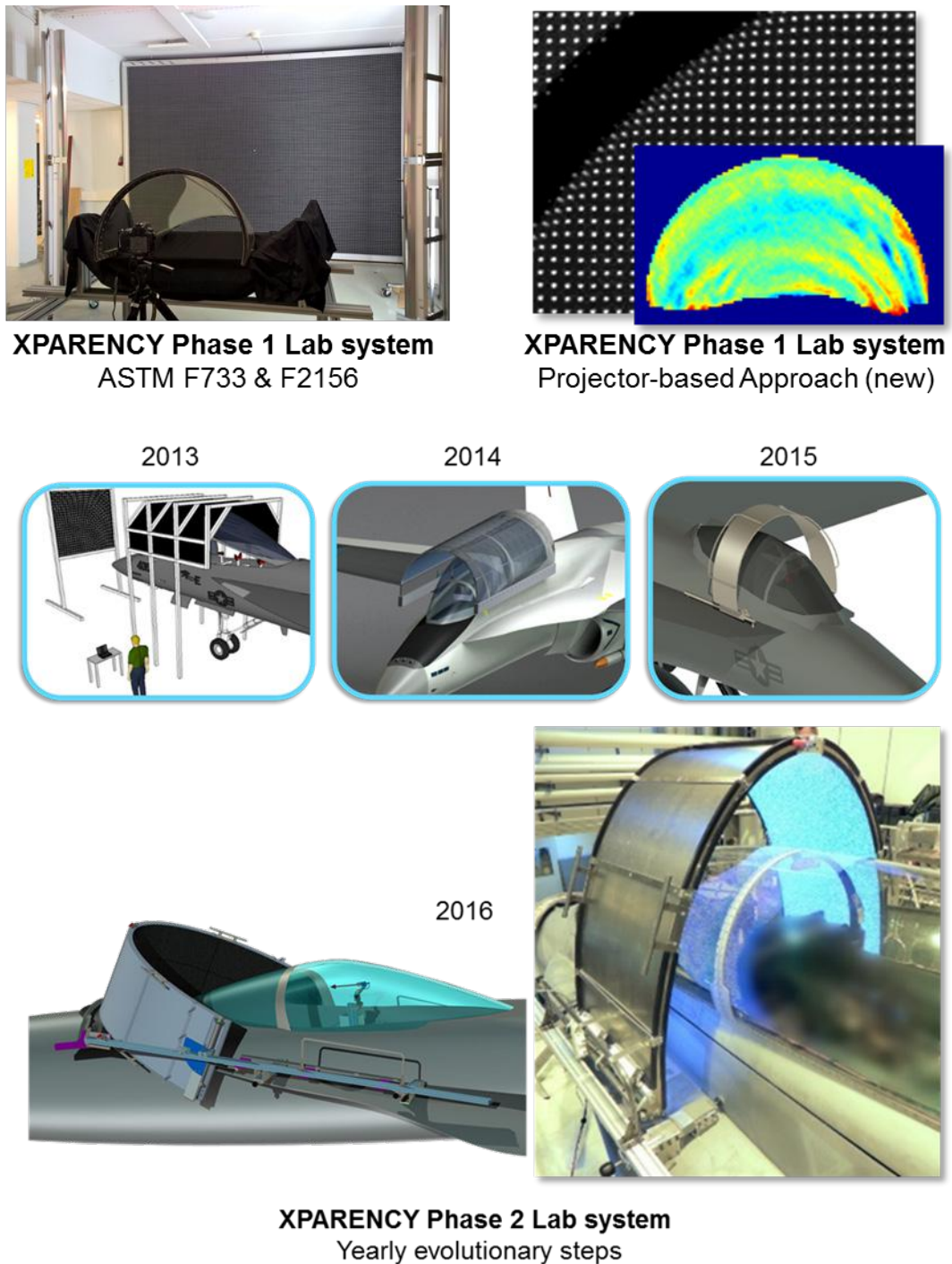
Figure 68: *An overview of the XPARENCY's "off-aircraft" Phase 1 (above) and "on-aircraft" Phase 2 (below) transparency optical distortion detection system [71]. Figure courtesy of VTT.*

As the "on-aircraft" optical distortion detection system's proof-of-concept was successful, efforts to have a Finnish company to upgrade the Technology Readiness Level (TRL) to match that of a new product are underway. Parallel to these industrialization activities, the FDFLOGCOM JSC tasked VTT to develop the system further, to build upon the existing XPARENCY proof-of-concept and expand to the detection and quantifying of scratches, dents and haze in the F/A-18C windshields and canopies (XPARENCY2, **Figure 69**). The follow-on project is well underway. Scratch/dent quantification methods have been investigated to measure in detail the scratches/dents detected (e.g. depth-from-

focus and Tilted Focal Plane Imaging). Repair simulation tools have been developed to verify if simulations of repair effects work in real life in view of resulting (new, anticipated) optical distortions.
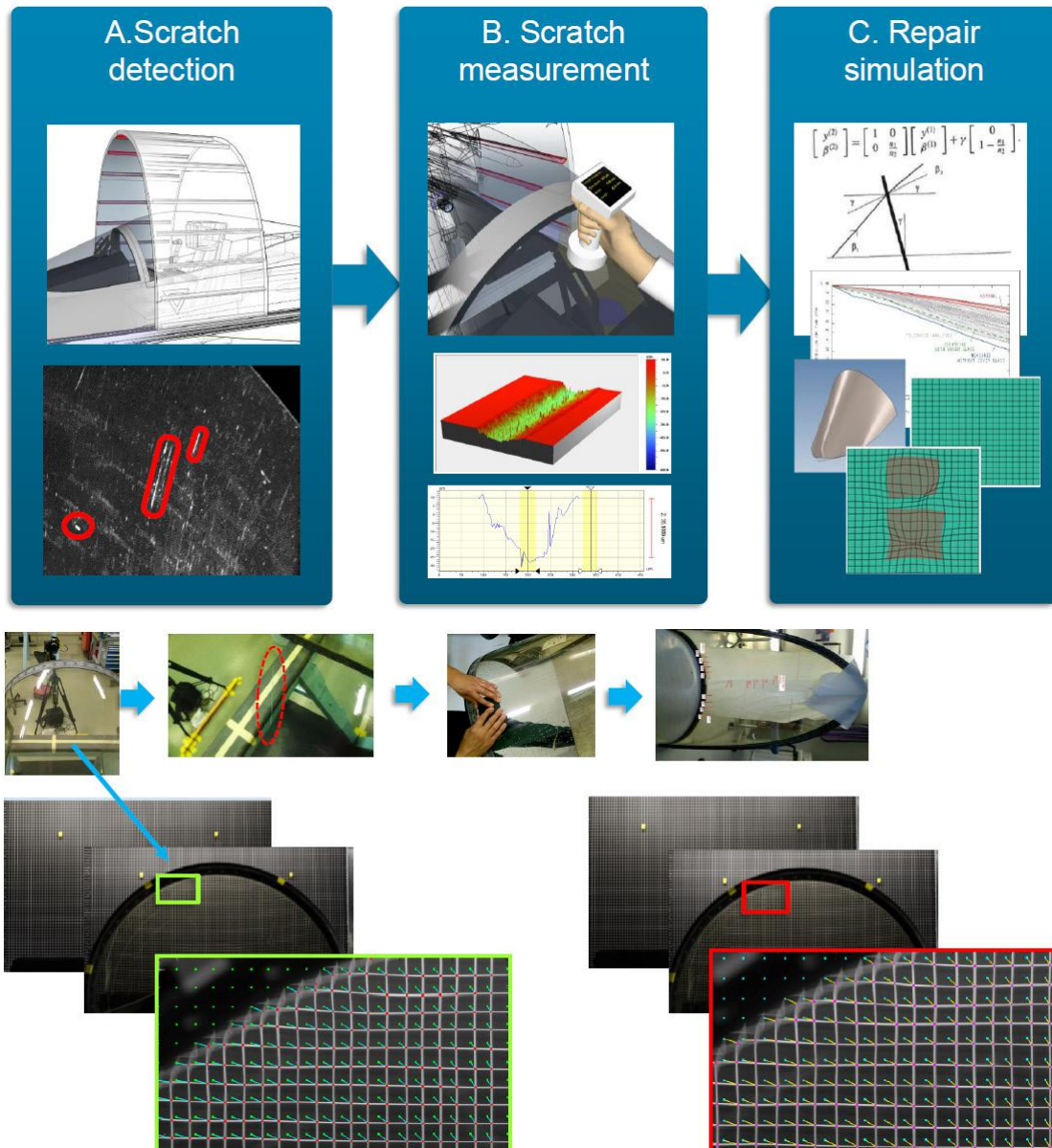
Figure 69: *An overview of the XPARENCY2 "on-aircraft" system to detect and quantify scratches, dents, and haze in the F/A-18C windshields and canopies [72]. Figure courtesy of VTT.*

References

[1] **From Observation Sorties to Multi-Role Fighters.** 2019. The Finnish Air Force web page. Retrieved from https://ilmavoimat.fi/en/history

[2] **Equipment of the Finnish Air Force.** 2019. The Finnish Air Force web page. Retrieved from http://ilmavoimat.fi/en/materiel1

[3] **All Finnish Air Force's Hornets Upgraded to MLU 2.** 2017. The Finnish Air Force web page. Retrieved from http://ilmavoimat.fi/en/article/-/asset_publisher/kaikki-ilmavoimien-hornetit-on-nyt-paivitetty-mlu-2-tasoon. Published in English on 5.1.2017 at 10.21.

[4] **HX Fighter Program.** 2019. Ministry of Defence web page. Retrieved from http://www.defmin.fi/en/administrative_branch/strategic_capability_projects/hx_fighter_program.

[5] **Preliminary Assessment for Replacing the Capabilities of the Hornet Fleet, Final Report.** 2015. Helsinki: Ministry of Defence. ISBN 978-951-25-2680-2. Available as pdf from http://www.defmin.fi/files/3182/HX-ENG.pdf.

[6] **New fighters will have a key role in Finland's defence capability.** 2019. Ministry of Defence web page. Retrieved from https://www.defmin.fi/en/administrative_branch/strategic_capability_projects/hx_fighter_program/hx_fighter_program/key_role_in_finlands_defence_capability.

[7] **Replies received to invitations to tender for HX Fighter Programme.** 2019. Ministry of Defence web page. Retrieved from https://www.defmin.fi/en/administrative_branch/strategic_capability_projects/hx_fighter_program/topical/replies_received_to_invitations_to_tender_for_hx_fighter_programme.9648.news.

[8] **Past Projects: F-18 High Alpha Research Vehicle (HARV).** 2009. The National Aeronautics and Space Administration (NASA) web page. Retrieved from https://www.nasa.gov/centers/dryden/history/pastprojects/HARV/index.html.

[9] Aakkula, J., Jokinen, J., Saarela, O. and Tervakangas, S. 2016. **Testing and modelling of DIARC plasma coated elastic-plastic steel wedge specimens.** International Journal of Adhesion & Adhesives, 68 (2016), 219-228, https://doi.org/10.1016/j.ijadhadh.2016.03.024.

[10] Aakkula, J., Jokinen, J. and Saarela, O. 2017. **Fatigue performance of DIARC® plasma coated bonded metal specimens.** International Journal of Adhesion & Adhesives, 79 (2017), 83-94, https://doi.org/10.1016/j.ijadhadh.2017.09.009.

[11] Amosov, N. I. 1958. **Estimating the optical distortion from curved automobile glass.** Glass and Ceramics, 15 (1958), 427-429, https://doi.org/10.1007/BF00678735.

[12] Antin, K.-N. 2018. **Residual stress changes due to cyclic loading.** Final report (in Finnish, classified). Espoo: Aalto University, School of Engineering.

[13] Arasto, E., Juntunen, J., Jäppinen, T., Koskinen, T., Marja-aho, M. and Metsäjoki, J. 2018. **Producing cracks for RUAG Case 02 –samples.** Research Report № VTT-R-06765-17 (in Finnish, classified). Espoo: VTT Technical Research Center of Finland Ltd.

[14] ASTM F733-09. 2009. **Standard Practice for Optical Distortion and Deviation of Transparent Parts Using the Double-Exposure Method.** ASTM International, West Conshohocken, PA, USA. https://doi.org/10.1520/F0733-09.

[15] ASTM F2156-11. 2011. **Standard Test Method for Measuring Optical Distortion in Transparent Parts Using Grid Line Slope.** ASTM International, West Conshohocken, PA, USA. https://doi.org/10.1520/F2156-11.

[16] Dixon, M., Glaubius, R., Freeman, P. et al. 2011. **Measuring optical distortion in aircraft transparencies: a fully automated system for quantitative evaluation.** Machine Vision and Applications, 22 (2011), 791-804, https://doi.org/10.1007/s00138-010-0258-z.

[17] ESDU 90018. 1990. **Fatigue of aluminium alloy joints with various fastener systems. High load transfer.** IHS ESDU. ISBN: 978 0 85679 744 6.

[18] Hoffren, J. 2017. **Heavy store carriers and external fuel tanks for NH90 helicopter flow simulation model.** Report № NH-S-0052 (in Finnish, classified). Tampere: Patria Aviation Oy.

[19] Hoffren, J. 2017. **Movable control surfaces for the Hawk flow simulation model.** Report № HW-S-0031 (in Finnish, classified). Tampere: Patria Aviation Oy.

[20] Hoffren, J. 2018. **Aerodynamic limit load computations for Hornet.** Report № HN-L-0303 (in Finnish , classified). Tampere: Patria Aviation Oy.

[21] Hoffren, J. 2019. **Generation of CFD grid for Grob 115E and its initial application to determine the aircraft characteristics.** Report № GO-S-0007 (in Finnish , classified). Tampere: Patria Aviation Oy.

[22] Hoffren, J. and Orpana, M. 2017. **Limit load cases for Hornet global FE model (Phase 1: selection of load cases).** Report № HN-L-0296 (in Finnish , classified). Tampere: Patria Aviation Oy.

[23] Hukkanen, T. and Keinonen, M. 2016. **FINAF F-18 Aircraft Structural Integrity Plan, Part II: Structural Integrity Plan.** Technical Report № HN-L-0173 Rev. F (in Finnish, classified). 563 p. Halli: Patria Aviation Oy.

[24] ICAF. 2001. *A Review of Recent Aeronautical Fatigue Investigations in Finland until March 2001*. (A. Siljander, Ed.). Research Report № BTUO33-011139. Espoo: VTT Technical Research Center of Finland.

[25] ICAF. 2003. *A Review of Aeronautical Fatigue Investigations in Finland during the Period February 2001 - March 2003*. (A. Siljander, Ed.). Research Report № BTUO33-031123. Espoo: VTT Technical Research Center of Finland.

[26] ICAF. 2005. *A Review of Aeronautical Fatigue Investigations in Finland during the Period April 2003 - April 2005*. (A. Siljander, Ed.). Research Report № BTUO33-051366. Espoo: VTT Technical Research Center of Finland.

[27] ICAF. 2007. *A Review of Aeronautical Fatigue Investigations in Finland during the Period May 2005 - April 2007*. (A. Siljander, Ed.). ICAF Doc № 2410 (Research Report № VTT-R-03406-07). Espoo: VTT Technical Research Center of Finland.

[28] ICAF. 2009. *A Review of Aeronautical Fatigue Investigations in Finland May 2007 - April 2009*. (A. Siljander, Ed.). ICAF Doc № 2418 (Research Report № VTT-R-02540-09). Espoo: VTT Technical Research Center of Finland.

[29] ICAF. 2011. *A Review of Aeronautical Fatigue Investigations in Finland May 2009 - March 2011*. (E. Peltoniemi, A. Siljander, Eds.). ICAF Doc № 2427 (Research Report № VTT-R-02827-11). Espoo: VTT Technical Research Center of Finland.

[30] ICAF. 2013. *A Review of Aeronautical Fatigue Investigations in Finland April 2011 - February 2013*. (A. Siljander, Ed.). ICAF Doc № 2429 (Research Report № VTT-R-02105-13). Espoo: VTT Technical Research Center of Finland.

[31] ICAF. 2015. *A Review of Aeronautical Fatigue Investigations in Finland March 2013 - February 2015*. (A. Siljander, P. Varis, Eds.). ICAF Doc № 2432 (Research Report № VTT-CR-01811-15. Espoo: VTT Technical Research Center of Finland Ltd.

[32] ICAF. 2017. *A Review of Aeronautical Fatigue Investigations in Finland March 2015 - March 2017*. (T. Viitanen, P. Varis, A. Siljander, Eds.). ICAF Doc № 2433 (Research Report № VTT-CR-02002-17. Espoo: VTT Technical Research Center of Finland Ltd.

[33] Ilkko, J., Salminen, E. and Siikonen, T. 2017. **Time-dependent flow simulations 4 and DES/DDES comparisons with Hornet grid.** Technical Reports № F-112 (in Finnish). Espoo: Finflo Ltd.

[34] Ilkko, J., Salminen, E. and Siikonen, T. 2017. **Time-dependent flow simulations 5 and DES/DDES comparisons with Hornet grid.** Technical Reports № F-114 (in Finnish). Espoo: Finflo Ltd.

[35] Jokinen, J. and Kanerva, M. 2018. **Simulation of delamination growth at CFRP-tungsten aerospace laminates using VCCT and CZM modelling techniques.** Applied Composite Materials (2018), 1-13, https://doi.org/10.1007/s10443-018-9746-5.

[36] Jokinen, J. and Kanerva, M. 2017. **Analysis of cracked lap shear testing of tungsten-CFRP hybrid laminates.** Engineering Fracture Mechanics 175 (2017), 184-200, https://doi.org/10.1016/j.engfracmech.2017.01.029.

[37] Jokinen, J. and Kanerva, M. 2017. **Crack onset analysis of adhesives for the CZM-VCCT method.** XIV International Conference on Computational Plasticity (Complas 2017), Barcelona, Spain. 5-7 September 2017.

[38] Jokinen, J., Kanerva, M., Wallin, M. and Saarela, O. 2019. **The simulation of a double cantilever beam test using the virtual crack closure technique with the cohesive zone modelling.** International Journal of Adhesion and Adhesives, 88 (2019), 50-58, https://doi.org/10.1016/j.ijadhadh.2018.10.015.

[39] Jokinen, J., Wallin, M. and Saarela, O. 2015. **Delamination analysis of a trailing edge flap.** In: Siljander, A. (Ed.) Embracing the future – respecting the past; supporting aging fleets with new technologies, Proceedings of the 34th Conference and the 28th Symposium of the International Committee on Aeronautical Fatigue and Structural Integrity, Helsinki, Finland. 1-5 June 2015, pp. 879-888. ISBN 978-951-38-7442-1.

[40] Jokinen, J., Kanerva, M. and Saarela, O. 2018. **Multi-site delamination using virtual crack closure technique for a composite aircraft wing flap.** 31st Congress of the International Council of the Aeronautical Sciences (ICAS), Belo Horizonte, Brazil. September 9-14, 2018.

[41] Kauppila, H. 2019. **HolGer Development and MLG Hotspot Study.** Report № HN-S-0088 (classified). Tampere: Patria Aviation Oy. [in preparation]

[42] Keinonen, M. 2015. **F-18 C/D Hornet Structures Summary, SRP2 (SSP) Definition.** Technical Report № HN-L-0254 (classified). 25 p. Halli: Patria Aviation Oy.

[43] Kettunen, J. 2019. **HW-368 centre fuselage vibration measurement flight.** Technical Report № HW-L-0142 (in Finnish, classified). Halli: Patria Aviation Oy.

[44] Kettunen, J. and Mattila, M. 2016. **Mk 66 mini-OLM Fatigue Analysis.** Technical Report № HW-L-0130A (in Finnish, classified). Halli: Patria Aviation Oy.

[45] Koski, K. 2019. **Bolted joint tests.** Research Report № VTT-R-00065-19 (classified). Espoo: VTT Technical Research Center of Finland Ltd.

[46]   Kunnari, A. 2017. **A4EI Analysis Procedure for Inner Wing Step Lap Joint Disbonds.** Technical Report № HN-L-0285 (classified). Halli: Patria Aviation Oy.

[47]   Laakso, R. 2019. **HW-368 MINIDATA: extra work 2, version 3.** Memorandum № VTT-M-06919-18 (in Finnish, classified). Espoo: VTT Technical Research Center of Finland Ltd.

[48]   Laakso, R. 2018. **Fit parameter calculation.** Memorandum № VTT-M-01576-18 (in Finnish, classified). Espoo: VTT Technical Research Center of Finland Ltd.

[49]   Laakso, R. 2017. **HW TP FSFT.** Customer Report № VTT-CR-00791-17 (in Finnish, classified). Espoo: VTT Technical Research Center of Finland Ltd.

[50]   Laakso, R., Kettunen, J. and Lähteenmäki, J. 2019. **Hawk Mk 51/51A/66 Tailplane Full-Scale Fatigue Tests.** Oral presentation at the 30th ICAF Symposium, 5-7 June 2019. Krakow, Poland.

[51]   Laakso, R., Jessen-Juhler, O., Juntunen, J., Koski, K., Koskinen, T., Metsäjoki, J., Mäkinen, J., Rinta-aho, J., Siljander, A. and Tuhti, A. 2018. **Producing cracks for POD3 samples.** Customer Report № VTT-CR-05448-18 (in Finnish, classified). Espoo: VTT Technical Research Center of Finland Ltd.

[52]   Laakso, R., Juntunen, J., Aitoniemi, J., Mäkinen, J. and Salonen, L. 2017. **HW TP FSFT: Supporting structures and load implementations.** Customer Report № VTT-CR-00832-17 (in Finnish, classified). Espoo: VTT Technical Research Center of Finland Ltd.

[53]   Laakso, R., Varis, P., Merinen, S., Eskola, S., Teittinen, T. and Juntunen, J. 2017. **HW TP FSFT: Intrumentation, data acquisition, and calibrations.** Customer Report № VTT-CR-00833-17 (in Finnish, classified). Espoo: VTT Technical Research Center of Finland Ltd.

[54]   Laakso, R., Arasto, E., Varis, P. and Juntunen, J. 2017. **HW TP FSFT: Loading spectrum.** Customer Report № VTT-CR-00834-17 (in Finnish, classified). Espoo: VTT Technical Research Center of Finland Ltd.

[55]   Laakso, R., Varis, P., Arasto, E., Juntunen, J., Aitoniemi, J., Tuhti, A., Koskinen, T., Siljander, A. and Lahti, J. 2017. **HW TP FSFT: Fatigue tests and NDI.** Customer Report № VTT-CR-00835-17 (in Finnish, classified). Espoo: VTT Technical Research Center of Finland Ltd.

[56]   Larsson, S. E. 1969. **The development of a calculation method for the fatigue strength of lugs and a study of test results for lugs of aluminium alloys.** In Fatigue Design Procedures, Proceedings of the 4th ICAF Symposium, Pergamon Press, 1969, pp. 309-339.

[57]   Liius, M., Malmi, S. and Salo, J. 2017. **Detailed FE model of Hornet Bulkhead Y557.5 Vertical Tail Stub.** Report № HN-L-0294 (in Finnish, classified). Tampere: Patria Aviation Oy.

[58]   Liius, M., Malmi, S. and Niiranen, O. 2017. **Detailed FE model of Hornet Frame Y566 Vertical Tail Stub.** Report № HN-L-0295 (in Finnish, classified). Tampere: Patria Aviation Oy.

[59]   Liukkonen, S. 2017. **FINAF HOLM Bootstrap Instrumentation and Mechanical Ground Calibrations.** Research Report № VTT-R-02431-17 (classified). Espoo: VTT Technical Research Center of Finland Ltd.

[60]   Liukkonen, S. 2016. **Hawk Mk.66 strain sensor installation for the SHM system of HW-360.** Research Report № VTT-R-04284-16 (in Finnish, classified). Espoo: VTT Technical Research Center of Finland Ltd.

[61] Liukkonen, S. 2016. **HW Mk.66 Mini-OLM test flight measurements.** Research Report № VTT-R-05320-15 (in Finnish, classified). Espoo: VTT Technical Research Center of Finland Ltd.

[62] Liukkonen, S. 2017. **HN-416 Onboard HOLM System's Electrical Calibration 2017.** Research Report № VTT-R-03212-17 (in Finnish, classified). Espoo: VTT Technical Research Center of Finland Ltd.

[63] Liukkonen, S. 2018. **Hawk Mk.66 strain sensor installation for the SHM system of HW-344.** Research Report № VTT-R-02624-18 (in Finnish, classified). Espoo: VTT Technical Research Center of Finland Ltd.

[64] Liukkonen, S. 2018. **Hawk Mk.66 strain sensor installation for the SHM system of HW-361.** Research Report № VTT-R-05121-18 (in Finnish, classified). Espoo: VTT Technical Research Center of Finland Ltd.

[65] Liukkonen, S. 2018. **Hawk Mk.66 strain sensor installation for the SHM system of HW-367.** Research Report № VTT-R-05122-18 (in Finnish, classified). Espoo: VTT Technical Research Center of Finland Ltd.

[66] Malmi, S. 2018. **Training procedures and analysis capability.** Report № HN-L-0062, Rev. E. (classified). Tampere: Patria Aviation Oy.

[67] Morton, S., Steenman, M., Cummings, R. and Forsythe, J. 2003. **DES Grid Resolution Issues for Vortical Flows on a Delta Wing and an F-18C.** In 41st Aerospace Sciences Meeting and Exhibit, Reno, Nevada, USA, (AIAA 2003-1103), p. 1103, https://doi.org/10.2514/6.2003-1103.

[68] Morton, S. A., Cummings, R. M. and Kholodar, D. B. 2007. **High Resolution Turbulence Treatment of F/A-18 Tail Buffet.** Journal of Aircraft, 44 (2007), 1769-1775, https://doi.org/10.2514/1.29577.

[69] Niiranen, O. and Liius, M. 2018. **Detailed FE model of Hornet Center Fuselage Dorsal Longeron FS374-447.** Report № HN-L-0306 (in Finnish, classified). Tampere: Patria Aviation Oy.

[70] Nordeen, L. 2017. **F/A-18 Hornet, Still Got Sting, World Fleet Review.** Air International, Vol. 92, No. 1, p. 81. Stamford: Key Publishing Ltd.

[71] Okkonen, M. et al. 2016. **XPARENCY final report.** Customer Report № VTT-CR-00840-16 (in Finnish, classified). Oulu: VTT Technical Research Center of Finland Ltd.

[72] Okkonen, M. and Mäyrä, A. 2018. **Optical Simulation of Scratch Repair in F/A-18's.** ASTM Committee F07.08 on Aerospace Transparent Materials and Enclosures, Washington DC, USA. 7 November, 2018.

[73] Orell, O., Vuorinen, J., Jokinen, J., Kettunen, H., Hytönen, P., Turunen, J. and Kanerva, M. 2018. **Characterization of elastic constants of anisotropic composites in compression using digital image correlation.** Composite Structures, 185 (2018), 176-185, https://doi.org/10.1016/j.compstruct.2017.11.008.

[74] Orpana, M. 2018. **F/A-18 Hornet, SAFE Fatigue Tracking of Structures, Management Report, Period 3, 2018.** Report № HN-L-1064 (classified, in Finnish). Tampere: Patria Aviation Oy.

[75] Palmberg, B. 1986. **Fatigue life and fastener flexibility of single shear joints with countersunk fasteners.** Report № FFA TN 1986-01. Stockholm: The Aeronautical Research Institute of Sweden.

[76]   Pirtola, J. and Kunnari, A. 2015. **Experiences on a Propability of Detection Project.** In: Proceedings of the 36th Conference and the 29th Symposium of the International Committee on Aeronautical Fatigue and Structural Integrity, Nagoya, Japan. 5-9 June 2017, pp. 2075-2085.

[77]   Salo, J. and Liius, M. 2018. **Detailed FE model of Hornet Aft Fuselage Upper Outboard Longeron FS633-657.** Report № HN-L-0307 (in Finnish, classified). Tampere: Patria Aviation Oy.

[78]   Salonen, T. 2016. **Neural Network Development for Hawk Mk 66 Tail Fatigue Monitoring.** Technical Report № HW-S-0028 (in Finnish, classified). Tampere: Patria Aviation Oy.

[79]   Tikka, J. and Salonen, T. 2007. **Parameter Based Fatigue Life Analysis of F18 Aircraft.** In: Lazzeri, L. and Salvetti, A. (Eds.) Durability and Damage Tolerance of Aircraft Structures: Metals vs. Composites, Volume I, Proceedings of the the 24th Symposium of the International Committee on Aeronautical Fatigue, Naples, Italy. 16-18 May 2007. Pisa, Italy: Pacini Editore, 2007, pp. 412-426. ICAF-Doc. 2417.

[80]   Tikka, J. and Salonen, T. 2015. **Practical Experience of Neural Network Based Fatigue Life Monitoring.** In: Siljander, A. (Ed.) Embracing the future – respecting the past; supporting aging fleets with new technologies, Proceedings of the 34th Conference and the 28th Symposium of the International Committee on Aeronautical Fatigue and Structural Integrity, Helsinki, Finland. 1-5 June 2015, pp. 879-888. ISBN 978-951-38-7442-1.

[81]   TOPINS. 2017. Retrieved from http://www.topinssolution.com/

[82]   Vos, J. B., Charbonnier, D., Siikonen, T., Salminen, E., Hoffren, J., Gehri, A. and Stefani, P. 2018. **Swiss/Finnish Collaboration on Aero-elastic simulations for the F/A-18 fighter.** In 2018 Applied Aerodynamics Conference, Atlanta, Georgia, USA, (AIAA 2018-3642), https://doi.org/10.2514/6.2018-3642.

[83]   Vos, J. B., Charbonnier, D., Ludwig, T., Merazzi, S., Gehri, A. and Stephani, P. 2017. **Recent Developments on Fluid Structure Interaction Using the Navier Stokes Multi Block (NSMB) CFD Solver.** In 35th AIAA Applied Aerodynamics Conference, Denver, Colorado, USA, (AIAA 2017-4458), https://doi.org/10.2514/6.2017-4458.

[84]   Varis, P. and Koski, K. 2017. **Modification of the HOLM ground analysis environment for the crack growth approach.** Research Report № VTT-R-05384-17 (in Finnish, classified). Espoo: VTT Technical Research Center of Finland Ltd.

[85]   Varis, P. and Laakso, R. 2018. **The FINAF average spectrum for Hawk Mk.66 (HW-368) aircraft, and data delivery for Hawk neural network.** Customer Report № VTT-CR-03626-18 (in Finnish, classified). Espoo: VTT Technical Research Center of Finland Ltd.

[86]   Varis, P., Juntunen, J., Isotahdon, E., Marja-aho, M., Siljander, A. and Metsäjoki, J. 2019. **Small crack growth study.** Customer Report № VTT-CR-03255-18 (in Finnish, classified). Espoo: VTT Technical Research Center of Finland Ltd. [in preparation]

[87]   Viitanen, T. 2018. **HN-432 Onboard HOLM System's Electrical Calibration 2018.** Research Report № VTT-R-04572-18 (in Finnish, classified). Espoo: VTT Technical Research Center of Finland Ltd.

[88]   Viitanen, T. and Janhunen, H. 2017. **Provided flight parameters for CFD analyses.** Research Report № VTT-R-06461-17 (in Finnish, classified). Espoo: VTT Technical Research Center of Finland Ltd.

[89]   Viitanen, T. and Janhunen, H. 2018. **FINAF data package 4, Rev. C.** Memorandum № VTT-M-02829-17 Rev. C (classified). Espoo: VTT Technical Research Center of Finland Ltd.

[90] Viitanen, T. and Janhunen, H. 2018. **FINAF data package 5, Rev. A.** Memorandum № VTT-M-01298-18 Rev. A (classified). Espoo: VTT Technical Research Center of Finland Ltd.

[91] Viitanen, T. and Janhunen, H. 2018. **FINAF data package 6, Rev. A.** Memorandum № VTT-M-01299-18 Rev. A (classified). Espoo: VTT Technical Research Center of Finland Ltd.

[92] Viitanen, T. and Janhunen, H. 2018. **FINAF data package 7.** Memorandum № VTT-M-01300-18 Rev. A (classified). Espoo: VTT Technical Research Center of Finland Ltd.

[93] Viitanen, T. and Laakso, R. 2018. **HOLM Analyses Database v5.0.0.** Research Report № VTT-M-05129-16 (in Finnish, classified). Espoo: VTT Technical Research Center of Finland Ltd. [in preparation]

[94] Viitanen, T., Laakso, R. and Liukkonen, S. 2018. **In response to "Known HOLM Data Issues/Data Requests".** Memorandum № VTT-M-04405-18 (classified). Espoo: VTT Technical Research Center of Finland Ltd.

[95] Viitanen, T., Laakso, R., Varis, P. and Arasto, E. 2018. **HOLM fatigue analyses, Annual Report 2018.** Research Report № VTT-M-05141-16 (in Finnish, classified). Espoo: VTT Technical Research Center of Finland Ltd.

[96] Viitanen, T. and Janhunen, H. 2008. **F-18C Hornet Landing Simulations, Phase 2.** Research Report № VTT-R-07158-08. (classified). Espoo: VTT Technical Research Center of Finland.

[97] Väkevä, V. 2018. **The effect of compressive residual stresses at the surface on fatigue life of an aluminium alloy.** Bachelor's Thesis (in Finnish). Espoo: Aalto University, School of Engineering.

[98] Wallin, M. 2017. **FE Analysis Tools for Inner Wing Step Lap Joint.** Technical Report № HN-L-0293 (classified). Halli: Patria Aviation Oy.

[99] Wallin, M. 2019. **Test Spesification for Step Lap Joint Repair Validation.** Technical Report № HN-K-0037 (classified). Halli: Patria Aviation Oy.

[100] Wallin, M. 2019. **Design and Analysis of IWSLJ Repair Concepts.** Technical Report № HN-K-0038 (classified). Halli: Patria Aviation Oy.

[101] Yli-Olli, S. and Koski, K. 2019. **Fractographic and metallographic evaluation of fatigue test pieces.** Customer Report VTT-CR-00308-19 (classified). Espoo: VTT Technical Research Center of Finland Ltd.

[102] Öström, J. 2007. **F-18C Hornet Landing Simulations.** Research Report № VTT-R-08770-07. (classified). Espoo: VTT Technical Research Center of Finland.

[103] Öström, J. 2008. **The main landing gear model's integration in the HUTFLY2 flight simulator.** Research Report № VTT-R-02564-08. (in Finnish, classified). Espoo: VTT Technical Research Center of Finland.

[104] Öström, J., Lähteenmäki, J. and Viitanen, T. 2008. **F-18 Hornet Landing Simulations Using Adams and Simulink Co-Simulation.** In: AIAA Modeling and Simulation Technologies Conference. Honolulu, Hawaii, USA, (AIAA 2008-6850), https://doi.org/10.2514/6.2008-6850.

Report's title	
A REVIEW OF AERONAUTICAL FATIGUE INVESTIGATIONS IN FINLAND APRIL 2017 – MARCH 2019	
Customer, contact person, address Finnish Defence Force Logistics Command, Joint System Centre, Air Systems Division Mr. Ari Kivistö P. O. Box 69; FI-33541 Tampere; Finland	
Project name PIIKKI - ICAF2019NR	Project number 122893 - 1.1
Editors Tomi Viitanen, Aslak Siljander	Pages 75
Keywords ICAF, aeronautical fatigue, military aircraft, fixed wing, structural integrity, FDF, FINAF, Finland	Report identification code VTT-CR-00352-19/ 30.4.2019

Summary

This document was prepared for the delivery to the 36th Conference of the International Committee on Aeronautical Fatigue and Structural Integrity (ICAF) scheduled to be held in Krakow, Poland on 3-4 June 2019.

A review is given of the aircraft structural fatigue research and associated activities which form part of the programs within the Finnish Air Force Command (AFCOMFIN), the Finnish Defence Force Logistics Command, Joint Systems Centre (FDFLOGCOM JSC), Air Systems Division; Aalto University; Elomatic/ Finflo Ltd; Emmecon Ltd; Eurofins Expert Services Oy; Patria Aviation Oy; Tampere University; Trueflaw Ltd; and VTT Technical Research Centre of Finland Ltd (VTT).

The review summarizes fatigue related research programs and investigations on specific military fixed wing aircraft since the previous Finnish National Review (presented in the 35th Conference, ICAF, Nagoya, Japan) up to March 2019.

Confidentiality	Public

Espoo 30 April 2019
Tomi Viitanen   Aslak Siljander ICAF National Delegate Finland (VTT)   Principal Scientist (VTT)
Editors' contact address VTT, P. O. Box 1000, FI-02044 VTT, Finland (Street: Vuorimiehentie 3, Espoo, Finland)
Distribution
Unclassified. Distribution unlimited. This document has been authorized by the FDFLOGCOM JSC for unlimited public release [Permission № BP7150 / 26.4.2019].